NCAR/TN-382+STR
NCAR TECHNICAL NOTE

June 1993

Description of the NCAR Community Climate Model (CCM2)

JAMES J. HACK
BYRON A. BOVILLE
BRUCE P. BRIEGLEB
JEFFREY T. KIEHL
PHILIP J. RASCH
DAVID L. WILLIAMSON

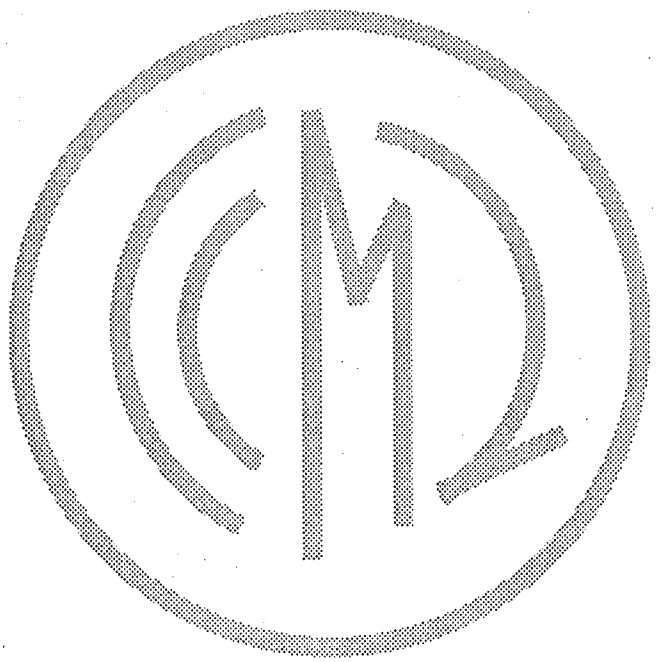

CLIMATE AND GLOBAL DYNAMICS DIVISION

NATIONAL CENTER FOR ATMOSPHERIC RESEARCH
BOULDER, COLORADO

CONTENTS

CONTENTS—Continued

LIST OF FIGURES

1. INTRODUCTION

This report presents the details of the governing equations, physical parameterizations, and numerical algorithms defining the version of the NCAR Community Climate Model designated CCM2. The material provides an overview of the major model components, and the way in which they interact as the numerical integration proceeds. Details on the coding implementation, along with in-depth information on running the CCM2 code, are given in a separate technical report entitled "User's Guide to NCAR CCM2" (Bath *et al.*, 1992). As before, it is our objective that this model provide NCAR and the university research community with a reliable, well documented atmospheric general circulation model. In contrast with earlier versions of the CCM, however, the CCM2 represents a wholly new state-of-the-art atmospheric general circulation model, both functionally and in terms of its implementation. As such, this version of the CCM represents a major break from the evolutionary nature of earlier releases, and should provide the research community with a significantly improved atmospheric modeling capability.

a. Brief History

Over the last decade, the NCAR Climate and Global Dynamics (CGD) Division has provided a comprehensive, three-dimensional global atmospheric model to university and NCAR scientists for use in the analysis and understanding of global climate. Because of its widespread use, the model was designated a Community Climate Model (CCM). The original version of the NCAR Community Climate Model (designated CCM0A) was based on the Australian spectral model developed by W. Bourke, B. McAvaney, K. Puri, and R. Thurling (Bourke *et al.*, 1977; McAvaney *et al.*, 1978), and was described in Washington (1982). The model was adapted to the NCAR computers by K. Puri (Australian Numerical Meteorological Research Centre—ANMRC) during an extended visit. It was subsequently modified by E. Pitcher (University of Miami) and R. Malone (Los Alamos/Department of Energy) to adopt more efficient Fourier transform routines and the improved radiation/cloudiness parameterizations of Ramanathan and Dickinson. The radiation and cloud models were subsequently revised to their CCM0A versions by Ramanathan. Results of January and July simulations produced by CCM0A are presented by Pitcher *et al.* (1983). The response of the model to refinements in the radiative processes is described by Ramanathan *et al.* (1983).

An important broadening of the concept of the NCAR community model occurred in late 1981 with NCAR's decision to utilize the same basic code for global forecast studies (both medium– and long–range) and for climate simulation. Economy and increased efficiency could then be achieved by documenting and maintaining only one set of codes. Changes from one application to the other would also be relatively straightforward in a model with modular design. The use of one basic model for both forecasting and climate studies also has potential scientific value since a major part of long–range (one– to two–

week) forecast errors is due to the drift toward a model climate which differs from that of the atmosphere. Thus, improvements in the climate aspects of the model should be expected to lead to improvements in intermediate to long-range forecasts. A similar scientific benefit is that many physical parameterizations are deterministic rather than statistical, in the sense that they are based on the details of the current model state, rather than on some past statistical properties. Thus, many of their properties can be studied, improved, and verified by examining them in a forecast mode.

Because of the extension of the role of the CCM to include forecast studies as well as climate studies, and because of the expected widespread use for both purposes by university and NCAR scientists, a versatile, modular, and well–documented code became essential. The version designated CCM0B was developed to meet these requirements. This code originated with an adiabatic, inviscid version of the spectral model developed at the European Centre for Medium Range Weather Forecasts (ECMWF) by A. P. M. Baede, M. Jarraud, and U. Cubasch (Baede *et al.,* 1979). Physical parameterizations and numerical approximations matching those of CCM0A were added to this model. The physical parameterizations included the radiation and cloud routines developed at NCAR (Ramanathan *et al.,* 1983), convective adjustment, stable condensation, vertical diffusion, surface fluxes, and surface–energy–balance prescription developed at the Geophysical Fluid Dynamics Laboratory (GFDL) (Smagorinsky, 1963; Manabe *et al.,* 1965; Smagorinsky *et al.,* 1965; Holloway and Manabe, 1971). The vertical and temporal finite differences matched those of the Australian spectral model (Bourke *et al.,* 1977). This combination was designated the NCAR CCM0B. It was described in a series of technical notes, which included a Users' Guide (Sato *et al.,* 1983) that provided details of the code logic, flow, and style and illustrated how to modify and run that model and a note describing each subroutine in the model library that was designed to be used in conjunction with the code itself (Williamson *et al.,* 1983). The details of the algorithms were given in Williamson (1983), and circulation statistics from long January and July simulations were presented in Williamson and Williamson (1984). The latter report provided prospective users with a brief, concise summary of the climate produced by the model. In addition, it demonstrated that the climate produced by the CCM0B version matched the original CCM0A version to within the natural variability.

The advantages of the community model concept, in which many scientists use the same basic model for a variety of scientific studies, were demonstrated in workshops held at NCAR in July 1985 (Anthes, 1986), July 1987, and July 1990. Fundamental strengths and weaknesses of the model have been identified at these workshops through the presentation of a diverse number of applications of the CCM. Much constructive dialogue has taken place between experts in several disciplines at these meetings, leading to continued improvements in the CCM with each release.

The first such example was the introduction of the NCAR CCM1, which followed CCM0B in July of 1987 and included a similar set of detailed technical documentation

(Williamson *et al.*, 1987; Bath *et al.*, 1987a; Bath *et al.*, 1987b; Williamson and Williamson, 1987; Hack *et al.*, 1989). Substantial changes were incorporated in the radiation scheme, including a new solar albedo parameterization accounting for the solar zenith-angle dependence of albedo on various surface types. Other changes included improvements to the absorption of solar radiation by H_2O and O_2; improvements to the longwave absorptance algorithms for H_2O, CO_2, and O_3; changes to account for the liquid water content of stratiform clouds in determining their emissivity; and incorporation of a new finite-difference scheme in the longwave part of the radiation model (Kiehl *et al.*, 1987). The vertical finite-difference approximations were modified to conserve energy without adversely affecting the model simulations, and frictional heating was included so that the momentum diffusion produced a corresponding heating term in the thermodynamic equation. The latter two improvements resulted in the energy in the model being conserved to the order of one W m^{-2} and, moisture to one-hundredth W m^{-2} energy equivalent over 90-day periods. The horizontal diffusion was modified to a ∇^4 form in the troposphere and included a partial correction for evaluating the operator on pressure surfaces rather than sigma surfaces. The local moisture adjustment was generalized to provide for a global horizontal borrowing (Royer, 1986) in a conserving manner. The vertical diffusion was converted to a nonlinear form for which the eddy-mixing coefficient depended on local shear and stability. The diffusion was applied throughout the atmosphere rather than only below 500 mb, as done in CCM0B, and eliminated the need for a dry convective adjustment in the troposphere. The surface drag coefficient was made a function of stability following Deardorff (1972), and the equation of state was modified to formally correctly account for moisture in the atmosphere (i.e., virtual temperature was used where appropriate and the variation with moisture of the specific heat at constant pressure was accounted for). In addition to the above changes to the physics, CCM1 included new capabilities such as a seasonal mode in which the specified surface conditions vary with time, and an optional interactive surface hydrology (Budyko, 1956), which followed the formulation presented by Manabe (1969). Since the CCM1 could also be used as a global forecast model, codes to prepare initial data in the CCM history tape format from analyzed observed atmospheric data, such as FGGE Level IIIb analyses (Mayer, 1988), and codes to perform nonlinear normal mode initialization (Errico and Eaton, 1987; Errico 1986) were made available.

The latest version of the NCAR Community Climate Model, CCM2, incorporates the most ambitious set of improvements to date. A brief overview of the CCM2 is provided in the next section.

b. Overview of CCM2

The bulk of the effort in the NCAR Climate Modeling Section over the last four years has been to improve the physical representation of a wide range of key climate processes in the NCAR Community Climate Model, including clouds and radiation, moist

convection, the planetary boundary layer, and transport. The resulting changes to the model have resulted in a significantly improved climate simulation, particularly in low latitudes. Changes to the model formulation are so extensive that the model cannot be thought of as having evolved from the earlier CCM1 version. Instead, the NCAR CCM2 represents an entirely new atmospheric general circulation model in both function and implementation.

The model has been developed for a standard horizontal spectral resolution of T42 (approximately a 2.8 x 2.8 degree transform grid), with 18 vertical levels and a top at 2.917 mb. In addition to changes in model formulation, the model code has been entirely re-implemented with three major objectives: much greater ease of use and modification; conformation to a plug-compatible physics interface standard; and the incorporation of single-job multitasking capabilities. As before, a User's Guide (Bath *et al.,* 1992) is available that provides details of the code logic, flow, data structures and style, and explains how to modify and run CCM2. In contrast with CCM1, the code is internally documented, obviating the need for a separate technical note that describes each subroutine and common block in the model library. Thus, the code itself, the Users' Guide, the present report, and a series of reviewed scientific publications are designed to completely document CCM2. Aspects of the CCM2 dynamic, thermodynamic, and radiative climate statistics are documented in Climate Modeling Section (1993) and Kiehl *et al.*, (1993). No reference to the earlier technical reports documenting the CCM should be required.

It is worthwhile to begin this discussion by noting the principal algorithmic approaches that have been carried forward from CCM1 to CCM2: the use of a semi-implicit, leap frog time integration scheme; the spectral transform method for treating the dry dynamics; and a bi-harmonic horizontal diffusion operator. In most other respects, the CCM2 makes use of new algorithms for both resolved dynamics and parameterized physics.

It is well known that the large-scale moisture field is very difficult to model accurately due to large horizontal and vertical spatial variations, coupled with the large-amplitude, small-scale character of its sources and sinks. Spectral models often introduce negative values of water vapor that are generally "fixed" in some fashion (Rasch and Williamson, 1990). These techniques can also be the source of anomalous rainfall (sometimes referred to as "spectral rain") caused by overshoots introduced by the spectral representation, which cannot be monitored or fixed (Williamson, 1990). Shape preserving Semi-Lagrangian Transport (SLT) methods do not suffer from these particular drawbacks. They transport information downwind only, and are sensitive to the local characteristics of the wind and moisture fields only. Consequently, a shape-preserving semi-Lagrangian transport scheme (Williamson and Rasch, 1989; Rasch and Williamson, 1990, 1991; Williamson and Rasch, 1993) is the method used for advecting water vapor as well as an arbitrary number of other scalar fields (e.g., cloud water variables, chemical constituents, etc.) in the CCM2.

A second change in the CCM2 dynamical formalism is the incorporation of a terrain-following hybrid vertical coordinate. The hybrid coordinate was developed by Simmons and Strüfing (1981) to provide a general framework for a terrain-following vertical coordinate that reduces to a pressure coordinate at an arbitrary point above the surface. The specific form of the hybrid coordinate in CCM2 differs from Simmons and Strüfing (1981) by allowing for an upper boundary at finite height (nonzero pressure), as in the original development of generalized vertical coordinates by Kasahara (1974). In addition, the vertical finite difference approximations collapse to those of CCM1 when the hybrid scheme is reduced to a σ system.

The CCM2 employs a δ-Eddington approximation to calculate solar absorption, using 18 spectral intervals to achieve reasonable agreement with clear sky and cloudy sky absorption (Briegleb, 1992). These include 7 intervals between 0.20 and 0.35μm to capture O_3 Hartley-Huggins band absorption and Rayleigh scattering; 1 interval in the visible between 0.35 and 0.70μm to capture Rayleigh scattering, O_3 Chappius band absorption, and O_2 B band absorption; 7 intervals between 0.70 and 5.0μm to capture vapor and liquid water absorption of H_2O, as well as O_2 A band absorption; and finally, 3 bands to capture CO_2 absorption in the 2.7μm and 4.3μm bands. A simple empirical scaling approximation is used to accurately capture the stratospheric heating limit for CO_2, O_2, and H_2O. To incorporate the effects of clouds, the scheme makes use of the cloud radiative parameterization of Slingo (1989). The optical properties for liquid droplet cloud particles are parameterized in terms of the liquid water path and effective radius. Comparisons with available references suggests that this scheme reasonably captures radiative heating from the surface through the mesosphere ($\sim$ 0.01 mb around 80km) and particularly improves estimates of atmospheric absorption/heating below cloud decks. The δ-Eddington approximation allows an estimate of the photon flux necessary to compute photodissociation rates for chemistry applications and provides a versatile way to incorporate the effects of aerosols. The use of adjustable monochromatic intervals also allows for applications that require finer spectral resolution than those discussed above.

The treatment of longwave radiation remains much the same as in CCM1. The major modification is the incorporation of a Voigt line shape to more accurately treat infrared radiative cooling in the stratosphere.

A diurnal cycle is incorporated in CCM2 in order to include the interactions between the radiative effects of the diurnal cycle and the surface fluxes of sensible and latent heat (and the associated free-atmosphere response). For the diurnal cycle, both solar and longwave heating rates are updated every model hour in the standard configuration. These heating rates and associated surface radiative fluxes are fixed and applied to the dynamics until the next heating rate update is completed. The longwave absorptivities and emissivities are updated every twelve hours in the standard configuration. In the CCM1, two types of radiation calculations were performed: a "full" calculation (both fluxes and atmospheric heating rates), and a "partial" (only surface

radiative fluxes) calculation, (see Williamson *et al.*, 1987, p. 46–47). The "partial" radiation calculation is not an option in CCM2.

Land and sea ice surfaces, with and without snow cover, are modeled as horizontally homogeneous media with vertically varying thermal properties. The subsurface temperatures are assumed to obey a thermal diffusion equation where the net energy flux at the surface/atmosphere interface is calculated using bulk exchange formulae in which the transfer coefficients are stability dependent. At the lower boundary over land surfaces, a zero heat flux condition is imposed, while over sea ice a constant ocean temperature condition is maintained, allowing for heat transfer between the lowest sea ice layer and the underlying ocean. The time dependent thermal diffusion equation is solved in finite difference form for an arbitrary number of layers, using a fully implicit Crank-Nicholson scheme. The standard configuration of CCM2 has four soil layers.

The cloud fraction parameterization in CCM2 is a generalization of Slingo (1987). Clouds can form in any tropospheric layer, except the first layer above the surface, and cloud fraction depends on relative humidity, vertical motion, static stability and the convective precipitation rate. The cloud emissivities are determined from the local liquid water path. The liquid water path is diagnosed by vertically integrating a specified liquid water concentration profile, which is also a function of latitude.

Turbulence in the atmospheric boundary layer (ABL), sometimes referred to as the planetary boundary layer (PBL), is responsible for the mixing of heat, moisture, momentum, and passive scalars. A non-local ABL parameterization, based on the work of Troen and Mahrt (1986) and Holtslag *et al.* (1990), is used in the NCAR CCM2 to represent these processes. The parameterization scheme determines an eddy diffusivity profile based on a diagnosed boundary layer height and a turbulent velocity scale. It also incorporates non-local (vertical) transport by large eddies, thus providing a more comprehensive representation of the physics of boundary layer transport. Subgrid scale vertical transport of passive scalars by boundary layer turbulence is also treated.

A simple mass flux scheme developed by Hack (1993) is used to represent all types of moist convection. This scheme utilizes a three level conceptual cloud model with convergence and entrainment in the first level, condensation and rain out in the middle level and limited detrainment in the top level. The convective model is applied to three contiguous CCM levels, starting from the bottom of the model and shifting up successively one level at a time, after which the column is stabilized. The convection parameterization makes use of temperature and moisture perturbations from the ABL parameterization to determine the thermodynamic properties of ascending parcels. This scheme also provides a consistent treatment of convective transports of an arbitrary number of passive scalars.

In the initial release of CCM2 the land surface had specified soil moisture. The Biosphere-Atmosphere Transfer Scheme (BATS) of Dickinson *et al.* (1986) is now available as an option and is documented in Dickinson et al. (1993) and Bonan (1993). As in CCM1, sea surface temperatures are specified by linear interpolation between the climatological monthly mean values, but now use the data of Shea *et al.* (1990).

2. OVERVIEW OF TIME DIFFERENCING

The temporal approximations are designed around a time-splitting formalism. In this section we provide the details of the splitting and relate the various steps to the individual processes described in later sections. When describing time-split algorithms, the notational details often become very complex and cumbersome (e.g., CCM1 in Williamson *et al.*, 1987), even though each process or sub-step in isolation can be described as a straightforward centered, forward or backward process. Therefore, we do not carry the detailed notation forward throughout this report, but rather, describe each process individually with simple, local notation and relate that simple notation to the complete, and therefore complex, notation adopted in this section only.

The general prognostic equations for a generic model variable ψ can be written as

$$\frac{\partial \psi}{\partial t} = P_T(\psi) + \Gamma(\psi) + F(\psi) + P_A(\psi) , \qquad (2.a.1)$$

where P_T represents those physical parameterizations applied as tendencies, P_A those parameterizations applied as adjustments, and Γ represents the dynamical components. The term F is an ad hoc correction to ensure conservation of atmospheric mass and water vapor by the dynamical processes.

We describe a basic time step assuming the unfiltered prognostic variables are known on the Gaussian grid at time $n, (\psi^n)$ and time filtered prognostic variables are known at time $n-1, \left(\overline{\psi}^{n-1}\right)$. The time step is complete after the predicted variables are available at grid points at time $n+1, \left(\psi^{n+1}\right)$, and time filtered values are available at time $n, \left(\overline{\psi}^{n}\right)$.

One complete time step proceeds as

$$\psi^- = \overline{\psi}^{n-1} + 2\Delta t P_T^n \left(\psi^-, \psi^n, \overline{\psi}^{n-1}\right) \qquad (2.a.2)$$

$$\begin{cases} \hat{\psi}^+ = \psi^- + 2\Delta t \Gamma \left(\hat{\psi}^+, \psi^n, \psi^-, \overline{\psi}^{n-1}\right) & (2.a.3a) \\ \hat{\psi}^+ = L^n_{\lambda\varphi\eta}\left(\psi^-\right) & (2.a.3b) \end{cases}$$

$$\psi^+ = \hat{\psi}^+ + 2\Delta t F \qquad (2.a.4)$$

$$\psi^{n+1} = P_A\left(\psi^+\right) \qquad (2.a.5)$$

$$\overline{\psi}^n = \psi^n + \alpha\left(\overline{\psi}^{n-1} - 2\psi^n + \psi^{n+1}\right) . \qquad (2.a.6)$$

The time filter, (2.a.6), was originally designed by Robert (1966) and later studied by Asselin (1972). The tendency physics (2.a.2) includes (in the following order) the cloud parameterization; radiative fluxes and atmospheric heating rates; soil temperature update; surface fluxes; free atmosphere vertical diffusivities, ABL height, diffusivities and countergradient term; vertical diffusion solution; gravity wave drag; and Rayleigh

friction. Note that for greater stability (2.*a*.2) is, in general, implicit with the unknown ψ^- appearing on the right-hand side. To make the solution practical, this step is further subdivided into time split steps for each component as described in Section 4.1. The end result of step (2.*a*.2) is the net tendency attributable to the tendency physics

$$P_T^n = \frac{\psi^- - \overline{\psi}^{n-1}}{2\Delta t} . \qquad (2.a.7)$$

The dynamical step (2.*a*.3) is written in two general forms, with (2.*a*.3*a*) for the semi-implicit spectral transform dynamical components and (2.*a*.3*b*) for the semi-Lagrangian advection of water vapor (and additional constituents). Because the tendency physics (2.*a*.2) is formulated in terms of u and v, but the dynamics (2.*a*.3*a*) is formulated in terms of ζ and δ, it is convenient to rewrite (2.*a*.3*a*) by substituting in (2.*a*.2):

$$\hat{\psi}^+ = \overline{\psi}^{n-1} + 2\Delta t \Gamma \left(\hat{\psi}^+, \psi^n, \psi^-, \overline{\psi}^{n-1} \right) + 2\Delta t P_T^n \left(\psi^-, \psi^n, \overline{\psi}^{n-1} \right) . \qquad (2.a.8)$$

One subtle point associated with the dynamics is that, in some minor ways, Γ explicitly depends on $\overline{\psi}^{n-1}$, as indicated in (2.*a*.3*a*). In a traditional time-split approach, this dependency would be replaced with an equivalent one on ψ^-, leading to the equation

$$\hat{\psi}^+ = \psi^- + 2\Delta t \Gamma \left(\hat{\psi}^+, \psi^n, \psi^- \right) . \qquad (2.a.9)$$

Formally, however, the approximation actually used in the model is as given in (2.*a*.3*a*), which yields (2.*a*.8). Equation (2.*a*.2) is used only to provide the tendencies, not for a provisional forecast value entering in the dynamics.

The dynamics step (2.*a*.3*a*), or more properly (2.*a*.8), is based on a centered semi-implicit, spectral transform method. It includes a transformation from grid to spectral space during the forecast and an inverse transform to grid space of the updated variables. Horizontal diffusion is applied on η surfaces in spectral space and a partial correction to p surfaces (consisting of the leading term only) is applied locally on the return to grid space. The details of this step are presented in Section 3.

The advection of water vapor and constituents is cleanly time split, as indicated in (2.*a*.3*b*). In this semi-Lagrangian step, L represents the interpolation operator applied to determine ψ^- at the departure point. The superscript n implies that the winds at time n are used to determine the departure point. Details are provided in Section 3.c.

The fixer step (2.*a*.4) applies a change to the surface pressure and water vapor (and constituents) such that the global average of dry atmosphere mass and water vapor are conserved in the advective process, *i.e.*,

$$\int \pi^+ dA - \int \left(\sum q^+ \Delta \hat{p}^+ \right) dA = \int \overline{\pi}^{n-1} dA - \int \left(\sum q^- \Delta \overline{p}^{n-1} \right) dA \qquad (2.a.10)$$

and

$$\int \left(\sum q^+ \Delta p^+ \right) dA = \int \left(\sum q^- \Delta \overline{p}^{n-1} \right) dA , \qquad (2.a.11)$$

where π is the surface pressure. The $\sum$ denotes an approximation to the integral by a vertical sum over the grid values, and the integral $\int (\quad) dA$ denotes the discrete horizontal Gaussian quadrature approximation to the integral. Equation (2.a.11) applies to all constituents, but only water vapor enters into (2.a.10). Details are given in Section 3.d.

The adjustment physics (2.a.5) consists of a number of adjustment type sub-steps also, each applied in a time-split manner. These sub-steps are mass flux convective parameterization, large scale stable condensation, and dry convective adjustment (at the levels activated). They are detailed in Section 4.2.

Finally, the time filtering (2.a.6) is applied to complete the time step. The form (2.a.6) is applied to u, v, T, q and π (where π is surface pressure). To be consistent with u and v, ζ and δ must also be filtered. To minimize data motion in the code, the filter is applied in two steps to ζ and δ only:

$$\widetilde{\psi}^n = \psi^n + \alpha\left(\overline{\psi}^{n-1} - 2\psi^n\right), \tag{2.a.12}$$

$$\overline{\psi}^n = \widetilde{\psi}^n + \alpha\left(\psi^{n+1}\right). \tag{2.a.13}$$

In the time split steps (2.a.2) through (2.a.6) all prognostic variables are not always affected by an individual sub-step, and thus by implication the "before" and "after" superscript notation denotes the same variable. For example, π (or $\ln \pi$) is not affected by the tendency physics so that π^- and $\overline{\pi}^{n-1}$ can be used interchangeably. Likewise, u, v (and ζ and δ) and T are not affected by the fixers, so $(\hat{\ })^+$ and $(\ )^+$ are interchangeable for them. In addition, u, v (and ζ and δ) and π (or $\ln \pi$) are unaffected by the adjustment physics, so $(\ )^{n+1}$ and $(\ )^+$ are interchangeable for them. By implication then, $(\ )^{n+1}$ and $(\hat{\ })^+$ also become interchangeable for u and v (and ζ and δ). This notational interchangeability should be kept in mind in the discussions in subsequent sections, relating the notations used there to this overview section.

The time step is complete after (2.a.6), at which point the temporal index is decremented and the calculation proceeds back to (2.a.2) for the next time step. In a circular structure such as this, the program code could easily start anywhere, and the temporal index could also be decremented anywhere. In fact, the CCM2 code appears not to start with (2.a.2), but rather to finish up the previous time step by solving (2.a.4), (2.a.5), and (2.a.6) first, at which time the history of state $\left(\overline{\psi}^n\right)$ is recorded if desired. The calculation then proceeds with (2.a.2) and part of (2.a.3a), up to the completion of the spectral transform. At this point the flow of the dynamics is interrupted while the semi-Lagrangian step (2.a.3b) is performed. After this, the dynamics (2.a.3a) is completed by solving the semi-implicit equations, applying the horizontal diffusion and performing the inverse transform. This appears to be the end of the process in the code, and the temporal indices are all shifted down one. However, as mentioned earlier, the time step as described by (2.a.2) through (2.a.6) is actually completed at the beginning of the code.

3. DYNAMICS

a. Hybrid Form of Governing Equations

The hybrid vertical coordinate that has been implemented in CCM2 is described in this section. The hybrid coordinate was developed by Simmons and Strüfing (1981) in order to provide a general framework for a vertical coordinate which is terrain following at the earth's surface, but reduces to a pressure coordinate at some point above the surface. The hybrid coordinate is more general in concept than the modified σ scheme of Sangster (1960), which is used in the GFDL SKYHI model. However, the hybrid coordinate is normally specified in such a way that the two coordinates are identical.

The following description uses the same general development as Simmons and Strüfing (1981), who based their development on the generalized vertical coordinate of Kasahara (1974). A specific form of the coordinate (the hybrid coordinate) is introduced at the latest possible point. The description here differs from Simmons and Strüfing (1981) in allowing for an upper boundary at finite height (nonzero pressure), as in the original development by Kasahara. Such an upper boundary may be required when the equations are solved using vertical finite differences.

Generalized terrain-following vertical coordinates

Deriving the primitive equations in a generalized terrain-following vertical coordinate requires only that certain basic properties of the coordinate be specified. If the surface pressure is π, then we require the generalized coordinate $\eta(p, \pi)$ to satisfy:

1. $\eta(p, \pi)$ is a monotonic function of p.
2. $\eta(\pi, \pi) = 1$
3. $\eta(0, \pi) = 0$
4. $\eta(p_t, \pi) = \eta_t$ where p_t is the top of the model.

The latter requirement provides that the top of the model will be a pressure surface, simplifying the specification of boundary conditions. In the case that $p_t = 0$, the last two requirements are identical and the system reduces to that described in Simmons and Strüfing (1981). The boundary conditions that are required to close the system are:

$$\dot{\eta}(\pi, \pi) = 0, \tag{3.a.1}$$

$$\dot{\eta}(p_t, \pi) = \omega(p_t) = 0. \tag{3.a.2}$$

Given the above description of the coordinate, the continuous system of equations can be written following Kasahara (1974) and Simmons and Strüfing (1981). The prognostic equations are:

$$\frac{\partial \zeta}{\partial t} = \mathbf{k} \cdot \nabla \times (\mathbf{n}/\cos\phi) + F_{\zeta_H}, \tag{3.a.3}$$

$$\frac{\partial \delta}{\partial t} = \nabla \cdot (\mathbf{n}/\cos\phi) - \nabla^2 (E + \Phi) + F_{\delta_H}, \tag{3.a.4}$$

$$\frac{\partial T}{\partial t} = \frac{-1}{a\cos^2\phi}\left[\frac{\partial}{\partial\lambda}(UT) + \cos\phi\frac{\partial}{\partial\phi}(VT)\right] + T\delta - \dot{\eta}\frac{\partial T}{\partial \eta} + \frac{R}{c_p^*}\mathcal{T}\frac{\omega}{p}$$

$$+ Q + F_{T_H} + F_{F_H}, \tag{3.a.5}$$

$$\frac{\partial q}{\partial t} = \frac{-1}{a\cos^2\phi}\left[\frac{\partial}{\partial\lambda}(Uq) + \cos\phi\frac{\partial}{\partial\phi}(Vq)\right] + q\delta - \dot{\eta}\frac{\partial q}{\partial \eta} + S, \tag{3.a.6}$$

$$\frac{\partial \pi}{\partial t} = -\int_1^{\eta_t} \nabla\cdot\left(\frac{\partial p}{\partial \eta}\mathbf{V}\right) d\eta. \tag{3.a.7}$$

The notation follows standard conventions except that the virtual temperature is represented by $\mathcal{T}$ and the following terms have been introduced, with $\mathbf{n} = (n_U, n_V)$:

$$n_U = +(\zeta + f)V - \dot{\eta}\frac{\partial U}{\partial \eta} - R\frac{\mathcal{T}}{p}\frac{1}{a}\frac{\partial p}{\partial\lambda} + F_U\,, \tag{3.a.8}$$

$$n_V = -(\zeta + f)U - \dot{\eta}\frac{\partial V}{\partial \eta} - R\frac{\mathcal{T}}{p}\frac{\cos\phi}{a}\frac{\partial p}{\partial\phi} + F_V\,, \tag{3.a.9}$$

$$E = \frac{U^2 + V^2}{2\cos^2\phi}\,, \tag{3.a.10}$$

$$(U, V) = (u, v)\cos\phi\,, \tag{3.a.11}$$

$$\mathcal{T} = \left[1 + \left(\frac{R_v}{R} - 1\right)q\right]T\,, \tag{3.a.12}$$

$$c_p^* = \left[1 + \left(\frac{c_{p_v}}{c_p} - 1\right)q\right]c_p\,. \tag{3.a.13}$$

The terms F_U, F_V, Q, and S represent the sources and sinks as determined by the tendency physics for momentum (in terms of U and V), temperature, and moisture, respectively. This is discussed in the overview (Section 2) and in detail in Section 4. The terms F_{ζ_H} and F_{δ_H} represent sources due to horizontal diffusion of momentum, while F_{T_H} and F_{F_H} represent sources attributable to horizontal diffusion of temperature and a contribution from frictional heating (see sections on horizontal diffusion and horizontal diffusion correction).

In addition to the prognostic equations, three diagnostic equations are required:

$$\Phi = \Phi_s + R\int_{p(\eta)}^{p(1)} \mathcal{T}\, d\ln p, \tag{3.a.14}$$

$$\dot{\eta}\frac{\partial p}{\partial \eta} = -\frac{\partial p}{\partial t} - \int_{\eta_t}^{\eta} \nabla\cdot\left(\frac{\partial p}{\partial \eta}\mathbf{V}\right) d\eta, \tag{3.a.15}$$

$$\omega = \mathbf{V} \cdot \nabla p - \int_{\eta_t}^{\eta} \nabla \cdot \left(\frac{\partial p}{\partial \eta} \mathbf{V} \right) d\eta. \qquad (3.a.16)$$

Note that the bounds on the vertical integrals are specified as values of η (e.g., η_t, 1) or as functions of p (e.g., p (1), which is the pressure at $\eta = 1$).

Conversion to final form

Equations (3.a.1) – (3.a.16) are the complete set which must be solved by a GCM. However, in order to solve them, the function $\eta(p, \pi)$ must be specified. In advance of actually specifying $\eta(p, \pi)$, the equations will be cast in a more convenient form. Most of the changes to the equations involve simple applications of the chain rule for derivatives, in order to obtain terms that will be easy to evaluate using the predicted variables in the model. For example, terms involving horizontal derivatives of p must be converted to terms involving only $\partial p/\partial \pi$ and horizontal derivatives of π. The former can be evaluated once the function $\eta(p, \pi)$ is specified.

The vertical advection terms in (3.a.5), (3.a.6), (3.a.8), and (3.a.9) may be rewritten as:

$$\dot{\eta} \frac{\partial \psi}{\partial \eta} = \dot{\eta} \frac{\partial p}{\partial \eta} \frac{\partial \psi}{\partial p}, \qquad (3.a.17)$$

since $\dot{\eta} \partial p/\partial \eta$ is given by (3.a.15). Similarly, the first term on the right-hand side of (3.a.15) can be expanded as

$$\frac{\partial p}{\partial t} = \frac{\partial p}{\partial \pi} \frac{\partial \pi}{\partial t}, \qquad (3.a.18)$$

and (3.a.7) invoked to specify $\partial \pi/\partial t$.

The integrals which appear in (3.a.7), (3.a.15), and (3.a.16) can be written more conveniently by expanding the kernel as

$$\nabla \cdot \left(\frac{\partial p}{\partial \eta} \mathbf{V} \right) = \mathbf{V} \cdot \nabla \left(\frac{\partial p}{\partial \eta} \right) + \frac{\partial p}{\partial \eta} \nabla \cdot \mathbf{V} \, . \qquad (3.a.19)$$

The second term in (3.a.19) is easily treated in vertical integrals, since it reduces to an integral in pressure. The first term is expanded to:

$$\begin{aligned} \mathbf{V} \cdot \nabla \left(\frac{\partial p}{\partial \eta} \right) &= \mathbf{V} \cdot \frac{\partial}{\partial \eta} (\nabla p) \\ &= \mathbf{V} \cdot \frac{\partial}{\partial \eta} \left(\frac{\partial p}{\partial \pi} \nabla \pi \right) \end{aligned}$$

$$= \mathbf{V}\cdot\frac{\partial}{\partial\eta}\left(\frac{\partial p}{\partial\pi}\right)\nabla\pi + \mathbf{V}\cdot\frac{\partial p}{\partial\pi}\nabla\left(\frac{\partial\pi}{\partial\eta}\right). \qquad (3.a.20)$$

The second term in (3.a.20) vanishes because $\partial\pi/\partial\eta = 0$, while the first term is easily treated once $\eta(p,\pi)$ is specified. Substituting (3.a.20) into (3.a.19), one obtains:

$$\nabla\cdot\left(\frac{\partial p}{\partial\eta}\mathbf{V}\right) = \frac{\partial}{\partial\eta}\left(\frac{\partial p}{\partial\pi}\right)\mathbf{V}\cdot\nabla\pi + \frac{\partial p}{\partial\eta}\nabla\cdot\mathbf{V}. \qquad (3.a.21)$$

Using (3.a.21) as the kernel of the integral in (3.a.7), (3.a.15), and (3.a.16), one obtains integrals of the form

$$\int\nabla\cdot\left(\frac{\partial p}{\partial\eta}\mathbf{V}\right)d\eta = \int\left[\frac{\partial}{\partial\eta}\left(\frac{\partial p}{\partial\pi}\right)\mathbf{V}\cdot\nabla\pi + \frac{\partial p}{\partial\eta}\nabla\cdot\mathbf{V}\right]d\eta$$

$$= \int\mathbf{V}\cdot\nabla\pi d\left(\frac{\partial p}{\partial\pi}\right) + \int\delta dp. \qquad (3.a.22)$$

The original primitive equations (3.a.3) – (3.a.7), together with (3.a.8), (3.a.9), and (3.a.14) – (3.a.16) can now be rewritten with the aid of (3.a.17), (3.a.18), and (3.a.22).

$$\frac{\partial\zeta}{\partial t} = \mathbf{k}\cdot\nabla\times(\mathbf{n}/\cos\phi) + F_{\zeta_H}\ , \qquad (3.a.23)$$

$$\frac{\partial\delta}{\partial t} = \nabla\cdot(\mathbf{n}/\cos\phi) - \nabla^2(E+\Phi) + F_{\delta_H}\ , \qquad (3.a.24)$$

$$\frac{\partial T}{\partial t} = \frac{-1}{a\cos^2\phi}\left[\frac{\partial}{\partial\lambda}(UT) + \cos\phi\frac{\partial}{\partial\phi}(VT)\right] + T\delta - \dot\eta\frac{\partial p}{\partial\eta}\frac{\partial T}{\partial p} + \frac{R}{c_p^*}\mathcal{T}\frac{\omega}{p}$$

$$+ Q + F_{T_H} + F_{F_H} \qquad (3.a.25)$$

$$\frac{\partial q}{\partial t} = \frac{-1}{a\cos^2\phi}\left[\frac{\partial}{\partial\lambda}(Uq) + \cos\phi\frac{\partial}{\partial\phi}(Vq)\right] + q\delta - \dot\eta\frac{\partial p}{\partial\eta}\frac{\partial q}{\partial p} + S, \qquad (3.a.26)$$

$$\frac{\partial\pi}{\partial t} = -\int_{(\eta_t)}^{(1)}\mathbf{V}\cdot\nabla\pi d\left(\frac{\partial p}{\partial\pi}\right) - \int_{p(\eta_t)}^{p(1)}\delta dp, \qquad (3.a.27)$$

$$n_U = +(\zeta+f)V - \dot\eta\frac{\partial p}{\partial\eta}\frac{\partial U}{\partial p} - R\frac{\mathcal{T}}{a}\frac{1}{p}\frac{\partial p}{\partial\pi}\frac{\partial\pi}{\partial\lambda} + F_U, \qquad (3.a.28)$$

$$n_V = -(\zeta+f)U - \dot\eta\frac{\partial p}{\partial\eta}\frac{\partial V}{\partial p} - R\frac{\mathcal{T}\cos\phi}{a}\frac{1}{p}\frac{\partial p}{\partial\pi}\frac{\partial\pi}{\partial\phi} + F_V, \qquad (3.a.29)$$

$$\Phi = \Phi_s + R\int_{p(\eta)}^{p(1)} \mathcal{T} d\ln p, \tag{3.a.30}$$

$$\dot{\eta}\frac{\partial p}{\partial \eta} = \frac{\partial p}{\partial \pi}\left[\int_{(\eta_t)}^{(1)} \mathbf{V}\cdot\nabla\pi d\left(\frac{\partial p}{\partial \pi}\right) + \int_{p(\eta_t)}^{p(1)} \delta dp\right]$$

$$-\int_{(\eta_t)}^{(\eta)} \mathbf{V}\cdot\nabla\pi d\left(\frac{\partial p}{\partial \pi}\right) - \int_{p(\eta_t)}^{p(\eta)} \delta dp, \tag{3.a.31}$$

$$\omega = \frac{\partial p}{\partial \pi}\mathbf{V}\cdot\nabla\pi - \int_{(\eta_t)}^{(\eta)} \mathbf{V}\cdot\nabla\pi d\left(\frac{\partial p}{\partial \pi}\right) - \int_{p(\eta_t)}^{p(\eta)} \delta dp. \tag{3.a.32}$$

Once $\eta(p,\pi)$ is specified, then $\partial p/\partial\pi$ can be determined and (3.*a*.23) – (3.*a*.32) can be solved in a GCM.

In the actual definition of the hybrid coordinate, it is not necessary to specify $\eta(p,\pi)$ explicitly, since (3.*a*.23) – (3.*a*.32) only requires that p and $\partial p/\partial\pi$ be determined. It is sufficient to specify $p(\eta,\pi)$ and to let η be defined implicitly. This is will be done in a later section. In the case that $p(\eta,\pi) = \sigma\pi$ and $\eta_t = 0$, (3.*a*.23) – (3.*a*.32) can be reduced to the set of equations solved by CCM1.

Continuous equations using $\partial\ln(\pi)/\partial t$

In practice, the solutions generated by solving the above equations are excessively noisy. This problem appears to arise from aliasing problems in the hydrostatic equation (3.*a*.30). The $\ln p$ integral introduces a high order nonlinearity which enters directly into the divergence equation (3.*a*.24). Large gravity waves are generated in the vicinity of steep orography, such as in the Pacific Ocean west of the Andes.

The equations given above, using π as a prognostic variable, may be easily converted to equations using $\Pi = \ln(\pi)$, resulting in the hydrostatic equation becoming only quadratically nonlinear except for moisture contributions to virtual temperature. Since the spectral transform method will be used to solve the equations, gradients will be obtained during the transform from wave to grid space. Outside of the prognostic equation for Π, all terms involving $\nabla\pi$ will then appear as $\pi\nabla\Pi$.

Equations (3.*a*.23) – (3.*a*.32) become:

$$\frac{\partial\zeta}{\partial t} = \mathbf{k}\cdot\nabla\times(\mathbf{n}/\cos\phi) + F_{\zeta_H}, \tag{3.a.33}$$

$$\frac{\partial\delta}{\partial t} = \nabla\cdot(\mathbf{n}/\cos\phi) - \nabla^2(E+\Phi) + F_{\delta_H}, \tag{3.a.34}$$

$$\frac{\partial T}{\partial t} = \frac{-1}{a\cos^2\phi}\left[\frac{\partial}{\partial\lambda}(UT) + \cos\phi\frac{\partial}{\partial\phi}(VT)\right] + T\delta - \dot{\eta}\frac{\partial p}{\partial\eta}\frac{\partial T}{\partial p} + \frac{R}{c_p^*}\mathcal{T}\frac{\omega}{p}$$

$$+ Q + F_{T_H} + F_{F_H}, \tag{3.a.35}$$

$$\frac{\partial q}{\partial t} = \frac{-1}{a\cos^2\phi}\left[\frac{\partial}{\partial\lambda}(Uq) + \cos\phi\frac{\partial}{\partial\phi}(Vq)\right] + q\delta - \dot{\eta}\frac{\partial p}{\partial\eta}\frac{\partial q}{\partial p} + S\,, \tag{3.a.36}$$

$$\frac{\partial\Pi}{\partial t} = -\int_{(\eta_t)}^{(1)}\mathbf{V}\cdot\nabla\Pi d\left(\frac{\partial p}{\partial\pi}\right) - \frac{1}{\pi}\int_{p(\eta_t)}^{p(1)}\delta dp, \tag{3.a.37}$$

$$n_U = +(\zeta+f)V - \dot{\eta}\frac{\partial p}{\partial\eta}\frac{\partial U}{\partial p} - R\frac{\mathcal{T}}{a}\frac{\pi}{p}\frac{\partial p}{\partial\pi}\frac{\partial\Pi}{\partial\lambda} + F_U, \tag{3.a.38}$$

$$n_V = -(\zeta+f)U - \dot{\eta}\frac{\partial p}{\partial\eta}\frac{\partial V}{\partial p} - R\frac{\mathcal{T}\cos\phi}{a}\frac{\pi}{p}\frac{\partial p}{\partial\pi}\frac{\partial\Pi}{\partial\phi} + F_V, \tag{3.a.39}$$

$$\Phi = \Phi_s + R\int_{p(\eta)}^{p(1)}\mathcal{T}d\ln p, \tag{3.a.40}$$

$$\dot{\eta}\frac{\partial p}{\partial\eta} = \frac{\partial p}{\partial\pi}\left[\int_{(\eta_t)}^{(1)}\pi\mathbf{V}\cdot\nabla\Pi d\left(\frac{\partial p}{\partial\pi}\right) + \int_{p(\eta_t)}^{p(1)}\delta dp\right]$$

$$-\int_{(\eta_t)}^{(\eta)}\pi\mathbf{V}\cdot\nabla\Pi d\left(\frac{\partial p}{\partial\pi}\right) - \int_{p(\eta_t)}^{p(\eta)}\delta dp, \tag{3.a.41}$$

$$\omega = \frac{\partial p}{\partial\pi}\pi\mathbf{V}\cdot\nabla\Pi - \int_{(\eta_t)}^{(\eta)}\pi\mathbf{V}\cdot\nabla\Pi d\left(\frac{\partial p}{\partial\pi}\right) - \int_{p(\eta_t)}^{p(\eta)}\delta dp. \tag{3.a.42}$$

The above equations reduce to the standard σ equations used in CCM1 if $\eta = \sigma$ and $\eta_t = 0$. (Note that in this case $\partial p/\partial\pi = p/\pi = \sigma$.)

Semi-implicit formulation

The model described by (3.*a*.33) – (3.*a*.42), without the horizontal diffusion terms, together with boundary conditions (3.*a*.1) and (3.*a*.2), is integrated in time using the semi-implicit leapfrog scheme described below. The semi-implicit form of the time differencing will be applied to (3.*a*.34) and (3.*a*.35) without the horizontal diffusion sources, and to (3.*a*.37). In order to derive the semi-implicit form, one must linearize these equations about a reference state. Isolating the terms that will have their linear parts treated

implicitly, the prognostic equations (3.*a*.33), (3.*a*.34), and (3.*a*.37) may be rewritten as:

$$\frac{\partial \delta}{\partial t} = -RT\nabla^2 \ln p - \nabla^2 \Phi + X_1, \tag{3.a.43}$$

$$\frac{\partial T}{\partial t} = +\frac{R}{c_p^*} \mathcal{T} \frac{\omega}{p} - \dot{\eta} \frac{\partial p}{\partial \eta} \frac{\partial T}{\partial p} + Y_1, \tag{3.a.44}$$

$$\frac{\partial \Pi}{\partial t} = -\frac{1}{\pi} \int_{p(\eta_t)}^{p(1)} \delta dp + Z_1, \tag{3.a.45}$$

where X_1, Y_1, Z_1 are the remaining nonlinear terms not explicitly written in (3.*a*.43) – (3.*a*.45). The terms involving Φ and ω may be expanded into vertical integrals using (3.*a*.40) and (3.*a*.42), while the $\nabla^2 \ln p$ term can be converted to $\nabla^2 \Pi$, giving:

$$\frac{\partial \delta}{\partial t} = -RT\frac{\pi}{p}\frac{\partial p}{\partial \pi}\nabla^2 \Pi - R\nabla^2 \int_{p(\eta)}^{p(1)} T d\ln p \; + X_2, \tag{3.a.46}$$

$$\frac{\partial T}{\partial t} = -\frac{R}{c_p}\frac{T}{p}\int_{p(\eta_t)}^{p(\eta)} \delta dp - \left[\frac{\partial p}{\partial \pi}\int_{p(\eta_t)}^{p(1)} \delta dp - \int_{p(\eta_t)}^{p(\eta)} \delta dp\right] \frac{\partial T}{\partial p} + Y_2, \tag{3.a.47}$$

$$\frac{\partial \Pi}{\partial t} = -\frac{1}{\pi}\int_{p(\eta_t)}^{p(1)} \delta dp + Z_2. \tag{3.a.48}$$

Once again, only terms that will be linearized have been explicitly represented in (3.*a*.46) – (3.*a*.48), and the remaining terms are included in X_2, Y_2, and Z_2. Anticipating the linearization, $\mathcal{T}$ and c_p^* have been replaced by T and c_p in (3.*a*.46) and (3.*a*.47). Furthermore, the virtual temperature corrections are included with the other nonlinear terms.

In order to linearize (3.*a*.46) – (3.*a*.48), one specifies a reference state for temperature and pressure, then expands the equations about the reference state:

$$T = T^r + T', \tag{3.a.49}$$

$$\pi = \pi^r + \pi', \tag{3.a.50}$$

$$p = p^r(\eta, \pi^r) + p'. \tag{3.a.51}$$

In the special case that $p(\eta, \pi) = \sigma\pi$, (3.*a*.46) – (3.*a*.48) can be converted into equations involving only $\Pi = \ln \pi$ instead of p, and (3.*a*.50) and (3.*a*.51) are not required. This is a major difference between the hybrid coordinate scheme being developed here and the σ coordinate scheme in CCM1.

Expanding (3.*a*.46) – (3.*a*.48) about the reference state (3.*a*.49) – (3.*a*.51) and retaining only the linear terms explicitly, one obtains:

$$\frac{\partial \delta}{\partial t} = -R\nabla^2 \left[T^r \frac{\pi^r}{p^r} \left(\frac{\partial p}{\partial \pi} \right)^r \Pi + \int_{p^r(\eta)}^{p^r(1)} T' d \ln p^r + \int_{p'(\eta)}^{p'(1)} \frac{T^r}{p^r} dp' \right] + X_3, \qquad (3.a.52)$$

$$\frac{\partial T}{\partial t} = -\frac{R}{c_p} \frac{T^r}{p^r} \int_{p^r(\eta_t)}^{p^r(\eta)} \delta dp^r - \left[\left(\frac{\partial p}{\partial \pi} \right)^r \int_{p^r(\eta_t)}^{p^r(1)} \delta dp^r - \int_{p^r(\eta_t)}^{p^r(\eta)} \delta dp^r \right] \frac{\partial T^r}{\partial p^r} + Y_3, \qquad (3.a.53)$$

$$\frac{\partial \Pi}{\partial t} = -\frac{1}{\pi^r} \int_{p^r(\eta_t)}^{p^r(1)} \delta dp^r + Z_3. \qquad (3.a.54)$$

The semi-implicit time differencing scheme treats the linear terms in (3.*a*.52) – (3.*a*.54) by averaging in time. The last integral in (3.*a*.52) is reduced to purely linear form by the relation

$$dp' = \pi' d \left(\frac{\partial p}{\partial \pi} \right)^r + x\,. \qquad (3.a.55)$$

In the hybrid coordinate described below, p is a linear function of π, so x above is zero.

We will assume that centered differences are to be used for the nonlinear terms, and the linear terms are to be treated implicitly by averaging the previous and next time steps. Finite differences are used in the vertical, and are described in the following sections. At this stage only some very general properties of the finite difference representation must be specified. A layering structure is assumed in which field values are predicted on K layer midpoints denoted by an integer index, η_k. The interface between η_k and η_{k+1} is denoted by a half-integer index, $\eta_{k+1/2}$. The model top is at $\eta_{1/2} = \eta_t$, and the earth's surface is at $\eta_{K+1/2} = 1$. It is further assumed that vertical integrals may be written as a matrix (of order K) times a column vector representing the values of a field at the η_k grid points in the vertical. The column vectors representing a vertical column of grid points will be denoted by underbars, the matrices will be denoted by bold-faced capital letters, and superscript T will denote the vector transpose.

The finite difference forms of (3.*a*.52) – (3.*a*.54) may then be written down as:

$$\begin{aligned} \underline{\delta}^{n+1} = {} & \underline{\delta}^{n-1} + 2\Delta t \underline{X}^n \\ & - 2\Delta t R \underline{b}^r \nabla^2 \left(\frac{\Pi^{n-1} + \Pi^{n+1}}{2} - \Pi^n \right) \\ & - 2\Delta t R \mathbf{H}^r \nabla^2 \left(\frac{(\underline{T}')^{n-1} + (\underline{T}')^{n+1}}{2} - (\underline{T}')^n \right) \\ & - 2\Delta t R \underline{h}^r \nabla^2 \left(\frac{\Pi^{n-1} + \Pi^{n+1}}{2} - \Pi^n \right), \end{aligned} \qquad (3.a.56)$$

$$\underline{T}^{n+1} = \underline{T}^{n-1} + 2\Delta t \underline{Y}^n - 2\Delta t \mathbf{D}^r \left(\frac{\underline{\delta}^{n-1} + \underline{\delta}^{n+1}}{2} - \underline{\delta}^n \right), \tag{3.a.57}$$

$$\Pi^{n+1} = \Pi^{n-1} + 2\Delta t Z^n - 2\Delta t \left(\frac{\underline{\delta}^{n-1} + \underline{\delta}^{n+1}}{2} - \underline{\delta}^n \right)^T \underline{\Delta p}^r, \tag{3.a.58}$$

where $()^n$ denotes a time varying value at time step n. The quantities $\underline{X}^n, \underline{Y}^n$, and Z^n are defined so as to complete the right-hand sides of (3.*a*.43) – (3.*a*.45). The components of $\underline{\Delta p}^r$ are given by $\Delta p_k^r = p_{k+\frac{1}{2}}^r - p_{k-\frac{1}{2}}^r$. This definition of the vertical difference operator Δ will be used in subsequent equations. The reference matrices $\mathbf{H}^r$ and $\mathbf{D}^r$, and the reference column vectors $\underline{b}^r$ and $\underline{h}^r$, depend on the precise specification of the vertical coordinate and will be defined later.

Energy conservation

We shall impose a requirement on the vertical finite differences of the model that they conserve the global integral of total energy *in the absence of sources and sinks.* We need to derive equations for kinetic and internal energy in order to impose this constraint. The momentum equations (more painfully, the vorticity and divergence equations) without the F_U, F_V, F_{ζ_H} and F_{δ_H} contributions, can be combined with the continuity equation

$$\frac{\partial}{\partial t}\left(\frac{\partial p}{\partial \eta}\right) + \nabla \cdot \left(\frac{\partial p}{\partial \eta}\mathbf{V}\right) + \frac{\partial}{\partial \eta}\left(\frac{\partial p}{\partial \eta}\dot{\eta}\right) = 0 \tag{3.a.59}$$

to give an equation for the rate of change of kinetic energy:

$$\frac{\partial}{\partial t}\left(\frac{\partial p}{\partial \eta}E\right) = -\nabla \cdot \left(\frac{\partial p}{\partial \eta}E\mathbf{V}\right) - \frac{\partial}{\partial \eta}\left(\frac{\partial p}{\partial \eta}E\dot{\eta}\right)$$

$$- \frac{RT}{p}\frac{\partial p}{\partial \eta}\mathbf{V} \cdot \nabla p - \frac{\partial p}{\partial \eta}\mathbf{V} \cdot \nabla \Phi \,. \tag{3.a.60}$$

The first two terms on the right-hand side of (3.*a*.60) are transport terms. The horizontal integral of the first (horizontal) transport term should be zero, and it is relatively straightforward to construct horizontal finite difference schemes that ensure this. For spectral models, the integral of the horizontal transport term will not vanish in general, but we shall ignore this problem.

The vertical integral of the second (vertical) transport term on the right-hand side of (3.*a*.60) should vanish. Since this term is obtained from the vertical advection terms for momentum, which will be finite differenced, we can construct a finite difference operator that will ensure that the vertical integral vanishes.

The vertical advection terms are the product of a vertical velocity ($\dot{\eta}\partial p/\partial \eta$) and the vertical derivative of a field ($\partial \psi/\partial p$). The vertical velocity is defined in terms of

vertical integrals of fields (3.a.41), which are naturally taken to interfaces. The vertical derivatives are also naturally taken to interfaces, so the product is formed there, and then adjacent interface values of the products are averaged to give a midpoint value. It is the definition of the average that must be correct in order to conserve kinetic energy under vertical advection in (3.a.60). The derivation will be omitted here, the resulting vertical advection terms are of the form:

$$\left(\dot{\eta}\frac{\partial p}{\partial \eta}\frac{\partial \psi}{\partial p}\right)_k = \frac{1}{2\Delta p_k}\left[\left(\dot{\eta}\frac{\partial p}{\partial \eta}\right)_{k+1/2}(\psi_{k+1}-\psi_k)+\left(\dot{\eta}\frac{\partial p}{\partial \eta}\right)_{k-1/2}(\psi_k-\psi_{k-1})\right], \quad (3.a.61)$$

$$\Delta p_k = p_{k+1/2} - p_{k-1/2}. \quad (3.a.62)$$

The choice of definitions for the vertical velocity at interfaces is not crucial to the energy conservation (although not completely arbitrary), and we shall defer its definition until later. The vertical advection of temperature is not required to use (3.a.61) in order to conserve mass or energy. Other constraints can be imposed that result in different forms for temperature advection, but we will simply use (3.a.61) in the system described below.

The last two terms in (3.a.60) contain the conversion between kinetic and internal (potential) energy and the form drag. Neglecting the transport terms, under assumption that global integrals will be taken, noting that $\nabla p = \frac{\pi}{p}\frac{\partial p}{\partial \pi}\nabla\Pi$, and substituting for the geopotential using (3.a.40), (3.a.60) can be written as:

$$\frac{\partial}{\partial t}\left(\frac{\partial p}{\partial \eta}E\right) = -RT\frac{\partial p}{\partial \eta}\mathbf{V}\cdot\left(\frac{\pi}{p}\frac{\partial p}{\partial \pi}\nabla\Pi\right) - \frac{\partial p}{\partial \eta}\mathbf{V}\cdot\nabla\Phi_s - \frac{\partial p}{\partial \eta}\mathbf{V}\cdot\nabla\int_{p(\eta)}^{p(1)} RT\,d\ln p + \ldots \quad (3.a.63)$$

The second term on the right-hand side of (3.a.63) is a source (form drag) term that can be neglected as we are only interested in internal conservation properties. The last term on the right-hand side of (3.a.63) can be rewritten as

$$\frac{\partial p}{\partial \eta}\mathbf{V}\cdot\nabla\int_{p(\eta)}^{p(1)} RT\,d\ln p = \nabla\cdot\left\{\frac{\partial p}{\partial \eta}\mathbf{V}\int_{p(\eta)}^{p(1)} RT\,d\ln p\right\} - \nabla\cdot\left(\frac{\partial p}{\partial \eta}\mathbf{V}\right)\int_{p(\eta)}^{p(1)} RT\,d\ln p. \quad (3.a.64)$$

The global integral of the first term on the right-hand side of (3.a.64) is obviously zero, so that (3.a.63) can now be written as:

$$\frac{\partial}{\partial t}\left(\frac{\partial p}{\partial \eta}E\right) = -RT\frac{\partial p}{\partial \eta}\mathbf{V}\cdot\left(\frac{\pi}{p}\frac{\partial p}{\partial \pi}\nabla\Pi\right)$$
$$+\nabla\cdot\left(\frac{\partial p}{\partial \eta}\mathbf{V}\right)\int_{p(\eta)}^{p(1)} RT\,d\ln p + \ldots \qquad (3.a.65)$$

We now turn to the internal energy equation, obtained by combining the thermodynamic equation (3.a.35), without the Q, F_{T_H}, and F_{F_H} terms, and the continuity equation (3.a.59):

$$\frac{\partial}{\partial t}\left(\frac{\partial p}{\partial \eta}c_p^* T\right) = -\nabla\cdot\left(\frac{\partial p}{\partial \eta}c_p^* T\mathbf{V}\right) - \frac{\partial}{\partial \eta}\left(\frac{\partial p}{\partial \eta}c_p^* T\dot{\eta}\right)$$
$$+RT\frac{\partial p}{\partial \eta}\frac{\omega}{p}. \qquad (3.a.66)$$

As in (3.a.60), the first two terms on the right-hand side are advection terms that can be neglected under global integrals. Using (3.a.16), (3.a.66) can be written as:

$$\frac{\partial}{\partial t}\left(\frac{\partial p}{\partial \eta}c_p^* T\right) = RT\frac{\partial p}{\partial \eta}\mathbf{V}\cdot\left(\frac{\pi}{p}\frac{\partial p}{\partial \pi}\nabla\Pi\right)$$
$$-RT\frac{\partial p}{\partial \eta}\frac{1}{p}\int_{\eta_t}^{\eta}\nabla\cdot\left(\frac{\partial p}{\partial \eta}\mathbf{V}\right)d\eta + \ldots \qquad (3.a.67)$$

The rate of change of total energy due to internal processes is obtained by adding (3.a.65) and (3.a.67) and must vanish. The first terms on the right-hand side of (3.a.65) and (3.a.67) obviously cancel in the continuous form. When the equations are discretized in the vertical, the terms will still cancel, providing that the same definition is used for $(1/p\ \partial p/\partial \pi)_k$ in the nonlinear terms of the vorticity and divergence equations (3.a.38) and (3.a.39), and in the ω term of (3.a.35) and (3.a.42).

The second terms on the right-hand side of (3.a.65) and (3.a.67) must also cancel in the global mean. This cancellation is enforced locally in the horizontal on the column integrals of (3.a.65) and (3.a.67), so that we require:

$$\int_{\eta_t}^{1}\left\{\nabla\cdot\left(\frac{\partial p}{\partial \eta}\mathbf{V}\right)\int_{p(\eta)}^{p(1)} RT\,d\ln p\right\}d\eta$$
$$=\int_{\eta_t}^{1}\left\{RT\frac{\partial p}{\partial \eta}\frac{1}{p}\int_{\eta_t}^{\eta}\nabla\cdot\left(\frac{\partial p}{\partial \eta'}\mathbf{V}\right)d\eta'\right\}d\eta. \qquad (3.a.68)$$

The inner integral on the left-hand side of (3.a.68) is derived from the hydrostatic equation (3.a.40), which we shall approximate as

$$\Phi_k = \Phi_s + R\sum_{\ell=k}^{K} H_{k\ell}\mathcal{T}_\ell,$$

$$= \Phi_s + R\sum_{\ell=1}^{K} H_{k\ell}\mathcal{T}_\ell, \tag{3.a.69}$$

$$\underline{\Phi} = \Phi_s\underline{1} + R\mathbf{H}\underline{\mathcal{T}}, \tag{3.a.70}$$

where $H_{k\ell} = 0$ for $\ell < k$. The quantity $\underline{1}$ is defined to be the unit vector. The inner integral on the right-hand side of (3.a.68) is derived from the vertical velocity equation (3.a.42), which we shall approximate as

$$\left(\frac{\omega}{p}\right)_k = \left(\frac{\pi}{p}\frac{\partial p}{\partial \pi}\right)_k \mathbf{V}_k\cdot\nabla\Pi$$

$$-\sum_{\ell=1}^{K} C_{k\ell}\left[\delta_\ell\Delta p_\ell + \pi\left(\mathbf{V}_\ell\cdot\nabla\Pi\right)\Delta\left(\frac{\partial p}{\partial\pi}\right)_\ell\right], \tag{3.a.71}$$

where $C_{k\ell} = 0$ for $\ell > k$, and $C_{k\ell}$ is included as an approximation to $1/p_k$ for $\ell \le k$ and the symbol Δ is similarly defined as in (3.a.62). $C_{k\ell}$ will be determined by requiring that the finite difference analog to (3.a.68) be satisfied. Using (3.a.69) and (3.a.71), the finite difference analog of (3.a.68) is

$$\sum_{k=1}^{K}\left\{\frac{1}{\Delta\eta_k}\left[\delta_k\Delta p_k + \pi\left(\mathbf{V}_k\cdot\nabla\Pi\right)\Delta\left(\frac{\partial p}{\partial\pi}\right)_k\right] R\sum_{\ell=1}^{K} H_{k\ell}\mathcal{T}_\ell\right\}\Delta\eta_k$$

$$= \sum_{k=1}^{K}\left\{R\mathcal{T}_k\frac{\Delta p_k}{\Delta\eta_k}\sum_{\ell=1}^{K} C_{k\ell}\left[\delta_\ell\Delta p_\ell + \pi\left(\mathbf{V}_\ell\cdot\nabla\Pi\right)\Delta\left(\frac{\partial p}{\partial\pi}\right)_\ell\right]\right\}\Delta\eta_k, \tag{3.a.72}$$

where we have used the relation $\nabla\cdot\mathbf{V}(\partial p/\partial\eta)_k = [\delta_k\Delta p_k + \pi\left(\mathbf{V}_k\cdot\nabla\Pi\right)\Delta\left(\partial p/\partial\pi\right)_k]/\Delta\eta_k$ (see 3.a.22). We can now combine the sums in (3.a.72) and simplify to give

$$\sum_{k=1}^{K}\sum_{\ell=1}^{K}\left\{\left[\delta_k\Delta p_k + \pi\left(\mathbf{V}_k\cdot\nabla\Pi\right)\Delta\left(\frac{\partial p}{\partial\pi}\right)_k\right] H_{k\ell}\mathcal{T}_\ell\right\}$$

$$= \sum_{k=1}^{K}\sum_{\ell=1}^{K}\left\{\left[\delta_\ell\Delta p_\ell + \pi\left(\mathbf{V}_\ell\cdot\nabla\Pi\right)\Delta\left(\frac{\partial p}{\partial\pi}\right)_\ell\right]\Delta p_k C_{k\ell}\mathcal{T}_k\right\}. \tag{3.a.73}$$

Interchanging the indexes on the left-hand side of (3.a.73) will obviously result in identical expressions if we require that

$$C_{k\ell} = H_{\ell k}/\Delta p_k. \tag{3.a.74}$$

Given the definitions of vertical integrals in (3.*a*.70) and (3.*a*.71) and of vertical advection in (3.*a*.61) and (3.*a*.62) the model will conserve energy as long as we require that $\mathbf{C}$ and $\mathbf{H}$ satisfy (3.*a*.74). We are, of course, still neglecting lack of conservation due to the truncation of the horizontal spherical harmonic expansions.

Horizontal diffusion

CCM2 contains a horizontal diffusion term for T, ζ, and δ to prevent spectral blocking and to provide reasonable kinetic energy spectra. The horizontal diffusion operator in CCM2 is also used to ensure that the CFL condition is not violated in the upper layers of the model. The horizontal diffusion is a linear ∇^2 form on η surfaces in the top few levels of the model and a linear ∇^4 form with a partial correction to pressure surfaces for temperature elsewhere.

In the top few model levels, the ∇^2 form of the horizontal diffusion is given by

$$F_{\zeta_H} = K^{(2)} \left[\nabla^2 (\zeta + f) + 2(\zeta + f)/a^2\right], \tag{3.a.75}$$

$$F_{\delta_H} = K^{(2)} \left[\nabla^2 \delta + 2(\delta/a^2)\right], \tag{3.a.76}$$

$$F_{T_H} = K^{(2)} \nabla^2 T. \tag{3.a.77}$$

Since these terms are linear, they are easily calculated in spectral space. The undifferentiated correction term is added to the vorticity and divergence diffusion operators to prevent damping of uniform ($n = 1$) rotations (Orszag, 1974; Bourke *et al.*, 1977). It is important to note that the ∇^2 form of the horizontal diffusion is applied *only* to pressure surfaces in the standard model configuration.

The horizontal diffusion operator is better applied to pressure surfaces than to terrain-following surfaces (applying the operator on isentropic surfaces would be still better). Although the governing system of equations derived above is designed to reduce to pressure surfaces above some level, problems can still occur from diffusion along the lower surfaces. Partial correction to pressure surfaces of harmonic horizontal diffusion ($\partial\xi/\partial t = K\nabla^2\xi$) can be included using the relations:

$$\begin{aligned} \nabla_p \xi &= \nabla_\eta \xi - p\frac{\partial \xi}{\partial p}\nabla_\eta \ln p \\ \nabla_p^2 \xi &= \nabla_\eta^2 \xi - p\frac{\partial \xi}{\partial p}\nabla_\eta^2 \ln p - 2\nabla_\eta\left(\frac{\partial \xi}{\partial p}\right)\cdot\nabla_\eta p + \frac{\partial^2 \xi}{\partial^2 p}\nabla_\eta^2 p. \end{aligned} \tag{3.a.78}$$

Retaining only the first two terms above gives a correction to the η surface diffusion which involves only a vertical derivative and the Laplacian of log surface pressure,

$$\nabla_p^2 \xi = \nabla_\eta^2 \xi - \pi \frac{\partial \xi}{\partial p} \frac{\partial p}{\partial \pi} \nabla^2 \Pi + \ldots \tag{3.a.79}$$

Similarly, biharmonic diffusion can be partially corrected to pressure surfaces as:

$$\nabla_p^4 \xi = \nabla_\eta^4 \xi - \pi \frac{\partial \xi}{\partial p} \frac{\partial p}{\partial \pi} \nabla^4 \Pi + \ldots \tag{3.a.80}$$

The bi-harmonic ∇^4 form of the diffusion operator is applied at all other levels (generally throughout the troposphere) as

$$F_{\zeta_H} = -K^{(4)} \left[\nabla^4 (\zeta + f) - (\zeta + f) \left(2/a^2 \right)^2 \right], \tag{3.a.81}$$

$$F_{\delta_H} = -K^{(4)} \left[\nabla^4 \delta - \delta (2/a^2)^2 \right], \tag{3.a.82}$$

$$F_{T_H} = -K^{(4)} \left[\nabla^4 T - \pi \frac{\partial T}{\partial p} \frac{\partial p}{\partial \pi} \nabla^4 \Pi \right]. \tag{3.a.83}$$

The second term in F_{T_H} consists of the leading term in the transformation of the ∇^4 operator to pressure surfaces. It is included to offset partially a spurious diffusion of T over mountains. As with the ∇^2 form, the ∇^4 operator can be conveniently calculated in spectral space. The correction term is then completed after transformation of T and $\nabla^4 \Pi$ back to grid–point space. As with the ∇^2 form, an undifferentiated term is added to the vorticity and divergence diffusion operators to prevent damping of uniform rotations.

Finite difference equations

It will be assumed that the governing equations will be solved using the spectral method in the horizontal, so that only the vertical and time differences are presented here. The schematic dynamics term Γ in equation $(2.a.3a)$ includes horizontal diffusion of $T, (\zeta + f)$, and δ. Only T has the leading term correction to pressure surfaces. Thus, equations that include the terms in this time split sub-step are of the form

$$\frac{\partial \psi}{\partial t} = \mathrm{Dyn}\,(\psi) + (-1)^i K^{(2i)} \nabla_\eta^{2i} \psi\,, \tag{3.a.84}$$

for $(\zeta + f)$ and δ, and

$$\frac{\partial T}{\partial t} = \mathrm{Dyn}\,(T) + (-1)^i K^{(2i)} \left\{ \nabla_\eta^{2i} T - \pi \frac{\partial T}{\partial p} \frac{\partial p}{\partial \pi} \nabla^{2i} \Pi \right\}, \tag{3.a.85}$$

where $i = 1$ in the top few model levels and $i = 2$ elsewhere (generally within the troposphere). These equations are further subdivided into time split components:

$$\psi^{n+1} = \psi^{n-1} + \mathrm{Dyn}\left(\psi^{n+1}, \psi^n, \psi^{n-1}\right) , \tag{3.a.86}$$

$$\psi^* = \psi^{n+1} + (-1)^i K^{2i} \nabla_\eta^{2i} \left(\psi^{*n+1}\right) , \tag{3.a.87}$$

$$\hat{\psi}^{n+1} = \psi^* , \tag{3.a.88}$$

for $(\zeta + f)$ and δ, and

$$T^{n+1} = T^{n-1} + \mathrm{Dyn}\left(T^{n+1}, T^n, T^{n-1}\right) , \tag{3.a.89}$$

$$T^* = T^{n+1} + (-1)^i K^{(2i)} \nabla^{2i} \eta \left(T^*\right) , \tag{3.a.90}$$

$$\hat{T}^{n+1} = T^* + (-1)^i K^{(2i)} \pi \frac{\partial T^*}{\partial p} \frac{\partial p}{\partial \pi} \nabla^{2i} \Pi , \tag{3.a.91}$$

for T, where in the standard model i only takes the value 2 in (3.a.91). The first step from $(\ )^{n-1}$ to $(\ )^{n+1}$ includes the transformation to spectral coefficients. The second step from $(\ )^{n+1}$ to $(\hat{\ })^{n+1}$ for δ and ζ, or $(\ )^{n+1}$ to $(\ )^*$ for T, is done on the spectral coefficients, and the final step from $(\ )^*$ to $(\hat{\ })^{n+1}$ for T is done after the inverse transform to the grid point representation.

The following finite-difference description details only the forecast given by (3.a.86) and (3.a.89). In what follows we use $(\ )^{n-1}$ instead of $\overline{(\ )}^{n-1}$ from (2.a.8). This notation is convenient for discussing the dynamical equations in isolation. The finite-difference form of the forecast equation for water vapor will be presented later in Section 3c. The general structure of the complete finite difference equations is determined by the semi-implicit time differencing and the energy conservation properties described above. In order to complete the specification of the finite differencing, we require a definition of the vertical coordinate. The actual specification of the generalized vertical coordinate takes advantage of the structure of the equations (3.a.33)$-$(3.a.42). The equations can be finite-differenced in the vertical and, in time, without having to know the value of η anywhere. The quantities that must be known are p and $\partial p/\partial \pi$ at the grid points. Therefore the coordinate is defined implicitly through the relation:

$$p(\eta, \pi) = A(\eta) p_0 + B(\eta) \pi , \tag{3.a.92}$$

which gives

$$\frac{\partial p}{\partial \pi} = B(\eta) . \tag{3.a.93}$$

A set of levels η_k may be specified by specifying A_k and B_k, and difference forms of (3.a.33) $-$ (3.a.42) may be derived.

The finite difference forms of the Dyn operator (3.a.33) $-$ (3.a.42), including semi-implicit time integration are:

$$\underline{\zeta}^{n+1} = \underline{\zeta}^{n-1} + 2\Delta t \mathbf{k} \cdot \nabla \times \left(\underline{\mathbf{n}}^n / \cos\phi\right) , \tag{3.a.94}$$

$$\underline{\delta}^{n+1} = \underline{\delta}^{n-1} + 2\Delta t \left[\nabla \cdot (\underline{\mathbf{n}}^n / \cos\phi) - \nabla^2 \left(\underline{E}^n + \Phi_s \underline{1} + R\mathbf{H}^n (\underline{T}')^n\right)\right]$$
$$- 2\Delta t R\mathbf{H}^r \nabla^2 \left(\frac{(\underline{T}')^{n-1} + (\underline{T}')^{n+1}}{2} - (\underline{T}')^n\right)$$
$$- 2\Delta t R \left(\underline{b}^r + \underline{h}^r\right) \nabla^2 \left(\frac{\Pi^{n-1} + \Pi^{n+1}}{2} - \Pi^n\right), \qquad (3.a.95)$$

$$(\underline{T}')^{n+1} = (\underline{T}')^{n-1} - 2\Delta t \left[\frac{1}{a\cos^2\phi}\frac{\partial}{\partial\lambda}\left(\underline{UT}'\right)^n + \frac{1}{a\cos\phi}\frac{\partial}{\partial\phi}\left(\underline{VT}'\right)^n - \underline{\Gamma}^n\right]$$
$$- 2\Delta t \mathbf{D}^r \left(\frac{\underline{\delta}^{n-1} + \underline{\delta}^{n+1}}{2} - \underline{\delta}^n\right), \qquad (3.a.96)$$

$$\Pi^{n+1} = \Pi^{n-1} - 2\Delta t \frac{1}{\pi^n}\left((\underline{\delta}^n)^T \underline{\Delta p}^n + (\underline{\mathbf{V}}^n)^T \nabla\Pi^n \pi^n \underline{\Delta B}\right)$$
$$- 2\Delta t \left(\frac{\underline{\delta}^{n-1} + \underline{\delta}^{n+1}}{2} - \underline{\delta}^n\right)^T \frac{1}{\pi^r}\underline{\Delta p}^r, \qquad (3.a.97)$$

$$(n_U)_k = (\zeta_k + f) V_k - R\mathcal{T}_k \left(\frac{1}{p}\frac{\partial p}{\partial \pi}\right)_k \pi \frac{1}{a}\frac{\partial \Pi}{\partial \lambda}$$
$$- \frac{1}{2\Delta p_k}\left[\left(\dot{\eta}\frac{\partial p}{\partial \eta}\right)_{k+1/2}(U_{k+1} - U_k) + \left(\dot{\eta}\frac{\partial p}{\partial \eta}\right)_{k-1/2}(U_k - U_{k-1})\right] \qquad (3.a.98)$$
$$+ (F_U)_k \ ,$$

$$(n_V)_k = -(\zeta_k + f) U_k - R\mathcal{T}_k \left(\frac{1}{p}\frac{\partial p}{\partial \pi}\right)_k \pi \frac{\cos\phi}{a}\frac{\partial \Pi}{\partial \phi}$$
$$- \frac{1}{2\Delta p_k}\left[\left(\dot{\eta}\frac{\partial p}{\partial \eta}\right)_{k+1/2}(V_{k+1} - V_k) + \left(\dot{\eta}\frac{\partial p}{\partial \eta}\right)_{k-1/2}(V_k - V_{k-1})\right] \qquad (3.a.99)$$
$$+ (F_V)_k \ ,$$

$$\Gamma_k = T'_k \delta_k + \frac{R\mathcal{T}_k}{(c_p^*)_k}\left(\frac{\omega}{p}\right)_k - Q$$
$$- \frac{1}{2\Delta p_k}\left[\left(\dot{\eta}\frac{\partial p}{\partial \eta}\right)_{k+1/2}(T_{k+1} - T_k) + \left(\dot{\eta}\frac{\partial p}{\partial \eta}\right)_{k-1/2}(T_k - T_{k-1})\right], \qquad (3.a.100)$$

$$E_k = (u_k)^2 + (v_k)^2, \qquad (3.a.101)$$

$$\frac{R\mathcal{T}_k}{(c_p^*)_k} = \frac{R}{c_p}\left(\frac{T_k^r + \mathcal{T}_k'}{1 + \left(\frac{c_{pv}}{c_p} - 1\right) q_k}\right), \tag{3.a.102}$$

$$\begin{aligned}\left(\dot{\eta}\frac{\partial p}{\partial \eta}\right)_{k+1/2} &= B_{k+1/2} \sum_{\ell=1}^{K} \left[\delta_\ell \Delta p_\ell + \mathbf{V}_\ell \cdot \pi \nabla \Pi \Delta B_\ell\right] \\ &\quad - \sum_{\ell=1}^{k} \left[\delta_\ell \Delta p_\ell + \mathbf{V}_\ell \cdot \pi \nabla \Pi \Delta B_\ell\right], \end{aligned} \tag{3.a.103}$$

$$\begin{aligned}\left(\frac{\omega}{p}\right)_k &= \left(\frac{1}{p}\frac{\partial p}{\partial \pi}\right)_k \mathbf{V}_k \cdot \pi \nabla \Pi \\ &\quad - \sum_{\ell=1}^{k} C_{k\ell} \left[\delta_\ell \Delta p_\ell + \mathbf{V}_\ell \cdot \pi \nabla \Pi \Delta B_\ell\right], \end{aligned} \tag{3.a.104}$$

$$C_{k\ell} = H_{\ell k} / \Delta p_k, \tag{3.a.105}$$

$$\begin{aligned} D_{k\ell}^r &= \Delta p_\ell^r \frac{R}{c_p} T_k^r C_{\ell k}^r \\ &\quad + \frac{\Delta p_\ell^r}{2\Delta p_k^r} \left(T_k^r - T_{k-1}^r\right) \left(\epsilon_{k\ell+1} - B_{k-1/2}\right) \\ &\quad + \frac{\Delta p_\ell^r}{2\Delta p_k^r} \left(T_{k+1}^r - T_k^r\right) \left(\epsilon_{k\ell} - B_{k+1/2}\right), \end{aligned} \tag{3.a.106}$$

$$\frac{\epsilon_{k\ell}}{R} = \begin{cases} 1, & \ell \le k \\ 0, & \ell > k, \end{cases} \tag{3.a.107}$$

where notation such as $\left(\underline{UT'}\right)^n$ denotes a column vector with components $\left(U_k T_k'\right)^n$. In order to complete the system, it remains to specify the hydrostatic matrix $\mathbf{H}$ and its accompanying reference vector $\underline{h}^r$, together with the term $(1/p\,\partial p/\partial \pi)$, which results from the pressure gradient terms and also appears in the semi-implicit reference vector $\underline{b}^r$:

$$\left(\frac{1}{p}\frac{\partial p}{\partial \pi}\right)_k = \left(\frac{1}{p}\right)_k \left(\frac{\partial p}{\partial \pi}\right)_k = \frac{B_k}{p_k}, \tag{3.a.108}$$

$$H_{k\ell} = \begin{cases} 0, & \ell < k, \\ \frac{1}{2}\ln\left(\frac{p_{k+1}}{p_k}\right), & \ell = k, k < K, \\ \frac{1}{2}\ln\left(\frac{p_{\ell+1}}{p_{\ell-1}}\right), & \ell > k, k < K, \\ \frac{1}{2}\ln\left(\frac{\pi^2}{p_{K-1}p_K}\right), & \ell = K, k < K, \\ \ln\left(\frac{\pi}{p_K}\right), & \ell = K, k = K, \end{cases} \tag{3.a.109}$$

$$\underline{b}^r = \underline{T}^r, \tag{3.a.110}$$

$$\underline{h}^r = 0. \tag{3.a.111}$$

The matrices $\mathbf{C}^n$ and $\mathbf{H}^n$ (*i.e.*, with components $C_{k\ell}$ and $H_{k\ell}$) must be evaluated at each time step and each point in the horizontal. It is more efficient computationally to substitute the definitions of these matrices into (3.*a*.95) and (3.*a*.104) at the cost of some loss of generality in the code. The finite difference equations have been written in the form (3.*a*.94) – (3.*a*.111) because this form is quite general. For example, the equations solved by Simmons and Strüfing (1981) at ECMWF can be obtained by changing only the vectors and hydrostatic matrix defined by (3.*a*.108) – (3.*a*.111).

b. Spectral Transform

The spectral transform method is used in the horizontal exactly as in CCM1. As shown earlier, the vertical and temporal aspects of the model are represented by finite–difference approximations. The horizontal aspects are treated by the spectral–transform method, which is described in this section. Thus, at certain points in the integration, the prognostic variables $(\zeta + f), \delta, T$, and Π are represented in terms of coefficients of a truncated series of spherical harmonic functions, while at other points they are given by grid–point values on a corresponding Gaussian grid. In general, physical parameterizations and nonlinear operations are carried out in grid–point space. Horizontal derivatives and linear operations are performed in spectral space. Externally, the model appears to the user to be a grid–point model, as far as data required and produced by it. Similarly, since all nonlinear parameterizations are developed and carried out in grid–point space, the model also appears as a grid–point model for the incorporation of physical parameterizations, and the user need not be too concerned with the spectral aspects. For users interested in diagnosing the balance of terms in the evolution equations, however, the details are important and care must be taken to understand which terms have been spectrally truncated and which have not. The algebra involved in the spectral transformations has been presented in several publications (Daley *et al.,* 1976; Bourke *et al.,* 1977; Machenhauer, 1979). In this report, we present only the details relevant to the model code; for more details and general philosophy, the reader is referred to these earlier papers.

Spectral algorithm overview

The horizontal representation of an arbitrary variable ψ consists of a truncated series of spherical harmonic functions,

$$\psi(\lambda,\mu) = \sum_{m=-M}^{M} \sum_{n=|m|}^{\mathcal{N}(m)} \psi_n^m P_n^m(\mu) e^{im\lambda}, \tag{3.b.1}$$

where $\mu = \sin\phi$, M is the highest Fourier wavenumber included in the east–west representation, and $\mathcal{N}(m)$ is the highest degree of the associated Legendre polynomials for longitudinal wavenumber m. The properties of the spherical harmonic functions used in the representation can be found in the review by Machenhauer (1979). The model is coded for a general pentagonal truncation, illustrated in Figure 1, defined by three parameters: M, K, and N, where M is defined above, K is the highest degree of the associated Legendre polynomials, and N is the highest degree of the Legendre polynomials for $m = 0$. The common truncations are subsets of this pentagonal case:

$$\begin{aligned} &\text{Triangular}: M = N = K, \\ &\text{Rhomboidal}: K = N + M, \\ &\text{Trapezoidal}: N = K > M. \end{aligned} \tag{3.b.2}$$

The quantity $\mathcal{N}(m)$ in (3.b.1) represents an arbitrary limit on the two-dimensional wavenumber n, and for the pentagonal truncation described above is simply given by $\mathcal{N}(m) = \min(N + |m|, K)$.

The associated Legendre polynomials used in the model are normalized such that

$$\int_{-1}^{1} [P_n^m(\mu)]^2 \, d\mu = 1. \tag{3.b.3}$$

With this normalization, the Coriolis parameter f is

$$f = \frac{\Omega}{\sqrt{0.375}} P_1^o, \tag{3.b.4}$$

which is required for the absolute vorticity.

The coefficients of the spectral representation (3.b.1) are given by

$$\psi_n^m = \int_{-1}^{1} \frac{1}{2\pi} \int_0^{2\pi} \psi(\lambda,\mu) e^{-im\lambda} d\lambda P_n^m(\mu) d\mu. \tag{3.b.5}$$

The inner integral represents a Fourier transform,

$$\psi^m(\mu) = \frac{1}{2\pi} \int_0^{2\pi} \psi(\lambda,\mu) e^{-im\lambda} d\lambda, \tag{3.b.6}$$

which is performed by a Fast Fourier Transform (FFT) subroutine. The outer integral is performed via Gaussian quadrature,

$$\psi_n^m = \sum_{j=1}^{J} \psi^m(\mu_j) P_n^m(\mu_j) w_j, \tag{3.b.7}$$

where μ_j denotes the Gaussian grid points in the meridional direction, w_j the Gaussian weight at point μ_j, and J the number of Gaussian grid points from pole to pole. The Gaussian grid points (μ_j) are given by the roots of the Legendre polynomial $P_J(\mu)$, and the corresponding weights are given by

$$w_j = \frac{2(1-\mu_j^2)}{[J\ P_{J-1}(\mu_j)]^2}. \tag{3.b.8}$$

The weights themselves satisfy

$$\sum_{j=1}^{J} w_j = 2.0\ . \tag{3.b.9}$$

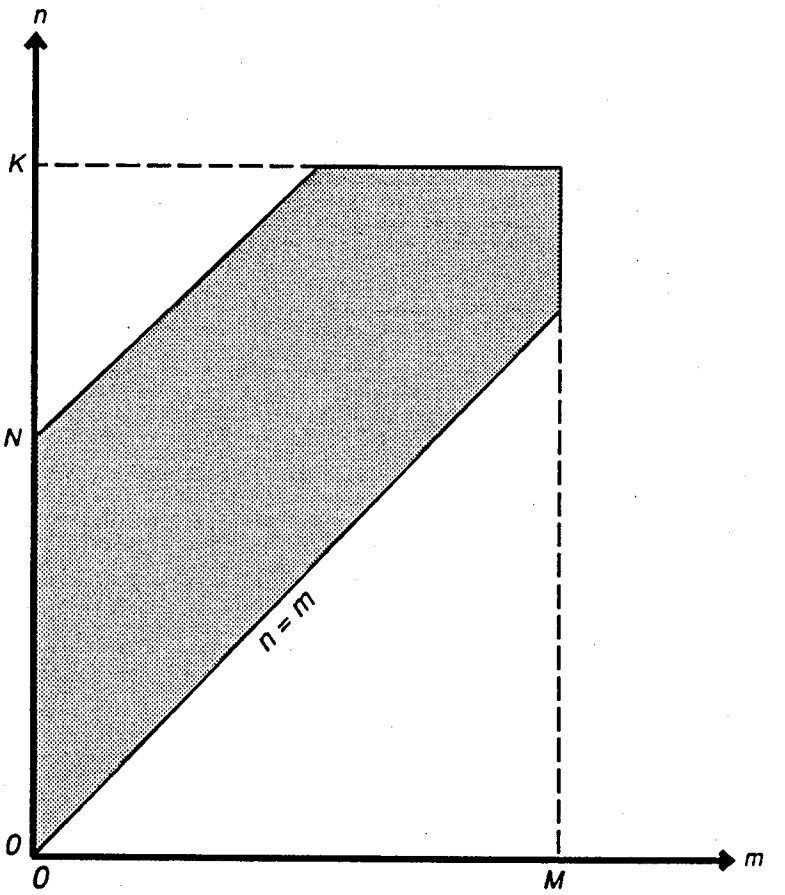

Figure 1. Pentagonal truncation parameters

The Gaussian grid used for the north–south transformation is generally chosen to allow un-aliased computations of quadratic terms only. In this case, the number of Gaussian latitudes J must satisfy

$$J \geq (2N + K + M + 1)/2 \quad \text{for M} \leq 2(\text{K} - \text{N}), \tag{3.b.10}$$

$$J \geq (3K + 1)/2 \qquad\qquad \text{for M} \geq 2(\text{K} - \text{N}). \tag{3.b.11}$$

For the common truncations, these become

$$J \geq (3K+1)/2 \qquad \text{for triangular and trapezoidal,} \tag{3.b.12}$$

$$J \geq (3N+2M+1)/2 \qquad \text{for rhomboidal.} \tag{3.b.13}$$

In order to allow exact Fourier transform of quadratic terms, the number of points P in the east–west direction must satisfy

$$P \geq 3M+1 \quad . \tag{3.b.14}$$

The actual values of J and P are often not set equal to the lower limit in order to allow use of more efficient transform programs.

Although in the next section of this model description, we continue to indicate the Gaussian quadrature as a sum from pole to pole, the code actually deals with the symmetric and antisymmetric components of variables and accumulates the sums from equator to pole only. The model requires an even number of latitudes to easily use the symmetry conditions. This may be slightly inefficient for some spectral resolutions. We define a new index, which goes from $-I$ at the point next to the south pole to $+I$ at the point next to the north pole and not including 0 (there are no points at the equator or pole in the Gaussian grid), *i.e.*, let $I = J/2$ and $i = j - J/2$ for $j \geq J/2+1$ and $i = j - J/2 - 1$ for $j \leq J/2$; then the summation in (3.*b*.7) can be rewritten as

$$\psi_n^m = \sum_{\substack{i=-I \\ i\neq 0}}^{I} \psi^m(\mu_i) P_n^m(\mu_i) w_i. \tag{3.b.15}$$

The symmetric (even) and antisymmetric (odd) components of ψ^m are defined by

$$\begin{aligned} (\psi_E)_i^m &= \frac{1}{2}\left(\psi_i^m + \psi_{-i}^m\right), \\ (\psi_O)_i^m &= \frac{1}{2}\left(\psi_i^m - \psi_{-i}^m\right). \end{aligned} \tag{3.b.16}$$

Since w_i is symmetric about the equator, (3.*b*.15) can be rewritten to give formulas for the coefficients of even and odd spherical harmonics:

$$\psi_n^m = \begin{cases} \sum_{i=1}^{I} (\psi_E)_i^m (\mu_i) P_n^m(\mu_i) 2w_i & \text{for } n-m \text{ even}, \\ \\ \sum_{i=1}^{I} (\psi_O)_i^m (\mu_i) P_n^m(\mu_i) 2w_i & \text{for } n-m \text{ odd}. \end{cases} \tag{3.b.17}$$

The model uses the spectral transform method (Machenhauer, 1979) for all nonlinear terms. However, the model can be thought of as starting from grid–point values at time t (consistent with the spectral representation) and producing a forecast of the grid–point values at time $t + \Delta t$ (again, consistent with the spectral resolution).

The forecast procedure involves computation of the nonlinear terms including physical parameterizations at grid points; transformation via Gaussian quadrature of the nonlinear terms from grid–point space to spectral space; computation of the spectral coefficients of the prognostic variables at time $t + \Delta t$ (with the implied spectral truncation to the model resolution); and transformation back to grid–point space. The details of the equations involved in the various transformations are given in the next section.

Combination of terms

In order to describe the transformation to spectral space, for each equation we first group together all undifferentiated explicit terms, all explicit terms with longitudinal derivatives, and all explicit terms with meridional derivatives appearing in the Dyn operator. Thus, the vorticity equation (3.*a*.94) is rewritten

$$\underline{(\zeta + f)}^{n+1} = \underline{V} + \frac{1}{a(1-\mu^2)} \left[\frac{\partial}{\partial \lambda}(\underline{V}_\lambda) - (1-\mu^2) \frac{\partial}{\partial \mu}(\underline{V}_\mu) \right], \tag{3.*b*.18}$$

where the explicit forms of the vectors $\underline{V}, \underline{V}_\lambda$, and $\underline{V}_\mu$ are given in Appendix A [(*A*1)–(*A*3).] The divergence equation (3.*a*.95) is

$$\begin{aligned} \underline{\delta}^{n+1} = \underline{D} + \frac{1}{a(1-\mu^2)} \left[\frac{\partial}{\partial \lambda}(\underline{D}_\lambda) + (1-\mu^2) \frac{\partial}{\partial \mu}(\underline{D}_\mu) \right] - \nabla^2 \underline{D}_\nabla \\ - \Delta t \nabla^2 (R \mathbf{H}^r \underline{T'}^{n+1} + R (\underline{b}^r + \underline{h}^r) \Pi^{n+1}). \end{aligned} \tag{3.*b*.19}$$

The mean component of the temperature is not included in the next–to–last term since the Laplacian of it is zero. The thermodynamic equation (3.*a*.96) is

$$\underline{T'}^{n+1} = \underline{T} - \frac{1}{a(1-\mu^2)} \left[\frac{\partial}{\partial \lambda}(\underline{T}_\lambda) + (1-\mu^2) \frac{\partial}{\partial \mu}(\underline{T}_\mu) \right] - \Delta t \mathbf{D}^r \, \underline{\delta}^{n+1}. \tag{3.*b*.20}$$

The surface–pressure tendency (3.*a*.97) is

$$\Pi^{n+1} = PS - \frac{1}{\pi^r} \left(\underline{\Delta p}^r \right)^T \underline{\delta}^{n+1}. \tag{3.*b*.21}$$

The grouped explicit terms in (3.*b*.19)–(3.*b*.21) are all given in Appendix A [(*A*4)–(*A*11)].

Transformation to spectral space

The coefficients of the spectral representation are obtained by integration,

$$\psi_n^m = \int_{-1}^{+1} \frac{1}{2\pi} \int_o^{2\pi} \psi(\lambda, \mu) e^{-im\lambda} d\lambda P_n^m(\mu) d\mu. \tag{3.*b*.22}$$

The inner integral is generally performed via an FFT subroutine. The result of this operation is denoted $\psi^m(\mu)$,

$$\psi^m(\mu) = \frac{1}{2\pi}\int_o^{2\pi} \psi(\lambda,\mu)e^{-im\lambda}d\lambda. \tag{3.b.23}$$

The outer integral is performed via Gaussian quadrature,

$$\psi_n^m = \sum_{j=1}^{J} \psi^m(\mu_j)P_n^m(\mu_j)w_j, \tag{3.b.24}$$

where μ_j denotes the Gaussian grid points in the meridional direction, w_j is the Gaussian weight at the jth grid point, and J the number of points from pole to pole.

Formally, Equations (3.b.18) – (3.b.21) are transformed to spectral space by performing the operations indicated in (3.b.22) to each term. We see that the equations basically contain three types of terms, for example, in the vorticity equation the undifferentiated term $\underline{V}$, the longitudinally differentiated term $\underline{V}_\lambda$, and the meridionally differentiated term $\underline{V}_\mu$. All terms in the original equations were grouped into one of these terms on the Gaussian grid so that they could be transformed at once.

Transformation of the undifferentiated term is obtained by straightforward application of (3.b.22) – (3.b.24),

$$\{\underline{V}\}_n^m = \sum_{j=1}^{J} \underline{V}^m(\mu_j)P_n^m(\mu_j)w_j, \tag{3.b.25}$$

where $\underline{V}^m(\mu_j)$ is the Fourier coefficient of $\underline{V}$ with wavenumber m at the Gaussian grid line μ_j. The longitudinally differentiated term is handled by integration by parts, using the cyclic boundary conditions,

$$\begin{aligned}\left\{\frac{\partial}{\partial\lambda}(\underline{V}_\lambda)\right\}^m &= \frac{1}{2\pi}\int_o^{2\pi}\frac{\partial \underline{V}_\lambda}{\partial\lambda}e^{-im\lambda}d\lambda, \\ &= im\frac{1}{2\pi}\int_o^{2\pi}\underline{V}_\lambda e^{-im\lambda}d\lambda,\end{aligned} \tag{3.b.26}$$

so that the Fourier transform is performed first, then the differentiation is carried out in spectral space. The transformation to spherical harmonic space then follows (3.b.25):

$$\left\{\frac{1}{a(1-\mu^2)}\frac{\partial}{\partial\lambda}(\underline{V}_\lambda)\right\}_n^m = im\sum_{j=1}^{J}\underline{V}_\lambda^m(\mu_j)\frac{P_n^m(\mu_j)}{a(1-\mu_j^2)}w_j, \tag{3.b.27}$$

where $\underline{V}_\lambda^m(\mu_j)$ is the Fourier coefficient of $\underline{V}_\lambda$ with wavenumber m at the Gaussian grid line μ_j.

The latitudinally differentiated term is handled by integration by parts using zero boundary conditions at the poles:

$$\left\{\frac{1}{a(1-\mu^2)}(1-\mu^2)\frac{\partial}{\partial\mu}(\underline{V}_\mu)\right\}_n^m = \int_{-1}^{1}\frac{1}{a(1-\mu^2)}(1-\mu^2)\frac{\partial}{\partial\mu}(\underline{V}_\mu)^m P_n^m d\mu, \tag{3.b.28}$$

$$= -\int_{-1}^{1}\frac{1}{a(1-\mu^2)}(\underline{V}_\mu)^m(1-\mu^2)\frac{dP_n^m}{d\mu}d\mu.$$

Defining the derivative of the associated Legendre polynomial by

$$H_n^m = (1-\mu^2)\frac{dP_n^m}{d\mu}, \tag{3.b.29}$$

(3.b.28) can be written

$$\left\{\frac{1}{a(1-\mu^2)}(1-\mu^2)\frac{\partial}{\partial\mu}(\underline{V}_\mu)\right\}_n^m = -\sum_{j=1}^{J}(\underline{V}_\mu)^m\frac{H_n^m(\mu_j)}{a(1-\mu_j^2)}w_j. \tag{3.b.30}$$

Similarly, the ∇^2 operator in the divergence equation can be converted to spectral space by sequential integration by parts and then application of the relationship

$$\nabla^2 P_n^m(\mu)e^{im\lambda} = \frac{-n(n+1)}{a^2}P_n^m(\mu)e^{im\lambda}, \tag{3.b.31}$$

to each spherical harmonic function individually so that

$$\{\nabla^2\underline{D}_\nabla\}_n^m = \frac{-n(n+1)}{a^2}\sum_{j=1}^{J}\underline{D}_\nabla^m(\mu_j)P_n^m(\mu_j)w_j, \tag{3.b.32}$$

where $\underline{D}_\nabla^m(\mu)$ is the Fourier coefficient of the original grid variable $\underline{D}_\nabla$.

Solution of semi–implicit equations

The prognostic equations can be converted to spectral form by summation over the Gaussian grid using (3.b.25), (3.b.27), and (3.b.30). The resulting equation for absolute vorticity is

$$\underline{(\zeta+f)}_n^m = \underline{VS}_n^m, \tag{3.b.33}$$

where $\underline{(\zeta+f)}_n^m$ denotes a spherical harmonic coefficient of $\underline{(\zeta+f)}^{n+1}$, and the form of $\underline{VS}_n^m$, as a summation over the Gaussian grid, is given in Appendix A (*A*12).

The spectral form of the divergence equation (3.b.19) becomes

$$\underline{\delta}_n^m = \underline{DS}_n^m + \Delta t\frac{n(n+1)}{a^2}\left[R\mathbf{H}^r\underline{T}_n'^m + R(\underline{b}^r+\underline{h}^r)\Pi_n^m\right], \tag{3.b.34}$$

where $\underline{\delta}_n^m$, $\underline{T}_n'^m$, and Π_n^m are spectral coefficients of $\underline{\delta}^{n+1}$, $\underline{T}'^{n+1}$, and Π^{n+1}. The Laplacian of the total temperature in (3.b.19) is replaced by the equivalent Laplacian of the perturbation temperature in (3.b.34). $\underline{DS}_n^m$ is given in Appendix A (*A*13). The

spectral thermodynamic equation is

$$\underline{T'}_n^m = \underline{TS}_n^m - \Delta t \mathbf{D}^r \underline{\delta}_n^m, \tag{3.b.35}$$

with $\underline{TS}_n^m$ defined in Appendix A ($A14$), while the surface pressure equation is

$$\Pi_n^m = PS_n^m - \left(\left(\underline{\Delta p}^r\right)^T \frac{1}{\pi^r} \right) \underline{\delta}_n^m \,, \tag{3.b.36}$$

where PS_n^m is also given in Appendix A ($A15$).

Equation (3.b.33) for vorticity is explicit and complete at this point. However, the remaining equations (3.b.34)–(3.b.36) are coupled. They are solved by eliminating all variables except $\underline{\delta}_n^m$:

$$\mathbf{A}_n \underline{\delta}_n^m = \underline{DS}_n^m + \Delta t \frac{n(n+1)}{a^2} \left[R\mathbf{H}^r (\underline{TS})_n^m + R\left(\underline{b}^r + \underline{h}^r\right)(PS)_n^m \right], \tag{3.b.37}$$

where

$$\mathbf{A}_n = \mathbf{I} + \Delta t^2 \frac{n(n+1)}{a^2} \left[R\mathbf{H}^r \mathbf{D}^r + R\left(\underline{b}^r + \underline{h}^r\right) \left(\left(\underline{\Delta p}^r\right)^T \frac{1}{\pi^r} \right) \right], \tag{3.b.38}$$

which is simply a set of K simultaneous equations for the coefficients with given wavenumbers (m,n) at each level and is solved by inverting $\mathbf{A}_n$. In order to prevent the accumulation of round–off error in the global mean divergence (which if exactly zero initially, should remain exactly zero) $(\mathbf{A}_o)^{-1}$ is set to the null matrix rather than the identity, and the formal application of (3.b.37) then always guarantees $\underline{\delta}_o^o = 0$. Once δ_n^m is known, $\underline{T'}_n^m$ and Π_n^m can be computed from (3.b.35) and (3.b.36), respectively, and all prognostic variables are known at time $n+1$ as spherical harmonic coefficients. Note that the mean component $\underline{T'}_o^o$ is not necessarily zero since the perturbations are taken with respect to a specified $\underline{T}^r$.

Horizontal diffusion

As mentioned earlier, the horizontal diffusion in (3.a.87) and (3.a.90) is computed implicitly via time splitting after the transformations into spectral space and solution of the semi-implicit equations. In the following, the ζ and δ equations have a similar form, so we write only the δ equation:

$$(\delta^*)_n^m = \left(\delta^{n+1}\right)_n^m - (-1)^i 2\Delta t K^{(2i)} \left[\nabla^{2i} (\delta^*)_n^m - (-1)^i (\delta^*)_n^m \left(2/a^2\right)^i \right], \tag{3.b.39}$$

$$(T^*)_n^m = \left(T^{n+1}\right)_n^m - (-1)^i 2\Delta t K^{(2i)} \left[\nabla^{2i} (T^*)_n^m \right] . \tag{3.b.40}$$

The extra term is present in (3.b.39), (3.b.43) and (3.b.45) to prevent damping of uniform rotations. The solutions are just

$$(\delta^*)_n^m = K_n^{(2i)}(\delta) \left(\delta^{n+1}\right)_n^m, \tag{3.b.41}$$

$$(T^*)_n^m = K_n^{(2i)}(T) \left(T^{n+1}\right)_n^m, \tag{3.b.42}$$

$$K_n^{(2)}(\delta) = \left\{1 + 2\Delta t D_n K^{(2)} \left[\left(\frac{n(n+1)}{a^2}\right) - \frac{2}{a^2}\right]\right\}^{-1}, \qquad (3.b.43)$$

$$K_n^{(2)}(T) = \left\{1 + 2\Delta t D_n K^{(2)} \left(\frac{n(n+1)}{a^2}\right)\right\}^{-1}, \qquad (3.b.44)$$

$$K_n^{(4)}(\delta) = \left\{1 + 2\Delta t D_n K^{(4)} \left[\left(\frac{n(n+1)}{a^2}\right)^2 - \frac{4}{a^4}\right]\right\}^{-1}, \qquad (3.b.45)$$

$$K_n^{(4)}(T) = \left\{1 + 2\Delta t D_n K^{(4)} \left(\frac{n(n+1)}{a^2}\right)^2\right\}^{-1}. \qquad (3.b.46)$$

$K_n^{(2)}(\delta)$ and $K_n^{(4)}(\delta)$ are both set to 1 for $n = 0$. The quantity D_n represents the "Courant number limiter", normally set to 1. However, D_n is modified to ensure that the CFL criterion is not violated in selected upper levels of the model. If the maximum wind speed in any of these upper levels is sufficiently large, then $D_n = 1000$ in that level for all $n > n_c$, where $n_c = a\Delta t / \max|\mathbf{V}|$. This condition is applied whenever the wind speed is large enough that $n_c < K$, the truncation parameter in (3.*b*.2), and temporarily reduces the effective resolution of the model in the affected levels. The number of levels at which this "Courant number limiter" may be applied is user-selectable, but it is only used in the top level of the 18 level CCM2 control runs.

The diffusion of T is not complete at this stage. In order to make the partial correction from η to p in (3.*a*.81) local, it is not included until grid-point values are available. This requires that $\nabla^4\Pi$ also be transformed from spectral to grid-point space. The values of the coefficients $K^{(2)}$ and $K^{(4)}$ for the standard T42 resolution are $2.5 \times 10^5 \mathrm{m}^2\mathrm{sec}^{-1}$ and $1.0 \times 10^{16}\mathrm{m}^2\mathrm{sec}^{-1}$, respectively.

Transformation from spectral to physical space

After the prognostic variables are completed at time $n+1$ in spectral space $\left(\underline{(\zeta+f)^*}\right)_n^m$, $(\underline{\delta^*})_n^m$, $(\underline{T^*})_n^m$, $\left(\Pi^{n+1}\right)_n^m$, they are transformed to grid space. For a variable ψ, the transformation is given by

$$\psi(\lambda,\mu) = \sum_{m=-M}^{M} \left[\sum_{n=|m|}^{\mathcal{N}(m)} \psi_n^m P_n^m(\mu)\right] e^{im\lambda}. \qquad (3.b.47)$$

The inner sum is done essentially as a vector product over n, and the outer is again performed by an FFT subroutine. The term needed for the remainder of the diffusion

terms, $\nabla^4\Pi$, is calculated from

$$\nabla^4\Pi^{n+1} = \sum_{m=-M}^{M}\left[\sum_{n=|m|}^{\mathcal{N}(m)}\left(\frac{n(n+1)}{a^2}\right)^2\left(\Pi^{n+1}\right)_n^m P_n^m(\mu)\right]e^{im\lambda}. \tag{3.b.48}$$

In addition, the derivatives of Π are needed on the grid for the terms involving $\nabla\Pi$ and $\mathbf{V}\cdot\nabla\Pi$,

$$\mathbf{V}\cdot\nabla\Pi = \frac{U}{a(1-\mu^2)}\frac{\partial\Pi}{\partial\lambda} + \frac{V}{a(1-\mu^2)}(1-\mu^2)\frac{\partial\Pi}{\partial\mu}. \tag{3.b.49}$$

These required derivatives are given by

$$\frac{\partial\Pi}{\partial\lambda} = \sum_{m=-M}^{M} im\left[\sum_{n=|m|}^{\mathcal{N}(m)}\Pi_n^m P_n^m(\mu)\right]e^{im\lambda}, \tag{3.b.50}$$

and using (3.b.29),

$$(1-\mu^2)\frac{\partial\Pi}{\partial\mu} = \sum_{m=-M}^{M}\left[\sum_{n=|m|}^{\mathcal{N}(m)}\Pi_n^m H_n^m(\mu)\right]e^{im\lambda}, \tag{3.b.51}$$

which involve basically the same operations as (3.b.48). The other variables needed on the grid are U and V. These can be computed directly from the absolute vorticity and divergence coefficients using the relations

$$(\zeta+f)_n^m = -\frac{n(n+1)}{a^2}\psi_n^m + f_n^m, \tag{3.b.52}$$

$$\delta_n^m = -\frac{n(n+1)}{a^2}\chi_n^m, \tag{3.b.53}$$

in which the only nonzero f_n^m is $f_1^o = \Omega/\sqrt{.375}$, and

$$U = \frac{1}{a}\frac{\partial\chi}{\partial\lambda} - \frac{(1-\mu^2)}{a}\frac{\partial\psi}{\partial\mu}, \tag{3.b.54}$$

$$V = \frac{1}{a}\frac{\partial\psi}{\partial\lambda} + \frac{(1-\mu^2)}{a}\frac{\partial\chi}{\partial\mu}. \tag{3.b.55}$$

Thus, the direct transformation is

$$U = -\sum_{m=-M}^{M} a\sum_{n=|m|}^{\mathcal{N}(m)}\left[\frac{im}{n(n+1)}\delta_n^m P_n^m(\mu) - \frac{1}{n(n+1)}(\zeta+f)_n^m H_n^m(\mu)\right]e^{im\lambda}$$

$$-\frac{a}{2}\frac{\Omega}{\sqrt{0.375}}H_1^o, \tag{3.b.56}$$

$$V = -\sum_{m=-M}^{M} a\sum_{n=|m|}^{\mathcal{N}(m)}\left[\frac{im}{n(n+1)}(\zeta+f)_n^m P_n^m(\mu) + \frac{1}{n(n+1)}\delta_n^m H_n^m(\mu)\right]e^{im\lambda}. \tag{3.b.57}$$

The horizontal diffusion tendencies are also transformed back to grid space. The spectral coefficients for the horizontal diffusion tendencies follow from (3.*b*.39) and (3.*b*.40):

$$F_{T_H}\left(T^*\right)_n^m = (-1)^{i+1} K^{2i} \left[\nabla^{2i}\left(T^*\right)\right]_n^m, \tag{3.b.58}$$

$$F_{\zeta_H}\left((\zeta+f)^*\right)_n^m = (-1)^{i+1} K^{2i} \left\{\nabla^{2i}(\zeta+f)^* - (-1)^i (\zeta+f)^* \left(2/a^2\right)^i\right\}, \tag{3.b.59}$$

$$F_{\delta_H}\left(\delta^*\right)_n^m = (-1) K^{2i} \left\{\nabla^{2i}\left(\delta^*\right) - (-1)^i \delta^* \left(2/a^2\right)^i\right\}, \tag{3.b.60}$$

using $i = 1$ or 2 as appropriate for the ∇^2 or ∇^4 forms. These coefficients are transformed to grid space following (3.*b*.1) for the T term and (3.*b*.56) and (3.*b*.57) for vorticity and divergence. Thus, the vorticity and divergence diffusion tendencies are converted to equivalent U and V diffusion tendencies.

Horizontal diffusion correction

After grid–point values are calculated, frictional heating rates are determined from the momentum diffusion tendencies and are added to the temperature, and the partial correction of the ∇^4 diffusion from η to p surfaces is applied to T. The frictional heating rate is calculated from the kinetic energy tendency produced by the momentum diffusion

$$F_{F_H} = -u^{n-1} F_{u_H}(u^*)/c_p^* - v^{n-1} F_{v_H}(v^*)/c_p^*, \tag{3.b.61}$$

where F_{u_H}, and F_{v_H} are the momentum equivalent diffusion tendencies, determined from F_{ζ_H} and F_{δ_H} just as U and V are determined from ζ and δ, and

$$c_p^* = c_p \left[1 + \left(\frac{c_{p_v}}{c_p} - 1\right) q^{n+1}\right]. \tag{3.b.62}$$

These heating rates are then combined with the correction,

$$\hat{T}_k^{n+1} = T_k^* + \left(2\Delta t F_{F_H}\right)_k + 2\Delta t \left(\pi B \frac{\partial T^*}{\partial p}\right)_k K^{(4)} \nabla^4 \Pi^{n+1}. \tag{3.b.63}$$

The vertical derivatives of T^* (where the * notation is dropped for convenience) are defined by

$$\begin{aligned}
\left(\pi B \frac{\partial T}{\partial p}\right)_1 &= \frac{\pi}{2\Delta p_1}\left[B_{1+\frac{1}{2}}\left(T_2 - T_1\right)\right], \\
\left(\pi B \frac{\partial T}{\partial p}\right)_k &= \frac{\pi}{2\Delta p_k}\left[B_{k+\frac{1}{2}}\left(T_{k+1} - T_k\right) + B_{k-\frac{1}{2}}\left(T_k - T_{k-1}\right)\right], \\
\left(\pi B \frac{\partial T}{\partial p}\right)_K &= \frac{\pi}{2\Delta p_K}\left[B_{K-\frac{1}{2}}\left(T_K - T_{K-1}\right)\right].
\end{aligned} \tag{3.b.64}$$

The corrections are added to the diffusion tendencies calculated earlier (3.*b*.58) to give the total temperature tendency for diagnostic purposes:

$$\hat{F}_{T_H}(T^*)_k = F_{T_H}(T^*)_k + (2\Delta t F_{F_H})_k + 2\Delta t B_k \left(\pi \frac{\partial T^*}{\partial p}\right)_k K^{(4)} \nabla^4 \Pi^{n+1}. \qquad (3.b.65)$$

c. Semi-Lagrangian Transport

The forecast equation for water vapor (and constituent) specific humidity in the η system is from (3.*a*.36) excluding sources and sinks.

$$\frac{dq}{dt} = \frac{\partial q}{\partial t} + \mathbf{V} \cdot \nabla q + \dot{\eta} \frac{\partial p}{\partial \eta} \frac{\partial q}{\partial p} = 0 \qquad (3.c.1)$$

or

$$\frac{dq}{dt} = \frac{\partial q}{\partial t} + \mathbf{V} \cdot \nabla q + \dot{\eta} \frac{\partial q}{\partial \eta} = 0. \qquad (3.c.2)$$

Equation (3.*c*.2) is more economical for the semi-Lagrangian vertical advection, as $\Delta\eta$ does not vary in the horizontal, while Δp does. Written in this form, the η advection equations look exactly like the σ equations.

These are the necessary equations for the time split subset (2.*a*.3*b*). For simplicity, in this section we will use the notation adopted in the previous section, *i.e.*, $(\ )^{n-1}$ for $(\ )^-$ of (2.*a*.3*b*) and $(\ )^{n+1}$ for $(\hat{})^+$. Thus, the tendency sources have already been added to the time level labeled $(n-1)$ here. The semi-Lagrangian advection step (2.*a*.3*b*) is further subdivided into horizontal and vertical advection sub-steps, which, in an Eulerian form, would be written

$$q^* = q^{n-1} + 2\Delta t \left(\mathbf{V} \cdot \nabla q\right)^n \qquad (3.c.3)$$

and

$$q^{n+1} = q^* + 2\Delta t \left(\dot{\eta} \frac{\partial q}{\partial n}\right)^n. \qquad (3.c.4)$$

In the semi-Lagrangian form used here, the general form is

$$q^* = \mathrm{L}_{\lambda\varphi}\left(q^{n-1}\right), \qquad (3.c.5)$$

$$q^{n+1} = \mathrm{L}_{\eta}\left(q^*\right). \qquad (3.c.6)$$

Equation (3.*c*.5) represents the horizontal interpolation of q^{n-1} at the departure point calculated assuming $\dot{\eta} = 0$. Equation (3.*c*.6) represents the vertical interpolation of q^* at the departure point, assuming $\mathbf{V} = 0$.

The horizontal departure points are found by first iterating for the mid-point of the trajectory, using winds at time n, and a first guess as the location of the mid-point of the previous time step

$$\lambda_M^{k+1} = \lambda_A - \Delta t u^n \left(\lambda_M^k, \varphi_M^k\right) / \cos\varphi_M^k, \qquad (3.c.7)$$

$$\varphi_M^{k+1} = \varphi_A - \Delta t v^n \left(\lambda_M^k, \varphi_M^k\right), \tag{3.c.8}$$

where subscript A denotes the arrival (Gaussian grid) point and subscript M the midpoint of the trajectory. The velocity components at $\left(\lambda_M^k, \varphi_M^k\right)$ are determined by Lagrange cubic interpolation. For economic reasons, the equivalent Hermite cubic interpolant with cubic derivative estimates is used at some places in this code. The equations will be presented later.

Once the iteration of (3.c.7) and (3.c.8) is complete, the departure point is given by

$$\lambda_D = \lambda_A - 2\Delta t u^n \left(\lambda_M, \varphi_M\right) / \cos\varphi_M, \tag{3.c.9}$$

$$\varphi_D = \lambda_A - 2\Delta t v^n \left(\lambda_M, \varphi_M\right), \tag{3.c.10}$$

where the subscript D denotes the departure point.

The form given by (3.c.7) – (3.c.10) is inaccurate near the poles and thus is only used for arrival points equatorward of 70° latitude. Poleward of 70° we transform to a local geodesic coordinate for the calculation at each arrival point. The local geodesic coordinate is essentially a rotated spherical coordinate system whose equator goes through the arrival point. Details are provided in Williamson and Rasch (1989). The transformed system is rotated about the axis through $\left(\lambda_A - \frac{\pi}{2}, 0\right)$ and $\left(\lambda_A + \frac{\pi}{2}, 0\right)$, by an angle φ_A so the equator goes through (λ_A, φ_A). The longitude of the transformed system is chosen to be zero at the arrival point. If the local geodesic system is denoted by (λ', φ'), with velocities (u', v'), the two systems are related by

$$\sin\phi' = \sin\phi\cos\phi_A - \cos\phi\sin\phi_A\cos\left(\lambda_A - \lambda\right), \tag{3.c.11}$$

$$\sin\phi = \sin\phi'\cos\phi_A + \cos\phi'\sin\prime_A\cos\lambda' \ , \tag{3.c.12}$$

$$\sin\lambda'\cos\phi' = -\sin\left(\lambda_A - \lambda\right)\cos\phi \ , \tag{3.c.13}$$

$$\begin{aligned} v'\cos\phi' = {} & v\left[\cos\phi\cos\phi_A + \sin\phi\sin\phi_A\cos\left(\lambda_A - \lambda\right)\right] \\ & - u\sin\phi_A\sin\left(\lambda_A - \lambda\right), \end{aligned} \tag{3.c.14}$$

$$u'\cos\lambda' - v'\sin\lambda'\sin\phi' = u\cos\left(\lambda_A - \lambda\right) + v\sin\phi\sin\left(\lambda_A - \lambda\right) \ . \tag{3.c.15}$$

The calculation of the departure point in the local geodesic system is identical to (3.c.7) – (3.c.10) with all variables carrying a prime. The equations can be simplified by noting that $\left(\lambda'_A, \varphi'_A\right) = (0, 0)$ by design and $u'\left(\lambda'_A, \varphi'_A\right) = u\left(\lambda_A, \varphi_A\right)$ and $v'\left(\lambda'_A, \varphi'_A\right) = v\left(\lambda_A, \varphi_A\right)$. The interpolations are always done in global spherical coordinates.

The interpolants are most easily defined on the interval $0 \leq \theta \leq 1$. Define

$$\theta = \left(x_D - x_i\right) / \left(x_{i+1} - x_i\right), \tag{3.c.16}$$

where x is either λ or φ and the departure point x_D falls within the interval (x_i, x_{i+1}). The Hermite cubic interpolant is given by

$$q_D = q_{i+1}\theta^3 + (3q_{i+1} - h_i d_{i+1})\,\theta^2(1-\theta) + (3q_i + h_i d_i)\,\theta(1-\theta)^2 + q_i(1-\theta)^3, \quad (3.c.17)$$

where q_i is the value at the gridpoint x_i, d_i is the derivative estimate given below, and $h_i = x_{i+1} - x_i$.

$$\begin{aligned} d_i = {} & q[x_i, x_{i-1}] + (x_i - x_{i-1})\,q[x_{i+1}, x_i, x_{i-1}] \\ & + (x_i - x_{i-1})(x_i - x_{i+1})\,q[x_{i+2}, x_{i+1}, x_i, x_{i-1}], \end{aligned} \quad (3.c.18)$$

$$\begin{aligned} d_{i+1} = {} & q[x_i, x_{i-1}] + [(x_{i+1} - x_i) + (x_{i+1} - x_{i-1})]\,q[x_{i+1}, x_i, x_{i-1}] \\ & + (x_{i+1} - x_{i-1})(x_{i+1} - x_i)\,q[x_{i+2}, x_{i+1}, x_i, x_{i-1}], \end{aligned} \quad (3.c.19)$$

using the normal divided difference notation

$$\begin{aligned} q[x_2, x_1] &= \{q(x_2) - q(x_1)\} / (x_2 - x_1) \\ q[x_n, x_{n-1}, \ldots, x_1] &= \{q[x_n, x_{n-1}, \ldots, x_2] - q[x_{n-1}, x_{n-2}, \ldots, x_1]\} / (x_n - x_1). \end{aligned} \quad (3.c.20)$$

The Lagrangian cubic interpolant used for the velocity interpolation, which is equivalent to (3.c.17) – (3.c.19), is

$$\begin{aligned} f_D = {} & (x_D - x_{i+2}) \Big\{ (x_D - x_{i+1})\,[(x_D - x_i)\,a_{i-1} f_{i-1} + (x_D - x_{i-1})\,a_i f_i] \\ & + (x_D - x_{i-1})(x_D - x_i)\,a_{i+1} f_{i+1} \Big\} \\ & + (x_D - x_{i-1})(x_D - x_i)(x_D - x_{i+1})\,a_{i+2} f_{i+2}, \end{aligned} \quad (3.c.21)$$

where

$$a_{i-1} = -[m(1+m)(1+m+p)]^{-1}, \quad (3.c.22)$$

$$a_i = [m(1+p)]^{-1}, \quad (3.c.23)$$

$$a_{i+1} = [p(1+m)]^{-1}, \quad (3.c.24)$$

$$a_{i+2} = -[p(1+p)(1+m+p)]^{-1}, \quad (3.c.25)$$

$$p = (x_{i+2} - x_{i+1}) / (x_{i+1} - x_i), \quad (3.c.26)$$

$$m = (x_i - x_{i-1}) / (x_{i+1} - x_i), \quad (3.c.27)$$

where f can represent either u or v, or their counterparts in the geodesic coordinate system. The two dimensional (λ, φ) interpolant is obtained as a tensor product application of the one-dimensional interpolants, with λ interpolations done first. Assume the

departure point falls in the grid box $(\lambda_i, \lambda_{i+1})$ and $(\varphi_i, \varphi_{i+1})$. Four λ interpolations are performed to find q values at $(\lambda_D, \varphi_{j-1}), (\lambda_D, \varphi_j), (\lambda_D, \varphi_{j+1})$, and $(\lambda_D, \varphi_{j+2})$. This is followed by one interpolation in φ using these four values to obtain the value at (λ_D, φ_D). Cyclic continuity is used in longitude. In latitude, the grid is extended to include a pole point (row) and one row across the pole. The pole row is set equal to the average of the row next to the pole for q and to wavenumber 1 components for u and v. The row across the pole is filled with the values from the first row below the pole shifted π in longitude for q and minus the value shifted by π in longitude for u and v.

Once the departure point is known, the constituent value of $q^* = q_D^{n-1}$ is obtained as indicated in (3.*c*.5) by Hermite cubic interpolation (3.*c*.17), with cubic derivative estimates (3.*c*.18) and (3.*c*.19) modified to satisfy the Sufficient Condition for Monotonicity with C° continuity (SCMO) described below. Define $\Delta_i q$ by

$$\Delta_i q = \frac{q_{i+1} - q_i}{x_{i+1} - x_i} \,. \tag{3.c.28}$$

First, if $\Delta_i q = 0$ then

$$d_i = d_{i+1} = 0 \,. \tag{3.c.29}$$

Then, if either

$$0 \leq \frac{d_i}{\Delta_i q} \leq 3 \tag{3.c.30}$$

or

$$0 \leq \frac{d_{i+1}}{\Delta_i q} \leq 3 \tag{3.c.31}$$

is violated, d_i or d_{i+1} is brought to the appropriate bound of the relationship. These conditions ensure that the Hermite cubic interpolant is monotonic in the interval $[x_i, x_{i+1}]$.

The horizontal semi-Lagrangian sub-step (3.*c*.5) is followed by the vertical step (3.*c*.6). The vertical velocity $\dot{\eta}$ is obtained from that diagnosed in the dynamical calculations (3.*a*.93) by

$$(\dot{\eta})_{k+\frac{1}{2}} = \left(\dot{\eta}\,\frac{\partial p}{\partial \eta}\right)_{k+\frac{1}{2}} \Bigg/ \left(\frac{p_{k+1} - p_k}{\eta_{k+1} - \eta_k}\right), \tag{3.c.32}$$

with $\eta_k = A_k + B_k$. Note, this is the only place that the model actually requires an explicit specification of η. The mid-point of the vertical trajectory is found by iteration

$$\eta_M^{k+1} = \eta_A - \Delta t \dot{\eta}^n \left(\eta_M^k\right). \tag{3.c.33}$$

Note, the arrival point η_A is a mid-level point where q is carried, while the $\dot{\eta}$ used for the interpolation to mid-points is at interfaces. We restrict η_M by

$$\eta_1 \leq \eta_M \leq \eta_K, \tag{3.c.34}$$

which is equivalent to assuming that q is constant from the surface to the first model level and above the top q level. Once the mid-point is determined, the departure point is

calculated from

$$\eta_D = \eta_A - 2\Delta t \dot{\eta}^n (\eta_M), \tag{3.c.35}$$

with the restriction

$$\eta_1 \leq \eta_D \leq \eta_K. \tag{3.c.36}$$

The appropriate values of $\dot{\eta}$ and q are determined by interpolation (3.c.17), with the derivative estimates given by (3.c.18) and (3.c.19) for $i = 2$ to $K-1$. At the top and bottom we assume a zero derivative (which is consistent with (3.c.34) and (3.c.36)), $d_i = 0$ for the interval $k = 1$, and $\delta_{i+1} = 0$ for the interval $k = K-1$. The estimate at the interior end of the first and last grid intervals is determined from an uncentered cubic approximation; that is d_{i+1} at the $k = 1$ interval is equal to d_i from the $k = 2$ interval, and d_i at the $k = K-1$ interval is equal to d_{i+1} at the $k = K-2$ interval. The monotonic conditions (3.c.30) to (3.c.31) are applied to the q derivative estimates.

d. Mass fixers

The fixers which ensure conservation (2.a.4) are applied to the dry mass and water vapor so that

$$\int_2 \pi^+ - \int_3 q^+ \Delta p^+ = \int_2 \pi^- - \int_3 q^- \Delta p^- = \mathbf{P}, \tag{3.d.1}$$

$$\int_3 q^+ \Delta p^+ = \int_3 q^- \Delta p^-, \tag{3.d.2}$$

where, from the definition of the vertical coordinate,

$$\Delta p = p_0 \Delta A + \pi \Delta B, \tag{3.d.3}$$

and the integral $\int_2$ denotes the normal Gaussian quadrature while $\int_3$ includes a vertical sum followed by Gaussian quadrature. The actual fixers are chosen to have the form

$$\pi^+ (\lambda, \varphi) = \mathbf{M} \hat{\pi}^+ (\lambda, \varphi), \tag{3.d.4}$$

preserving the horizontal gradient of Π, which was calculated earlier during the inverse spectral transform, and

$$q^+ (\lambda, \varphi, \eta) = \hat{q}^+ + \alpha \hat{q}^+ |\hat{q}^+ - q^-|^\beta, \tag{3.d.5}$$

with $\beta = \frac{3}{2}$. In (3.d.4) and (3.d.5) the ($\hat{}$) denotes the provisional value before adjustment. The form (3.d.5) forces the arbitrary corrections to be small when the mixing ratio is small and when the change made to the mixing ratio by the advection is small. Satisfying (3.d.1) and (3.d.2) sequentially gives

$$\alpha = \frac{\int\limits_3 q^- \Delta p^- - \int\limits_3 \hat{q}^+ \Delta \hat{p}^+}{\int\limits_3 \hat{q}^+ |\hat{q}^+ - q^-|^\beta \, \Delta \hat{p}^+} \tag{3.d.6}$$

and

$$\mathbf{M} = \left(\mathbf{P} + \int\limits_3 q^- \Delta p^- \right) \Big/ \int\limits_2 \hat{\pi}^+ \ . \tag{3.d.7}$$

The correction for dry mass depends on water vapor amount, and the correction for water vapor depends on the dry mass. These corrections should be done simultaneously. Because they are done sequentially in CCM2, neither is exactly conserved. In practice, the error associated with a sequential adjustment is negligible.

4. MODEL PHYSICS

4.1 Tendency Physics

As discussed earlier, the tendency physics include (in the following order) the parameterization of cloud amount; the evaluation of radiative fluxes and atmospheric heating rates; the evaluation of surface fluxes; the soil temperature update; evaluation of free atmosphere vertical diffusivities, diagnosis of the PBL height, PBL diffusivities and non-local transport term followed by the vertical diffusion solution; evaluation of gravity wave drag tendencies; and Rayleigh friction. Note that for greater stability the formulation of many of these processes is implicit, and the time step is further sub-divided into time split steps for each component to make the solution of the tendency terms more practical. The final result of the evaluation of these processes is the net tendency attributable to the tendency physics as shown in (2.a.7). Also note that we use the more conventional p_s notation for surface pressure (as opposed to π) for the following model physics discussion.

a. Cloud Parameterization

Cloud amount (or cloud fraction) in the CCM2 is evaluated via a diagnostic method. This approach amounts to a generalization of the scheme introduced by Slingo (1987), and depends on relative humidity, vertical velocity, atmospheric stability and the convective precipitation rate (i.e., precipitation arising from the parameterization of moist convection, section 4h). Three types of cloud are diagnosed by the scheme: convective cloud, layered cloud, and low-level marine stratus. Some of the major changes from Slingo (1987) are: clouds are allowed to form in any tropospheric layer, except the layer nearest the surface; the minimum convective cloud fraction is 20% (i.e., for nonprecipitating cases); low-level frontal clouds occur for all $\omega < 0$; and the relative humidity thresholds for mid- and upper-level layered clouds are functions of atmospheric stability.

Total column convective cloud amount between the base and top of convective activity is diagnosed on the basis of the presence of moist convective activity and the associated convective precipitation rate using

$$\overline{A}_{\text{conv}} = 0.20 + 0.125 \ln(1.0 + P), \qquad (4.a.1)$$

where P is the convective precipitation rate in mm/day (see 4.h.36) and $\overline{A}_{\text{conv}}$ is not allowed to exceed 80%. The convective cloud amount in each layer is assumed to be randomly overlapped within the convectively active region, the bounds of which are provided by the moist convection parameterization. Thus, the total cloud fraction in (4.a.1) is distributed in the vertical according to

$$A_{\text{conv}} = 1.0 - (1.0 - \overline{A}_{\text{conv}})^{1/N}, \qquad (4.a.2),$$

where N is the number of model levels within the convectively active region. For the subsequent cloud fraction calculation, the large scale relative humidity within the grid box is adjusted to account for the assumption that the fraction of convective cloud, $\overline{A}_{\rm conv}$, is saturated. The specific humidity grid value itself is unchanged. Thus, the adjusted large scale relative humidity, $RH^{'}$, is given by

$$RH^{'} = \frac{RH - A_{\rm conv}}{1 - A_{\rm conv}} \,, \tag{4.a.3}$$

where RH is the actual grid box relative humidity. Frontal and tropical low cloud fraction, *i.e.,* clouds occurring below 700 mb, is diagnosed according to

$$A_c = \left(\frac{RH^{'} - 0.9}{0.1} \right)^2 \qquad \omega < 0 \,, \tag{4.a.4}$$

while stratus associated with low-level inversions is determined from

$$A_c = \begin{cases} 0 & RH^{'} < 0.6 \\ (-6.67 \frac{\partial \theta}{\partial p} - 0.667) \times & (1 - \frac{0.9 - RH'}{0.3}) \times \left(\frac{P-750}{150}\right) \\ & 0.6 \leq RH^{'} \leq 0.9 \quad \text{and} \\ & \frac{\partial \theta}{\partial p} < -0.125, 750 \leq p \leq 900 \\ (-6.67 \frac{\partial \theta}{\partial p} - 0.667) \times & \left(\frac{P-750}{150}\right) RH^{'} > 0.9 \quad \text{and} \\ & \frac{\partial \theta}{\partial p} < -0.125 \end{cases} \tag{4.a.5}$$

where $\frac{\partial \theta}{\partial p}$ is the maximum inversion strength and $RH^{'}$ is the adjusted layer relative humidity given by (4.a.3). The pressure factor, $\left(\frac{P-750}{150}\right)$, accounts for the transition from marine stratus cloud for low level inversions to trade cumulus clouds that occur for a higher inversion.

Middle and upper level cloud is defined to occur between 750 mb and

$$P_{\rm top} = 250 - 165 \cos^2 \phi \,. \tag{4.a.6}$$

Mid- and high-level stratified (or layered) cloud amount is determined from the relation

$$A_c = \max \left\{ 0 \,, \left[\frac{RH^{'} - RH_{\rm lim}(p,\phi)}{1 - RH_{\rm lim}(p,\phi)} \right]^2 \right\}, \tag{4.a.7}$$

$$RH_{\rm lim}(p,\phi) = .999 - .10 \left[1 - \frac{N^2}{2.5 \times 10^{-4}} \right], \tag{4.a.8}$$

where N^2 is the square of the Brunt-Väisällä frequency:

$$N^2 = -\frac{g^2 p}{\theta} \frac{\partial \theta}{\partial p}. \tag{4.a.9}$$

Note that the ratio $N^2/2.5\times10^{-4}$ is not allowed to exceed 1. The cloud cover in any layer is finally defined as

$$A_c = (1.0 - A_{conv})A_c + A_{conv}\,, \tag{4.a.10}$$

where A_c is not allowed to exceed 0.999. Cloud liquid water paths (LWP) are computed from a prescribed, meridionally and height varying, but time independent, cloud liquid water density (ρ_ℓ), Kiehl (1991):

$$\text{LWP} = \int \rho_\ell dz, \tag{4.a.11}$$

where

$$\rho_\ell = \rho_\ell^0 e^{(-z/h_\ell)}, \tag{4.a.12}$$

ρ_ℓ^0 is equal to 0.18 g m^{-3}, and h_ℓ is a meridionally varying, empirically derived local liquid water scale height currently evaluated as

$$h_\ell = A + B\cos^2\phi, \tag{4.a.13}$$

with $A = 1080$ and $B = 2000$. Using (4.a.13) and (4.a.11) to evaluate the LWP between pressures p_{k+1} and p_k results in a cloud liquid water path in layer k of

$$\text{LWP}\,(k) = \rho_\ell^0 h_\ell \left[e^{-z_{k+1/h_\ell}} - e^{-z_{k/h_\ell}}\right], \tag{4.a.14}$$

where z_k is the height of the k^{th} layer interface.

For diagnostic purposes, the CCM2 calculates three levels of cloud fraction, assuming random overlap. These diagnostics, denoted as low, middle, and high cloud, are bounded by the pressure levels p_s to 700 mb, 700 mb to 400 mb, and 400 mb to the model top.

b. Physical Parameterization of Radiation

Diurnal cycle

A diurnal cycle has been included in the CCM2 with the objective of treating the detailed interactions between the radiative effects of the diurnal cycle and the surface sensible and latent heat exchanges. In the standard configuration, both the longwave and shortwave heating rates are evaluated every model hour as discussed in the following sections. Between hourly evaluations, the longwave and shortwave fluxes and heating rates are held constant. The surface radiative fluxes are also fixed between hourly calculations. The incorporation of the diurnal cycle has also required the introduction of heat storage capabilities over land and sea ice surfaces, and will be discussed later in this section.

The insolation at the top of the model atmosphere is given by

$$S_I = S_0\epsilon\cos\zeta, \tag{4.b.1}$$

where S_0 is the solar constant, ζ is the solar zenith angle, and ϵ is the eccentricity factor (square of the ratio of mean to actual distance that depends on the time of year). We

represent the annual and diurnal cycle of solar insolation with a repeatable solar year of exactly 365 days and with a mean solar day of exactly 24 hours, respectively. The repeatable solar year does not allow for leap years. The expressions defining the annual and diurnal variation of solar insolation are given by:

$$\cos\zeta = \sin\phi\sin\delta - \cos\phi\cos\delta\cos(2\pi t_{\text{local}})$$

$$\epsilon = 1.000110 + .034221\cos\theta_0 + .001280\sin\theta_0 + .000719\cos 2\theta_0 + .000077\sin 2\theta_0$$

$$\delta = .006918 - .399912\cos\theta_0 + .070257\sin\theta_0 - .006758\cos 2\theta_0 +$$

$$.000907\sin 2\theta_0 - .002697\cos 3\theta_0 + .001480\sin 3\theta_0$$

where

$$\theta_0 = \frac{2\pi d}{365}(\text{mean orbit angle})$$

and

d = calendar day of year(= 0, for January 1 and 364 for December 31)

ϕ = latitude in radians

δ = solar declination in radians

t_{local} = calendar day with local time (ranges from 0.0 to 365.0).

Note that the calendar day d varies continuously throughout the repeatable year and is updated every model time step.

The expression for $\cos\zeta$ was taken from Sellers (1965, p.15), while the expressions for ϵ and δ were obtained from Paltridge and Platt (1976), pages 57 and 63, respectively. The eccentricity factor ϵ is appropriate for the current earth orbit and, according to Paltridge and Platt (1976), is accurate to better than 10^{-4}. Maximum eccentricity factor (the orbit point closest to the sun (perhelion)) occurs about January 3 (calendar day 2.0), and minimum ϵ (the orbit point farthest from the sun (aphelion)) occurs about July 5 (calendar day 185).

The declination δ (the angle between the celestial equator and the sun) is appropriate for the present earth obliquity of about $23\frac{1}{2}°$. The declination expression above is accurate to better than $3'$ of arc (Paltridge and Platt, 1976); since the change in declination in 24 hours is never greater than $30'$ of arc, (and remembering that the disc of the sun itself subtends an angle of $\sim 30'$ of arc), the above expression is quite an adequate approximation. Minimum declination δ occurs on about December 22 (calendar day 355.0), and maximum declination δ occurs on about June 21 (calendar day 172.0).

It does not seem necessary to compute solar insolation more accurately (for example, accounting for equation of time changes in the solar day during the year, or

accounting for long-term secular changes in orbit) for two reasons: (1) the solar insolation given above multiplies approximate factors dealing with the scattering and absorption in the model's atmosphere/surface system (for example, the surface albedos in the model are not known to an accuracy of better than 1–2% of solar insolation (Briegleb *et al.*, 1986), and (2) for multiyear model runs, it is desirable when looking at interannual variability that the solar insolation repeat precisely every year in order to eliminate this source of variation. The loss (in a run of larger than 4 years) of the leap year day seems an acceptable approximation since this loss would only amount to 5 days after a 20-year run, for example.

The local time (t_{local}) in the expression for $\cos\zeta$ depends on the calendar day as well as model longitude:

$$t_{\text{local}} = d + \frac{\lambda}{360^\circ}, \tag{4.b.2}$$

where λ = model longitude in degrees starting from Greenwich running eastward. This would mean, for example, that a model calendar day d having no fraction (such as 182.00) would refer to local midnight at Greenwich, and to local noon at the date line (180° longitude).

Solar radiation

The δ-Eddington approximation of Joseph, Wiscombe, and Weinman (1976) and also Coakley, Cess and Yurevich, (1983) has been adopted and is described in Briegleb (1992). This approximation has been shown to simulate quite well the effects of multiple scattering.

The solar spectrum is divided into 18 discrete spectral intervals (7 for O_3, 1 for the visible, 7 for H_2O, and 3 for CO_2). The CCM2 model atmosphere consists of a discrete vertical set of horizontally homogeneous layers within which radiative heating rates are to be specified. Each of these layers is considered to be a homogeneous combination of several radiatively active constituents. Solar irradiance, as well as surface reflectivity for direct and diffuse radiation in each spectral interval, are specified, as well as the cosine of the solar zenith angle.

The δ-Eddington method for CCM2 involves evaluating the δ-Eddington solution for the reflectivity and transmissivity for each layer in the vertical. The layers are then combined together, accounting for multiple scattering between layers, which allows evaluation of upward and downward spectral fluxes at each interface boundary between layers. This procedure is repeated for all spectral intervals to accumulate broad band fluxes, from which the heating rate can be evaluated from flux differences across each layer.

The δ-Eddington approximation allows for gaseous absorption by O_3, CO_2, O_2, and H_2O. Molecular scattering and cloud water droplet scattering/absorption are included.

A summary of the spectral intervals and the absorption/scattering data used in the formulation is given in Briegleb (1992).

For cloud scattering and absorption, the radiative parameterization of Slingo [1989] for liquid water droplet clouds is employed. In this parameterization, the optical properties of the cloud droplets are represented in terms of the prescribed liquid water path (LWP in units of kg m^{-2}, see 4.*a*.11–14) and effective radius, $r_e = \int r^3 n(r) dr / \int r^2 n(r) dr$, where $n(r)$ is the cloud drop size distribution over radius r;

$$\begin{aligned} \tau_c &= \mathrm{LWP}(a + \frac{b}{r_e}) \\ \omega &= 1 - c - dr_e \\ g &= e + fr_e \quad . \end{aligned} \tag{4.*b*.3}$$

The quantity τ_c is the cloud extinction optical depth (0 to ∞), ω is the particle single scattering albedo (0 to 1), g is the asymmetry parameter (–1 to +1), and $a...f$ are positive constant coefficients for 4 spectral ranges: (.25-.69 μm, .69-1.19 μm, 1.19-2.38 μm, and 2.38-4.00 μm). These parametric expressions represent the basic physical dependencies of the optical properties on effective radius r_e: larger effective radius for fixed LWP means fewer droplets and smaller effective cross section, hence, smaller τ_c. Larger droplets mean more absorption of radiation transmitted through the droplets, hence, smaller ω; larger droplets mean more forward scattering and hence, larger g. However, for the purposes of CCM2, the cloud droplet effective radius is fixed at 10μm, appropriate for marine stratocumulus clouds (Slingo, 1989).

Partial cloudiness and cloud overlap radiative effects are represented in the following manner. A parameterization that gives results approximately equal to the random overlap assumption, *without* the computational cost of calculating the spectrum of cloud cases and which gives the proper limits of zero cloud cover and complete cloud cover in a single layer, is utilized. The cloud extinction optical depth (τ_c) for each layer is modified as: $\tau_c' = \tau_c A_c^{\frac{3}{2}}$ and A_c is the fractional cloud cover in the layer; the power $\frac{3}{2}$ was found necessary to give results approximately the same as the random overlap assumption. Despite the simplicity of this assumption for dealing with partial cloud cover and cloud overlap effects, the resulting heating rates in a cloudy atmosphere are better represented than they were for CCM1.

The δ-Eddington scheme is implemented so that the solar radiation is evaluated once every model hour over the sunlit portions of the model earth. The surface albedo is specified in two wavebands (0.2-0.7 μm, and 0.7-5.0 μm) and distinguishes albedos for direct and diffuse incident radiation. Albedos for ocean surfaces, geographically varying land surfaces, and sea ice surfaces are distinguished (and summarized in Briegleb, 1992). Ozone is prescribed, and CO_2 is assumed to be uniformly mixed with constant mass mixing ratio. Diagnostic cloud amount (A_c) is evaluated every model hour just prior to

the solar radiation calculation. As mentioned previously, the clouds are assumed to be composed of water droplets, with a globally constant effective cloud radius (r_e) of 10 μm.

For some diagnostic purposes, such as estimating cloud radiative forcing (Kiehl and Ramanathan, 1990) a clear-sky absorbed solar flux is required. A diagnostic calculation is included to give an estimate of clear-sky column absorbed and surface absorbed flux. For computational efficiency, the clear sky top of atmosphere and surface fluxes are evaluated assuming two homogeneous atmospheric layers. The top layer contains only O_3, while the lower layer contains all other absorbers/scatterers except clouds. The actual surface albedos are employed.

Details of the implementation are as follows. The CCM2 model atmosphere is divided into $K+1$ layers in the vertical; an extra top layer (beyond the K layers specified by CCM2) is added. This extra layer prevents excessive heating in the CCM2 top layer when the top pressure is not very low; also, as CCM2 does not specify absorber properties above its top layer, the optical properties of the CCM2 top layer must be used for the extra layer. Layers are assumed to be horizontally and vertically homogeneous for each model gridpoint and are bounded vertically by layer interfaces. For each spectral band, upward and downward fluxes are computed on the layer interfaces (which include the surface and top interface). The spectral fluxes are summed and differenced across layers to evaluate the solar heating rate. The following discussion refers to each of the spectral intervals.

In general, several constituents absorb and/or scatter in each homogeneous layer. Every constituent is defined in terms of a layer extinction optical depth τ, single scattering albedo ω, asymmetry parameter g, and the forward scattering fraction f. The forward scattering fraction (not mentioned previously, see 4.*b*.3) is the fraction of radiation scattered into the strong forward peak and is taken as g^2 (see Briegleb, 1992). To define bulk layer properties, the combination formulas of Cess [1985] are used:

$$\tau = \sum_i \tau_i, \tag{4.b.4}$$

$$\omega = \frac{\sum_i \omega_i \tau_i}{\tau}, \tag{4.b.5}$$

$$g = \frac{\sum_i g_i \omega_i \tau_i}{\omega \tau}, \tag{4.b.6}$$

$$f = \frac{\sum_i f_i \omega_i \tau_i}{\omega \tau}, \tag{4.b.7}$$

where the sums are over all constituents.

The δ-Eddington solution for each layer requires scaled properties for τ, ω, g, given by the expressions:

$$\tau^* = \tau(1 - \omega f), \tag{4.b.8}$$

$$\omega^* = \omega\left(\frac{1-f}{1-\omega f}\right), \tag{4.b.9}$$

$$g^* = \frac{g-f}{1-f}. \tag{4.b.10}$$

The scaling accounts for the scattering effects of the strong forward peak in water droplet scattering. The δ-Eddington nonconservative ($\omega < 1$) solutions for each layer for direct radiation at cosine zenith angle μ_0 are (following the notation of Coakley, Cess, and Yurevich, 1983):

$$R(\mu_0) = (\alpha-\gamma)\overline{T}e^{-\tau^*/\mu_0} + (\alpha+\gamma)\overline{R} - (\alpha-\gamma), \tag{4.b.11}$$

$$T(\mu_0) = (\alpha+\gamma)\overline{T} + (\alpha-\gamma)\overline{R}e^{-\tau^*/\mu_0} - (\alpha+\gamma-1)e^{-\tau^*/\mu_0}, \tag{4.b.12}$$

$$\overline{R} = (u+1)(u-1)(e^{\lambda\tau^*} - e^{-\lambda\tau^*})N^{-1}, \tag{4.b.13}$$

$$\overline{T} = 4uN^{-1}, \tag{4.b.14}$$

where

$$\alpha = \frac{3}{4}\omega^*\mu_0\left(\frac{1+g^*(1-\omega^*}{1-\lambda^2\mu_0^2}\right), \tag{4.b.15}$$

$$\gamma = \frac{1}{2}\omega^*\left(\frac{1+3g^*(1-\omega^*)\mu_0^2}{1-\lambda^2\mu_0^2}\right), \tag{4.b.16}$$

$$N = (u+1)^2e^{\lambda\tau^*} - (u-1)^2e^{-\lambda\tau^*}, \tag{4.b.17}$$

$$u = \frac{3}{2}\left(\frac{1-\omega^*g^*}{\lambda}\right), \tag{4.b.18}$$

$$\lambda = \sqrt{3(1-\omega^*)(1-\omega^*g^*)}, \tag{4.b.19}$$

where $\mathrm{R}(\mu_0)$, $\mathrm{T}(\mu_0)$ are the layer reflectivity and transmissivity to direct radiation respectively, and $\overline{\mathrm{R}}$, $\overline{\mathrm{T}}$ are the layer reflectivity and transmissivity to diffuse radiation respectively. It should be noted that in some cases of small but nonzero ω, the diffuse reflectivity can be negative. For these cases, $\overline{\mathrm{R}}$ is set to 0, which produces negligible impact on fluxes and the heating rate.

To combine layers, it is assumed that radiation, once scattered, is diffuse and isotropic (including from the surface). For an arbitrary layer 1 (or combination of layers with radiative properties $R_1(\mu_0)$, $T_1(\mu_0)$,$\overline{R}_1$,$\overline{T}_1$) overlying layer 2 (or combination of layers with radiative properties $R_2(\mu_0)$, $T_2(\mu_0)$, and $\overline{R}_2$,$\overline{T}_2$), the combination formulas for direct and diffuse radiation incident from above are:

$$R_{12}(\mu_0) = R_1(\mu_0) + \frac{\overline{T}_1\{(T_1(\mu_0) - e^{-\tau_1^*/\mu_0})\overline{R}_2 + e^{-\tau_1^*/\mu_0}R_2(\mu_0)\}}{1-\overline{R}_1\overline{R}_2}, \tag{4.b.20}$$

$$T_{12}(\mu_0) = e^{-\tau_1^*/\mu_0} T_2(\mu_0) + \frac{\overline{T}_2\{(T_1(\mu_0) - e^{-\tau_1^*/\mu_0}) + e^{-\tau_1^*/\mu_0} R_2(\mu_0)\overline{R}_1\}}{1 - \overline{R}_1\overline{R}_2}, \tag{4.b.21}$$

$$\overline{R}_{12} = \overline{R}_1 + \frac{\overline{T}_1\overline{R}_2\overline{T}_1}{1 - \overline{R}_1\overline{R}_2}, \tag{4.b.22}$$

$$\overline{T}_{12} = \frac{\overline{T}_1\overline{T}_2}{1 - \overline{R}_1\overline{R}_2}. \tag{4.b.23}$$

Note that the transmissions for each layer ($T_1(\mu_0), T_2(\mu_0)$) and for the combined layers ($T_{12}(\mu_0)$) are total transmissions, containing both direct and diffuse transmission. Note also that the two layers (or combination of layers), once combined, are no longer a homogeneous system.

To combine the layers over the entire column, two passes are made through the layers, one starting from the top and proceeding downward, the other starting from the surface and proceeding upward. (In passing from the top down, the layer δ-Eddington computation of R(μ_0), T(μ_0), $\overline{\text{R}}$, $\overline{\text{T}}$ is terminated if the total transmission to direct radiation for the spectral band (normalized to 1.0 at top) is less than .001; this produces a negligible error and saves computational overhead). The result is that for every interface, the following combined reflectivities and transmissivities are available:

$e^{-\tau^*/\mu_0}$ = direct beam transmission from top of atmosphere to the interface (τ^* is the scaled optical depth from top-of-atmosphere to the interface),

$R_{up}(\mu_0)$ = reflectivity to direct solar radiation of entire atmosphere *below* the interface,

$T_{dn}(\mu_0)$ = total transmission to direct solar radiation incident from above to entire atmosphere *above* the interface,

$\overline{R}_{up}$ = reflectivity of atmosphere *below* the interface to diffuse radiation from above,

$\overline{R}_{dn}$ = reflectivity of atmosphere *above* the interface to diffuse radiation from below.

With these quantities, the upward and downward fluxes at every interface can be computed. For example, the upward flux would be the directly transmitted flux ($e^{-\tau*/\mu_0}$) times the reflection of the entire column below the interface to direct radiation ($R_{up}(\mu_0)$), plus the diffusely transmitted radiation from above that reaches the interface ($T_{dn}(\mu_0) - e^{-\tau*/\mu_0}$) times the reflectivity of the entire atmosphere below the interface to diffuse radiation from above ($\overline{R}_{up}$), all times a factor that accounts for multiple reflections

at the interface. A similar derivation of the downward flux is straightforward. The resulting expressions for the upward and downward flux are:

$$F_{up} = \frac{e^{-\tau^*/\mu_0} R_{up}(\mu_0) + (T_{dn}(\mu_0) - e^{-\tau^*/\mu_0})\overline{R}_{up}}{1 - \overline{R}_{dn}\overline{R}_{up}}, \tag{4.b.24}$$

$$F_{dn} = e^{-\tau^*/\mu_0} + \frac{(T_{dn}(\mu_0) - e^{-\tau^*/\mu_0}) + e^{-\tau^*/\mu_0} R_{up}(\mu_0)\overline{R}_{dn}}{1 - \overline{R}_{dn}\overline{R}_{up}}. \tag{4.b.25}$$

The upward and downward spectral fluxes at each interface are summed to evaluate the spectrally integrated fluxes, then differenced to produce the solar heating rate,

$$Q_{\text{sol}} = \frac{g}{c_p} \frac{F_{dn}(p_{k+1}) - F_{\text{up}}(p_{k+1}) - F_{dn}(p_k) + F_{up}(p_k)}{p_{k+1} - p_k} \tag{4.b.26}$$

which is added to the nonlinear term (Q) in the thermodynamic equation.

Longwave radiation

Longwave fluxes are calculated at each model level in both up and down directions. The approach to solving the transfer equations is to employ absorptivities and emissivities. Thus, the clear–sky fluxes at a half–level k are

$$F^{\downarrow}_{clr}(p_k) = B(0)\epsilon(0, p_k) + \int_o^{p_k} \alpha(p', p_k) \frac{dB}{dp'}(p') dp', \tag{4.b.27}$$

and

$$F^{\uparrow}_{clr}(p_k) = \sigma_B T_S^4 - \int_{p_k}^{p_s} \alpha(p', p_k) \frac{dB}{dp'}(p') dp', \tag{4.b.28}$$

where $B(p) = \sigma_B T^4(p)$ is just Stefan–Boltzmann's law, and the absorptivity is defined as

$$\alpha(p, p') = \frac{1}{\frac{dB}{dT}(p')} \int A_{\tilde{\nu}}(p', p) \frac{dB_{\tilde{\nu}}}{dT}(p') d\tilde{\nu}, \tag{4.b.29}$$

and the emissivity is

$$\epsilon(0, p) = \frac{1}{B(0)} \int A_{\tilde{\nu}}(0, p) B_{\tilde{\nu}}(0) d\tilde{\nu}, \tag{4.b.30}$$

where $A_{\tilde{\nu}}$ is the absorptivity due to a given gas, $B_{\tilde{\nu}}(p')$ is Planck's function, and $\tilde{\nu}$ is the wavenumber. An isothermal layer is assumed to exist from the model top to $p = 0$. For CO_2 and O_3, the band–absorptance technique is used to evaluate α and ϵ. This method uses the fact that gas absorption is limited to a finite spectral width. The Planck functions are evaluated at the center of the bands, and integration over $\tilde{\nu}$ is carried out for $A_{\tilde{\nu}}$. Thus,

$$\alpha_{CO_2}(p, p') = \frac{1}{4\sigma T^3(p')} \frac{dB_{CO_2}}{dT'}(p') A_{CO_2}(p', p). \tag{4.b.31}$$

B_{CO_2} is evaluated for $\tilde{\nu} = 667$ cm^{-1}, where $A_{CO_2}(p',p)$ is the broad–band absorptance from Kiehl and Briegleb (1991). Similarly,

$$\epsilon_{CO_2}(0,p) = \frac{1}{\sigma T^4(0)} B_{CO_2}(0) A_{CO_2}(0,p). \tag{4.b.32}$$

For ozone,

$$\alpha_{O_3}(p,p') = \frac{1}{4\sigma T^3(p')} \frac{dB_{O_3}}{dT'}(p') A_{O_3}(p',p), \tag{4.b.33}$$

and

$$\epsilon_{O_3}(0,p) = \frac{1}{\sigma T^4(0)} B_{O_3}(0) A_{O_3}(0,p), \tag{4.b.34}$$

where A_{O_3} is the ozone broad–band absorptance from Ramanathan and Dickinson (1979). A new feature to the longwave absorptance formulation for CCM2 is the inclusion of Voigt line profile effects for CO_2 and O_3. For the mid-to-upper stratosphere ($p \lesssim 10$mb), spectral absorption lines are no longer Lorentzian in shape. To account for the transition to Voigt lines a method described in Kiehl and Briegleb (1991) is employed. Essentially the pressure appearing in the mean line width parameter, γ,

$$\gamma = \gamma_o \frac{p}{p_0} \tag{4.b.35}$$

is replaced with

$$\gamma = \gamma_0 \left[\frac{p}{p_0} + \delta \sqrt{\frac{T}{250}} \right], \tag{4.b.36}$$

where $\delta = 5.0 \times 10^{-3}$ for CO_2 and $\delta = 2.5 \times 10^{-3}$ for O_3. These values insure agreement with line-by-line cooling rate calculations up to $p \approx 0.3$ mb. Water vapor cannot employ the broad–band absorptance method since H_2O absorption extends throughout the entire longwave region. The method of Ramanathan and Downey (1986) is used for water–vapor absorptivities and emissivities. The overlap treatment between water vapor and other gases is also described in Ramanathan and Downey (1986). Thus, the total absorptivity is given by

$$\alpha(p,p') = \alpha_{CO_2}(p,p') + \alpha_{O_3}(p,p') + \alpha_{H_2O}(p,p'), \tag{4.b.37}$$

and the total emissivity is

$$\epsilon(0,p) = \epsilon_{CO_2}(0,p) + \epsilon_{O_3}(0,p) + \epsilon_{H_2O}(0,p). \tag{4.b.38}$$

Clear–sky fluxes are thus obtained by integrating Equations (4.b.30) and (4.b.31). Details of the integration of these equations are given in Section 4.b.

The downward longwave clear–sky flux at the surface is thus,

$$F^{\downarrow}_{clr}(p_s) = B(0)\epsilon(0,p_s) + \int_o^{p_s} \alpha(p',p_s) \frac{dB}{dp'}(p') dp', \tag{4.b.39}$$

while the upward flux at the surface is just

$$F^{\uparrow}(p_s) = \sigma_B T_S^4. \tag{4.b.40}$$

The downward cloudy–sky flux at the surface is

$$F^{\downarrow}(p_s) = F^{\downarrow}_{clr}(p_s) f_{clear} + \sigma T^4(p_{clbk}) A'(p_{cl2}) + \sum_{k=3}^{KMAX} \left\{ \sigma T^4(p_{clbk}) + \int_{p_{clbk}}^{p_s} \alpha(p_s, p') \frac{dB(p')}{dp'} dp' \right\} f_{cld}(k), \tag{4.b.41}$$

where p_{clbk} is the pressure level of the cloud base at k.

The cloud emissivity is accounted for by defining an effective cloud amount for each model layer,

$$A'_k = \epsilon(p_k) A_k \tag{4.b.42}$$

where the broad–band emissivity, ϵ, is defined as

$$\epsilon(p_k) = 1 - e^{-0.1\mathrm{LWP}(k)}, \tag{4.b.43}$$

where the cloud liquid water path, LWP, is defined by (4.a.11). The 0.1 $\mathrm{m^2 g^{-1}}$ factor is an absorption coefficient based on observations of Griffith *et al.* (1980). $f_{cld}(k)$ is the probability of a cloud existing in layer k, and clear sky below this layer,

$$f_{cld}(k) = A'_k \prod_{i=2}^{k-1} (1 - A'_i), \tag{4.b.44}$$

or

$$f_{cld}(k) = A'_k \frac{\prod_{i=2}^{K} (1 - A'_i)}{\prod_{i=k}^{K} (1 - A'_i)}. \tag{4.b.45}$$

The clear-sky fraction for the total atmospheric column, f_{clear}, is given by

$$f_{clear} = \prod_{i=1}^{N} (1 - A'_i), \tag{4.b.46}$$

where A'_i is the fractional cloud cover in layer i and N is the total number of atmospheric layers. The fractional cloud cover is provided by the cloud parameterization scheme discussed in Section 4a. The net longwave flux at the surface is

$$F^N(p_s) = F^{\uparrow}(p_s) + F^{\downarrow}(p_s). \tag{4.b.47}$$

Fluxes within the atmosphere are evaluated at each model half–layer for longwave heating–rate calculations on full pressure–levels. The upward flux between the surface and the lowest cloud layer is equal to the clear–sky upward flux,

$$F^{\uparrow}_{blw}(p_k) = F^{\uparrow}_{clr}(p_k). \tag{4.b.48}$$

Within the layers that contain clouds, the upward flux is

$$F^{\uparrow}_{cld}(p_k) = F^{\uparrow}_{clr}(p_k) f_{clear}(k) + \sum_{\ell=k_{low}}^{k} \left\{ \sigma T^4(p_{cltl}) \right.$$
$$\left. - \int_{p_{cltl}}^{p_k} \alpha(p', p_{cltl}) \frac{dB}{dp'}(p') dp' \right\} \times f_{cld}(\ell) \quad p_{k_{low}} \le p_k \le p_{k+1}, \tag{4.b.49}$$

where $f_{cld}(\ell)$ is the probability that a cloud is in layer ℓ and clear sky exists above layer ℓ:

$$f_{cld}(\ell) = A'_\ell \prod_{i=\ell+1}^{k} (1 - A'_i) = A'_\ell \frac{\prod_{i=\ell+1}^{K} (1 - A'_i)}{\prod_{i=k+1}^{K} (1 - A'_i)}. \tag{4.b.50}$$

k_{low} is the lowest level of cloud, k_{HI} is the highest layer of cloud, and p_{cltl} is the cloud–top level. The upward flux above the clouds is obtained from a similar expression. The downward flux above the cloudy region is equal to the clear–sky flux,

$$F^{\downarrow}_{abv}(p_k) = F^{\downarrow}_{clr}(p_k). \tag{4.b.51}$$

Within the clouds and below the clouds, the downward flux is

$$F^{\downarrow}_{cld,blw}(p_k) = F^{\downarrow}_{clr}(p_k) f_{cld}(k) + \sum_{\ell=k}^{k_{HI}} \left\{ \sigma T^4(p_{clbl}) + \int_{p_{clbl}}^{p_k} \alpha(p', p) \frac{dB}{dp'}(p') dp' \right\}$$
$$\times f_{cld}(\ell), \qquad p_s \le p_k \le p_{HI}, \tag{4.b.52}$$

where p_{clbl} is the cloud–base level, $f_{cld}(\ell)$ is the probability of a cloud existing in layer ℓ and clear sky below this level,

$$f_{cld(\ell)} = A'_\ell \prod_{i=k}^{\ell=1} (1 - A'_i) = A'_\ell \frac{\prod_{i=k}^{K} (1 - A'_i)}{\prod_{i=\ell}^{K} (1 - A'_i)}. \tag{4.b.53}$$

The longwave atmospheric heating rate is obtained from

$$Q_{\ell w}(p_k) = \frac{g}{c_p} \frac{F^{\uparrow}(p_{k+1}) - F^{\downarrow}(p_{k+1}) - F^{\uparrow}(p_k) + F^{\downarrow}(p_k)}{p_{k+1} - p_k}. \tag{4.b.54}$$

which is added to the nonlinear term (Q) in the thermodynamic equation.

The full calculation of longwave radiation (which includes heating rates as well as boundary fluxes) is computationally expensive. Therefore, modifications to the longwave scheme were developed to improve its efficiency for the diurnal framework. For illustration, consider the clear-sky fluxes defined in (4.b.27) and (4.b.28). Well over 90% of the longwave computational cost involves evaluating the absorptivity α and emissivity ϵ. To reduce this computational burden, α and ϵ are computed at a user defined frequency that is set to

every 12 model hours in the standard configuration, while longwave heating rates are computed at the diurnal cycle frequency of once every model hour.

Calculation of α and ϵ with a period longer than the evaluation of the longwave heating rates neglects the dependence of these quantities on variations in temperature, water vapor, and ozone. However, variations in radiative fluxes due to changes in cloud amount are fully accounted for at each radiation calculation, which is regarded to be the dominant effect on diurnal time scales. The dominant effect on the heating rates of changes in temperature occurs through the Planck function and is accounted for with this method.

Numerical algorithms

The continuous equations for the infrared calculations require a sophisticated vertical finite–differencing scheme due to the integral term $\int \alpha dB$ in Equations (4.*b*.30)–(4.*b*.31). The reason for the additional care in evaluating this integral arises from the nonlinear behavior of α across a given model layer. For example, if the flux at interface p_k is required, an integral of the form $\int_{p_s}^{p_k} \alpha(p', p_k) dB(p')$ must be evaluated. For the nearest layer to level p_k, the following terms will arise:

$$\int_{p_{k+1}}^{p_k} \alpha(p', p_k) dB(p') = \frac{[\alpha(p_{k+1}, p_k) + \alpha(p_k, p_k)]}{2} [B(p_k) - B(p_{k+1})], \qquad (4.b.55)$$

employing the trapezoidal rule. The problem arises with the second absorptivity $\alpha(p_k, p_k)$, since this term is zero. It is also known that α is nearly exponential in form within a layer. Thus, to accurately account for the variation of $\alpha(p, p')$ across a layer, many more grid points are required than are available in CCM2. The nearest layer must, therefore, be subdivided and α must be evaluated across the subdivided layers. The algorithm that is employed in CCM2 is to use a trapezoid method for all layers except the nearest layer. For the nearest layer a subdivision, as illustrated in Figure 2, is employed.

For the upward flux, the nearest layer contribution to the integral is evaluated from

$$\int_{p_H^k}^{p_H^{k+1}} \alpha dB(p') = \alpha_{22} [B(p_H^{k+1}) - B(p^k)] + \alpha_{21} [B(p^k) - B(p_H^k)], \qquad (4.b.56)$$

while for the downward flux, the integral is evaluated according to

$$\int_{p_H^{k+1}}^{p_H^k} \alpha dB(p') = \alpha_{11} [B(p^k) - B(p_H^k)] + \alpha_{12} [B(p_H^{k+1}) - B(p^k)]. \qquad (4.b.57)$$

The α_{ij}, $i = 1, 2$; $j = 1, 2$, are absorptivities evaluated for the subdivided paths shown in Figure 2. The path–length dependence for the absorptivities arises from the dependence on the absorptance $A(p, p')$ [*e.g.*, Eq. (4.*b*.33)]. Temperatures are known at layer midpoints. Temperatures at layer interfaces are determined through linear interpolation in $\log p$ between layer midpoint temperatures. Thus, $B(p_k) = \sigma_B T_k^4$ can be

evaluated at all required levels. The most involved calculation arises from the evaluation of the fraction of layers shown in Figure 2. In general, the absorptance of a layer can require the evaluation of the following path lengths:

$$\xi(p_k, p_{k+1}) = f(\overline{T})\overline{p}\Delta p, \tag{4.b.58}$$

and

$$u(p_k, p_{k+1}) = g(\overline{T})\Delta p, \tag{4.b.59}$$

and

$$\beta(p_k, p_{k+1}) = h(\overline{T})\overline{p}, \tag{4.b.60}$$

where f, g, and h are functions of temperature due to band parameters (see Kiehl and Ramanathan, 1983), and $\overline{T}$ is an absorber mass–weighted mean temperature.

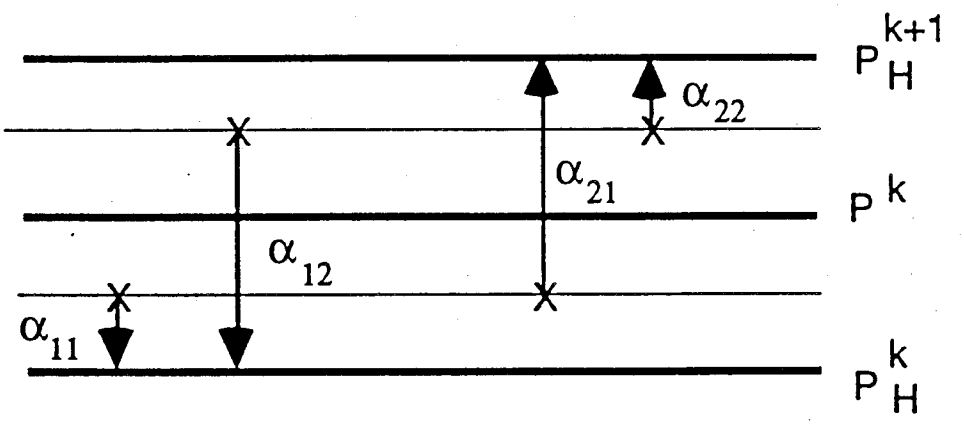

Figure 2. Subdivision of model layers for radiation flux calculation

These path lengths are, in particular, used extensively in the evaluation of A_{O_3} (Ramanathan and Dickinson, 1979) and A_{CO_2} (Kiehl and Briegleb, 1991). But path lengths dependent on both p^2 (*i.e.*, ξ) and p (*i.e.*, u) are also needed in calculating the water–vapor absorptivity, α_{H_2O} (Ramanathan and Downey, 1986). To account for the

subdivided layer, a fractional layer amount must be multiplied by ξ and u, *e.g.*,

$$\overline{\xi}_{11} = \xi(p_H^k, p_H^{k+1}) \times UINPL(1,k), \tag{4.b.61}$$

$$\overline{u}_{11} = u(p_H^k, p_H^{k+1}) \times WINPL(1,k), \tag{4.b.62}$$

and

$$\overline{\beta}_{11} = \beta(p_H^k, p_H^{k+1}) \times PINPL(1,k), \tag{4.b.63}$$

where $UINPL$, $WINPL$, and $PINPL$ are factors to account for the fractional subdivided layer amount. These quantities are derived for the case where the mixing ratio is assumed to be constant within a given layer (CO_2 and H_2O). For ozone, the mixing ratio is assumed to interpolate linearly in physical thickness; thus, another fractional layer amount $ZINPL$ is required for evaluating $A_{O_3}(p,p')$ across subdivided layers.

Consider the subdivided path for α_{22}; the total path length from p_H^k to p_H^{k+1} for the p^2 path length will be

$$\xi(p_H^k, p_H^{k+1}) \approx \overline{p}_H \left[p_H^k - p_H^{k+1}\right], \tag{4.b.64}$$

where $\overline{p}_H \equiv \frac{p_H^k + p_H^{k+1}}{2}$. The <u>total</u> layer path length is, therefore, proportional to

$$\xi(p_H^k, p_H^{k+1}) \approx \frac{1}{2}\left(\left(p_H^k\right)^2 - \left(p_H^{k+1}\right)^2\right). \tag{4.b.65}$$

The path length ξ for α_{22} requires the mean pressure

$$\overline{p}_{22} \approx \frac{1}{2}\left\{\frac{p^k + p_H^{k+1}}{2} + p_H^{k+1}\right\}, \tag{4.b.66}$$

and the pressure difference

$$\Delta p_{22} \approx \frac{p^k + p_H^{k+1}}{2} - p_H^{k+1}. \tag{4.b.67}$$

Therefore, the path ξ_{22} is

$$\xi_{22} \approx \overline{p}_{22}\ \Delta p_{22} = \frac{1}{2}\left\{\left(\frac{p^k + p_H^{k+1}}{2}\right)^2 - \left(p_H^{k+1}\right)^2\right\}. \tag{4.b.68}$$

The fractional path length is obtained by normalizing this by $\xi(p_H^k, p_H^{k+1})$,

$$UINPL(2,k) = DAF3(k)\left\{\left(\frac{p^k + p_H^{k+1}}{2}\right)^2 - \left(p_H^{k+1}\right)^2\right\}, \tag{4.b.69}$$

where

$$DAF3(k) = \frac{1}{\left(p_H^k\right)^2 - \left(p_H^{k+1}\right)^2}. \tag{4.b.70}$$

Similar reasoning leads to the following expressions for the remaining fractional path lengths, for α_{21},

$$UINPL(3,k) = DAF3(k)\left\{\left(\frac{p^k + p_H^k}{2}\right)^2 - \left(p_H^{k+1}\right)^2\right\}, \tag{4.b.71}$$

for α_{11},

$$UINPL(1,k) = DAF3(k)\left\{\left(p_H^k\right)^2 - \left(\frac{p^k + p_H^k}{2}\right)^2\right\}, \tag{4.b.72}$$

and for α_{12},

$$UINPL(4,k) = DAF3(k)\left\{\left(p_H^k\right)^2 - \left(\frac{p^k + p_H^{k+1}}{2}\right)^2\right\}. \tag{4.b.73}$$

The $UINPL$ are fractional layer amounts for path length that scale as p^2, *i.e.*, $\overline{\xi}_{ij}$.

For variables that scale linearly in p, *e.g.*, $\overline{u}_{ij}$, the following fractional layer amounts are used:

$$WINPL(1,k) = DAF4(k)\left\{\frac{p_H^k - p^k}{2}\right\}, \tag{4.b.74}$$

$$WINPL(2,k) = DAF4(k)\left\{\frac{p^k - p_H^{k+1}}{2}\right\}, \tag{4.b.75}$$

$$WINPL(3,k) = DAF4(k)\left\{\left(\frac{p_H^k + p^k}{2}\right) - p_H^{k+1}\right\}, \tag{4.b.76}$$

$$WINPL(4,k) = DAF4(k)\left\{p_H^k - \left(\frac{p_H^{k+1} + p^k}{2}\right)\right\}, \tag{4.b.77}$$

where

$$DAF4(k) = \frac{1}{p_H^k - p_H^{k+1}}. \tag{4.b.78}$$

These fractional layer amounts are directly analogous to the $UINPL$, but since $\overline{u}$ is linear in p, the squared terms are not present.

The variable $\overline{\beta}_{ij}$ requires a mean pressure for the subdivided layer. These are

$$PINPL(1,k) = \frac{1}{2}\left\{\frac{p^k + p_H^k}{2} + p_H^k\right\}, \tag{4.b.79}$$

$$PINPL(2,k) = \frac{1}{2}\left\{\frac{p^k + p_H^{k+1}}{2} + p_h^{k+1}\right\}, \tag{4.b.80}$$

$$PINPL(3,k) = \frac{1}{2}\left\{\frac{p^k + p_H^k}{2} + p_H^{k+1}\right\}, \tag{4.b.81}$$

$$PINPL(4,k) = \frac{1}{2}\left\{\frac{p^k + p_H^{k+1}}{2} + p_H^k\right\}. \tag{4.b.82}$$

Finally, fractional layer amounts for ozone path lengths are needed, since ozone is interpolated linearly in physical thickness. These are given by

$$ZINPL(1,k) = \frac{1}{2}\frac{\ell n\left(\frac{p_H^k}{p_k}\right)}{\ell n\left(\frac{p_H^k}{p_H^{k+1}}\right)}, \tag{4.b.83}$$

$$ZINPL(2,k) = \frac{1}{2}\frac{\ell n\left(\frac{p^k}{p_H^{k+1}}\right)}{\ell n\left(\frac{p_H^k}{p_H^{k+1}}\right)}, \tag{4.b.84}$$

$$ZINPL(3,k) = ZINPL(1,k) + 2ZINPL(2,k), \tag{4.b.85}$$

$$ZINPL(4,k) = ZINPL(2,k) + 2ZINPL(1,k). \tag{4.b.86}$$

c. Surface Energy Exchanges

The boundary condition on the surface/sub-surface temperature calculation discussed in the next section is the net surface energy flux given by

$$F_{\text{net}}(T_s) = F_{\text{RAD}} - \sigma T_s^4 - c_p\rho_1(\overline{w'\theta'})_s - L\rho_1(\overline{w'q'})_s, \tag{4.c.1}$$

where F_{RAD} is the absorbed solar flux plus the downward longwave flux (provided by the radiation parameterization); $c_p\rho_1(\overline{w'\theta'})_s$ is the surface sensible heat flux (positive *into* the atmosphere); $L\rho_1(\overline{w'q'})_s$ is the surface latent heat flux (positive *into* the atmosphere); and σT_s^4 is the longwave blackbody surface emission.

The surface sensible and latent heat fluxes, along with their momentum counterparts are defined by:

$$c_p\rho_1(\overline{w'\theta'})_s = c_p\rho_1 C_H|\mathbf{V}_1|(\theta_s - \theta_1), \tag{4.c.2}$$

$$L\rho_1(\overline{w'q'})_s = L\rho_1 D_w C_H\,|\mathbf{V}_1|\,(q_s^* - q_1), \tag{4.c.3}$$

$$\rho_1(\overline{w'u'})_s = -\rho_1 C_M|\mathbf{V}_1|u_1, \tag{4.c.4}$$

$$\rho_1(\overline{w'v'})_s = -\rho_1 C_M|\mathbf{V}_1|v_1, \tag{4.c.5}$$

where $\mathbf{V}, u, v, w, \theta, q,$ and ρ are the horizontal velocity vector, zonal, meridional and vertical wind components, potential temperature, specific humidity, and density, respectively. The subscripts s and 1 refer to values at the surface and at the lowest model level, respectively. The additional factor, D_w, in (4.c.3) is the potential evaporation which

represents the availability of water from the surface as a fraction of that available from a water surface. The variable q_s^* is defined as the saturation value of q at temperature T_s. We note that L is either the latent heat of vaporization L_v, or the sum of the latent heat of vaporization and latent heat of fusion L_i. The distinction between the two is noted where appropriate later in the text.

Following Louis *et al.* (1982) and Holtslag and Beljaars (1989), the two surface layer exchange coefficients used in (4.*c*.2)–(4.*c*.5) are defined as:

$$C_M = C_N f_M(Ri_s), \tag{4.c.6}$$

$$C_H = C_N f_H(Ri_s). \tag{4.c.7}$$

The neutral exchange coefficient is:

$$C_N = \frac{k^2}{\ln\left((z_1 + z_0)/z_0\right) \ln\left((z_1 + z_0)/z_0\right)}, \tag{4.c.8}$$

where $k = 0.4$ is the Von Karman constant, z_1 is the height of the lowest model level, and z_0 is the roughness length for momentum. Here we have assumed that the roughness lengths for momentum, heat, and constituents are the same, which is not true in general (see Beljaars and Holtslag 1991). If differing roughness lengths are accounted for, then the neutral exchange coefficients for heat and momentum differ. For heat, the denominator in (4.*c*.8) becomes $\ln\left((z_1 + z_{0M})/z_{0M}\right) \ln\left((z_1 + z_{0H})/z_{0H}\right)$, where z_{0M} and z_{0H} represent the roughness lengths for momentum and heat respectively. In CCM2, the roughness length over land varies geographically, based on surface type data (see Table 1), while over ocean $z_0 = 10^{-4}$ m. The roughness lengths (z_0) and potential evaporation (D_w) were determined by assigning values shown in Table 1 to Matthews' (1983) $1° \times 1°$ vegetation data and arithmetically averaging all values within each CCM2 grid box, including ocean values near coast lines. Over open water, sea-ice, and any land covered with snow, D_w=1. Further discussion can be found in Section 5b.

The surface layer Richardson number in (4.*c*.6) and (4.*c*.7) is defined as:

$$Ri_s = \frac{g z_1 (\theta_{v1} - \theta_{vs})}{\theta_1 |\mathbf{V}_1|^2}, \tag{4.c.9}$$

where g is the acceleration of gravity, θ_{v1} and θ_{vs} are the virtual potential temperatures, and $|\mathbf{V}_1|^2 \geq 1$. Under unstable conditions ($Ri_s < 0$), the functions which modify the neutral exchange coefficient are taken from Louis *et al.* (1982):

$$f_M(Ri_s) = 1 - \frac{10Ri}{1 + 75C_N \left\{\left((z_1 + z_0)/z_0\right) |Ri_s|\right\}^{1/2}}, \tag{4.c.10}$$

$$f_H(Ri_s) = 1 - \frac{15Ri}{1 + 75C_N \left\{\left((z_1 + z_0)/z_0\right) |Ri_s|\right\}^{1/2}}. \tag{4.c.11}$$

Under stable conditions ($Ri_s \geq 0$), the functions which modify the neutral exchange coefficient are taken from Holtslag and Beljaars (1989):

$$f_M(Ri_s) = f_H(Ri_s) = \frac{1}{1 + 10Ri_s\,(1 + 8Ri_s)}. \qquad (4.c.12)$$

The above forms for f_M and f_H are reasonable fits to available observations in the surface layer as shown by Holtslag and Beljaars (1989).

TABLE 1: Surface Data for Roughness Length, Potential Evaporation, and Thermal Surface Type

Type	Description[1]	Matthews' Vegetation Type[2]	Roughness[3] Length(m)	Potential Evaporation[4]	Thermal[5] Surface Type
1	Mixed farming tall grassland	W (Cultivation intensity>75%)	.06	.25	6
2A	Tall/medium grassland evergreen shrubland	H,I,O,Q,R	.10	.10	6
2B	Short grassland, meadow and shrubland	J,L,P,S,T	.05	.10	6
3	Evergreen forest (needleleaved)	4,5,7,8	1.00	.25	5
4	Mixed deciduous evergreen forest	A	.90	.25	5
5	Deciduous forest	9,B	.80	.25	5
6	Tropical evergreen broad-leafed forest	1,2,3	2.00	.25	4
7	Medium/tall grassland woodlands	6,C,D,E F,G,N	.60	.25	5
8	Desert	U	.05	.01	7
9	Tundra	K,M	.04	.25	6
10	Land Ice	—	.04	1.00	2

[1]See also Briegleb *et al.* (1986).
[2]The association of Matthews' (1983) more detailed types and the types here was done both by using Matthews' description, as well as surface albedos (Matthews, private communication), and other observations—see Briegleb and Ramanathan (1982) and Briegleb *et al.* (1986).
[3]Roughness Length z_0, from Dickinson *et al.*, (1986).
[4]Potential Evaporation, D_w
[5]Determines surface thermal properties; see Table 2.

Land surface properties, such as the potential evaporation, and snow cover are prescribed in the initial release of CCM2. These properties are internally determined by

the model when exercising the optional BATS land surface parameterization (Dickinson *et al.*, 1993; Bonan, 1993).

A seasonally varying snow cover that depends only on latitude and month is also prescribed. If S_{JAN} and S_{JULY} are respectively the January and July water equivalent snow depth values, then the water equivalent snow depth for calendar day d is given by

$$S(d) = \overline{S} + A_S \cos\left(\frac{2\pi}{365}(d - d_0)\right), \tag{4.c.13}$$

$$\overline{S} = \frac{1}{2}(S_{JAN} + S_{JULY}), \tag{4.c.14}$$

$$A_S = \frac{1}{2}(S_{JAN} - S_{JULY}), \tag{4.c.15}$$

where $d_0 = 46.0$ (phase of max/min in snow depth), and if $S < S_{MIN} = 0.001$ m, $S = 0$. The reference January and July values of the snow depth S are determined using the data of Forderhase *et al.*, (1980). Regions where the snow depth was undetermined are set to 30 mm for January and 10 mm for July on the original 5°×5° grid. Over the Antarctic, a constant (*i.e.*, seasonally invariant) value of 20 mm was assumed. Bilinear interpolation was used to evaluate the data on the model Gaussian grid.

Since surface albedo and potential evaporation are strongly influenced by variations in snow cover, the fraction of the surface covered by the prescribed snow amount (*i.e.*, the fraction which has snow properties) is estimated by

$$f_{snow} = \frac{20S}{20S + z_f} \tag{4.c.16}$$

(see Briegleb, 1992; Dickinson *et al.*, 1986). The surface aerodynamic roughness z_f equals z_0 when $z_0 \geq 0.25$ m, and has a minimum of 0.25 m.

Whenever a particular grid location has nonzero snow depth S, D_w is modified according to the relation

$$\widetilde{D_w} = f_{snow} + (1 - f_{snow})D_w, \tag{4.c.17}$$

where f_{snow} is the same horizontal snow cover fraction used in the surface albedo computation, and D_w is the fixed evaporation factor assigned to the underlying surface.

d. Surface/Soil Temperature Calculation

Land and sea ice surfaces, with and without snow cover, are modeled as horizontally homogeneous media of vertically varying thermal properties (see Table 2). The subsurface temperatures are assumed to obey the thermal diffusion equation:

$$\rho C \frac{\partial T}{\partial t} = -\frac{\partial F}{\partial z} \qquad F = -\kappa \frac{\partial T}{\partial z}, \tag{4.d.1}$$

where T is temperature, t time, ρ mass density (kg m^{-3}), C the mass heat capacity (J kg^{-1}K^{-1}), F the thermal flux (positive downward), z physical depth (m), and κ the

thermal conductivity (W $m^{-1}K^{-1}$). At the surface/atmosphere interface, the net energy flux and its first partial derivative, with respect to surface temperature, are assumed given. At the lower boundary over land surfaces, a zero heat flux condition is imposed. Over sea ice a constant ocean temperature condition (–2°C) is maintained, allowing for heat transfer between the lowest sea ice layer and the underlying ocean.

The thermal diffusion equation is solved in finite difference form for an arbitrary number of layers using a fully implicit Crank-Nicholson scheme (see Smith, 1965):

$$\rho_\ell C_\ell \left(\frac{T_\ell^{n+1} - T_\ell^n}{\Delta t} \right) = - \left(\frac{\partial F}{\partial z} \right)_\ell^{n+1} , \qquad (4.d.2)$$

where $\ell = 1, 2, \ldots,$ L refers to the layer index (1 = surface, increasing downward), n is the time index, and Δt = model time step. The implementation allows for variable κ, ρ, C and layer depths z. At the surface atmosphere interface, the net flux is allowed to have a linear temperature dependence making the scheme a backward-implicit method of solving for T (see Washington and Verplank, 1986).

As shown earlier (4.c.1), the net surface energy flux is given by

$$F_{\text{net}}(T_s) = F_{\text{RAD}} - \sigma T_s^4 - c_p \rho_1 (\overline{w'\theta'})_s - L\rho_1 (\overline{w'q'})_s . \qquad (4.d.3)$$

The net surface flux energy derivative with respect to temperature is assumed to be given by

$$\left. \frac{\partial F_{\text{net}}}{\partial T_s} \right|_{T_s^n} = - \left. \frac{\partial SH}{\partial T_s} \right|_{T_s^n} - \left. \frac{\partial LH}{\partial T_s} \right|_{T_s^n} , \qquad (4.d.4)$$

where $SH \equiv c_p \rho_1 \overline{(w'\theta')}_s$ and $LH \equiv L\rho_1 \overline{(w'q')}_s$. Note that the longwave surface emission temperature dependence is ignored in this relationship in order to fix all radiation dependencies on temperature during the surface temperature computation. This procedure is followed to be consistent with the time integration procedure, and to ensure that energetically, the precise energy fluxes used to forecast the temperature

$$\left(F_{net}(T_s^n) + \left. \frac{\partial F_{\text{net}}}{\partial T_s} \right|_{T_s^n} (T_s^{n+1} - T_s^n) \right) \qquad (4.d.5)$$

are consistent with the fluxes previously calculated by the radiation, and with those passed on to the vertical diffusion routines.

Once the forecast temperature T_s^{n+1} is available, the net flux terms of sensible and moisture flux from the surface into the lowest model atmospheric level (required by the vertical diffusion) are evaluated as:

$$SH^{n+1} = SH^n + \left. \frac{\partial SH}{\partial T_s} \right|_{T_s^n} (T_s^{n+1} - T_s^n) , \qquad (4.d.6)$$

$$Q^{n+1} = Q^n + \left. \frac{\partial Q}{\partial T_s} \right|_{T_s^n} (T_s^{n+1} - T_s^n) , \qquad (4.d.7)$$

where the moisture flux Q is the kinematic quantity $(\overline{w'q'})$ for surfaces above melting temperature and $\{LH/(\rho_1(L_v + L_i))\}$ for surfaces below melting temperature, where L_v and L_i are the latent heats of vaporization and fusion respectively.

TABLE 2: Surface Thermal Properties for Four Layers

Thermal Surface Type[1]	Description	κ_0[2]	θ	κ[2]	C_v[3]	C[4]	D_{top}[5]	D_{day}[5]	$D_{14\text{ days}}$[5]	D_{year}[5]	ρ[6]
2	sea ice	—	—	2.20	1.90×10^6	2.07×10^3	.50	.50	.50	.50	9.2×10^2
3	land ice	—	—	2.20	1.90×10^6	2.07×10^3	.25	.50	.50	8.50	9.2×10^2
4	equat forest	0.8	.40	1.408	2.60×10^6	1.04×10^3	.10	.366	1.369	6.99	2.5×10^3
5	mid-lat forest	0.8	.20	1.104	1.80×10^6	7.20×10^2	.09	.390	1.459	7.45	2.5×10^3
6	shrubland	0.9	.10	1.071	1.40×10^6	5.60×10^2	.08	.435	1.628	8.31	2.5×10^3
7	desert	1.0	.01	1.019	1.04×10^6	4.16×10^2	.06	.492	1.841	9.40	2.5×10^3

1 ocean is type 1
2 (W $m^{-1}K^{-1}$)
3 (J $m^{-3}K^{-1}$)
4 (J $kg^{-1}K^{-1}$)
5 (m)
6 (kg m^{-3})

The thermal properties of the surface were chosen as follows: the thermal surface type (see Table 1 and Table 2) is the *dominant* type (i.e. the most frequently occurring within a Gaussian grid box) determined by ascribing values of Table 1 to the 1°×1° resolution data of Matthews (1983). The thermal properties for each surface (thermal type) are based on a parameterization developed by Verstraete (1988): for all soil types at all times, the volume heat capacity is parameterized by

$$C_v(\theta) = (1 + 4\theta)10^6(\text{J m}^{-3}\text{K}^{-1}), \tag{4.d.8}$$

where θ is the volumetric soil water content, which can vary from 0 (completely dry soil) to 0.5 (water fills the available space in the soil, *i.e.*, 50%). Similarly, the soil thermal conductivity is given by

$$\kappa(\theta) = \kappa_0(1 + 1.9\theta)(\text{W m}^{-1}\text{K}^{-1}), \tag{4.d.9}$$

where κ_0 is 0.8 W $m^{-1}K^{-1}$ for loam, 0.9 W $m^{-1}K^{-1}$ for clay, and 1.0 W $m^{-1}K^{-1}$ for sand.

One can choose depths for any number of subsurface layers based on the soil penetration depth (taken to be three times the e-folding depth of a sinusoidally varying surface temperature $\sqrt{2\kappa/C_v\omega}$, where ω = circular frequency of surface temperature oscillation; see Sellers, 1965):

$$D = 3\sqrt{\frac{2\kappa}{C_v\omega}}, \tag{4.d.10}$$

where ω is taken for any desired list of times. The mass density is chosen to be a constant (2.5×10^3 kg m^{-3}).

The thickness of the topmost ground layer was chosen so that the diurnal range (maximum to minimum temperature) and phase (peak temperature lag with respect to solar incident maxima at local noon) compared reasonably well to observations referred to in Bhumralkar (1975).

As mentioned previously, the number of layers is arbitrary. In Table 2 we give an example of four layers (used in the standard implementation), where the lowest three layers from the top have equivalent periods of one day, two weeks, and one year, respectively. Over land, we are assuming that the top layer (of 6–10 cm thickness) absorbs all incident solar radiation. Over sea/land ice, which is partially transparent to solar radiation (compared to soil), we arbitrarily chose a constant layer thickness of 50 cm.

When snow cover is present over land we assume that the snow is homogeneously mixed by mass to determine the thermal properties of the surface:

$$
\begin{aligned}
\rho_1 &= \text{soil mass density of top layer} \\
C_1 &= \text{soil mass specific heat of top layer} \\
\kappa_1 &= \text{soil thermal conductivity of top layer} \\
z_1 &= \text{depth of top layer} \\
\rho_s, C_s, \kappa_s, z_s &= \text{same properties as above, but for snow} \\
m_1 &= \text{total mass of top layer} \equiv \rho_1 z_1 \text{ (without snow)} \\
m_s &= \text{total snow mass} \equiv \rho_s z_s \\
\rho_T &= \frac{m_1\rho_1 + m_s\rho_s}{m_1 + m_s} \\
C_T &= \frac{m_1 c_1 + m_s c_s}{m_1 + m_s} \\
\kappa_T &= \frac{m_1\kappa_1 + m_s\kappa_s}{m_1 + m_s} \\
z_T &= \frac{m_1 z_1 + m_s z_s}{m_1 + m_s} \quad .
\end{aligned}
$$

Rather than placing a horizontally uniform but arbitrarily thin snow layer over the surface, this mixing by mass was done to avoid numerical oscillations from occurring. In any case, homogeneous mass mixing to determine thermal properties was deemed physically realistic.

We note that the thermal properties of the snow (ρ, C, κ), *before* mixing with the top surface layer, are assumed to be equal to a 10% ice and 90% air mixture. We assume that the physical depth of the snow is 10 times its liquid water equivalent depth.

Numerical algorithms

The general diffusion equation is:

$$
\rho C \frac{\partial T}{\partial t} = -\frac{\partial F}{\partial z} = -\frac{\partial}{\partial z}\left(-\kappa \frac{\partial T}{\partial z}\right), \qquad (4.d.11)
$$

where the thermal heat flux F is positive downward; ρ is the mass density (kg m^{-3}), C is the heat capacity by mass (J kg^{-1} K^{-1}), and κ is the thermal conductivity (W m^{-1} K^{-1}).

We assume L homogeneous layers, for which the thermal and physical properties (κ, C, ρ) are constant within each layer, and allow variable layer thickness. The backward implicit top boundary condition is:

$$F_{\text{net}} + \frac{\partial F_{\text{net}}}{\partial T_s} |_{T_s^n} \left(T_s^{n+1} - T_s^n\right). \tag{4.d.12}$$

There are three general equations: for the *top* layer, for any intermediate layer, and for the bottom layer. All three equations will apply whenever L ≥ 3. The general fully implicit finite difference equation for times $n+1$ and n is

$$\rho_\ell C_\ell \left(\frac{T_\ell^{n+1} - T_\ell^n}{\Delta t}\right) = -\left(\frac{\partial F}{\partial z}\right)_\ell^{n+1}, \tag{4.d.13}$$

where ℓ = layer index (1,2, ... L from top to bottom), and where Δt = model time step. (Note that $T_s = T_1$).

We approximate the flux and temperature derivatives as follows (and suppress the time index n for simplicity):

$$\left(\kappa \frac{\partial T}{\partial z}\right)_\ell = \overline{\kappa}_{\ell+1,\ell} \frac{T_{\ell+1} - T_\ell}{\overline{z}_{\ell+1} - \overline{z}_\ell}, \tag{4.d.14}$$

where $\overline{z}_\ell$ is the mid-point depth of layer $\ell = \frac{1}{2}(z_\ell + z_{\ell-1})$, z_ℓ is the geometrical depth of layer interfaces where $\ell = 0$ is the surface/atmosphere top interface and z_{L} is the bottom interface with a perfectly insulated medium, and $\overline{\kappa}_{\ell+1,\ell} = \frac{1}{2}(\kappa_\ell + \kappa_{\ell+1})$.

The flux derivative is then:

$$\left(-\frac{\partial F}{\partial z}\right)_\ell = \frac{\overline{\kappa}_{\ell+1,\ell}\left(\frac{T_{\ell+1}-T_\ell}{\overline{z}_{\ell+1}-\overline{z}_\ell}\right) - \overline{\kappa}_{\ell,\ell-1}\left(\frac{T_\ell - T_{\ell-1}}{\overline{z}_\ell - \overline{z}_{\ell-1}}\right)}{z_\ell - z_{\ell-1}}. \tag{4.d.15}$$

Defining $\Delta z_\ell = z_\ell - z_{\ell-1}$ (ℓ^{th} layer physical thickness)
$\Delta z_\ell^+ = \overline{z}_{\ell+1} - \overline{z}_\ell$ (ℓ^{th} layer mid-point physical thickness with layer below)
$\Delta z_\ell^- = \overline{z}_\ell - \overline{z}_{\ell-1}$ (ℓ^{th} layer mid-point physical thickness with layer above)

gives:

$$\begin{aligned}\left(-\frac{\partial F}{\partial z}\right)_\ell &= \frac{1}{\Delta z_\ell}\left\{\frac{\overline{\kappa}_{\ell+1,\ell}}{\Delta z_\ell^+}(T_{\ell+1} - T_\ell) - \frac{\overline{\kappa}_{\ell,\ell-1}}{\Delta z_\ell^-}(T_\ell - T_{\ell-1})\right\} \\ &= \frac{1}{\Delta z_\ell}\left\{\frac{\overline{\kappa}_{\ell+1,\ell}}{\Delta z_\ell^+} T_{\ell+1} - \left(\frac{\overline{\kappa}_{\ell,\ell-1}}{\Delta z_\ell^-} + \frac{\overline{\kappa}_{\ell+1,\ell}}{\Delta z_\ell^+}\right) T_\ell + \frac{\overline{\kappa}_{\ell,\ell-1}}{\Delta z_\ell^-} T_{\ell-1}\right\}.\end{aligned} \tag{4.d.16}$$

Defining

$$f_\ell^+ = \frac{1}{\Delta z_\ell \Delta z_\ell^+} \qquad f_\ell^- = \frac{1}{\Delta z_\ell \Delta z_\ell^-} \tag{4.d.17}$$

gives:

$$\left(-\frac{\partial F}{\partial z}\right)_\ell = \left(\overline{\kappa}_{\ell+1,\ell}\, f_\ell^+\right) T_{\ell+1} - \left(\overline{\kappa}_{\ell,\ell-1}\, f_\ell^- + \overline{\kappa}_{\ell+1,\ell}\, f_\ell^+\right) T_\ell + \left(\overline{\kappa}_{\ell,\ell-1}\, f_\ell^-\right) T_{\ell-1}. \tag{4.d.18}$$

Consider the *top layer* equation first:

$$\rho_1 C_1 \left(\frac{T_1^{n+1} - T_1^n}{\Delta t} \right) = - \left(\frac{\partial F}{\partial z} \right)_1^{n+1}$$

$$= \left(\frac{\left(\frac{\overline{\kappa}_{21}(T_2^{n+1} - T_1^{n+1})}{\overline{z}_2 - \overline{z}_1} \right) + F_{\text{net}}^n + \left. \frac{\partial F_{\text{net}}}{\partial T_s} \right|_{T_1^n} (T_1^{n+1} - T_1^n)}{z_1 - z_0} \right). \qquad (4.d.19)$$

Collecting the $n+1$ temperatures on the left-hand side and all known terms n on the right-hand side gives

$$\left\{ \frac{\rho_1 C_1}{\Delta t} + \overline{\kappa}_{21}\, f_1^+ - \left(\frac{\left. \frac{\partial F_{\text{net}}}{\partial T_s} \right|_{T_s^n}}{z_1 - z_0} \right) \right\} T_1^{n+1} +$$

$$\left\{ -\overline{\kappa}_{21}\, f_1^+ \right\} T_2^{n+1} = \frac{F_{\text{net}}}{z_1 - z_0} + \left\{ \frac{\rho_1 C_1}{\Delta t} - \frac{\left. \frac{\partial F_{\text{net}}}{\partial T_s} \right|_{T_s^n}}{z_1 - z_0} \right\} T_1^n \qquad (4.d.20)$$

Next, consider an *intermediate layer* ℓ ($\ell \geq 2$ and $\ell \leq L-1$):

$$\left(-\overline{\kappa}_{\ell,\ell-1}\, f_\ell^- \right) T_{\ell-1}^{n+1} + \left\{ \frac{\rho_\ell C_\ell}{\Delta t} + \left(\overline{\kappa}_{\ell,\ell-1}\, f_\ell^- + \overline{\kappa}_{\ell+1\ell}\, f_\ell^+ \right) \right\} T_\ell^{n+1}$$

$$- \left(\overline{\kappa}_{\ell+1\ell}\, f_\ell^+ \right) T_{\ell+1}^{n+1} = \frac{\rho_\ell C_\ell}{\Delta t} T_\ell^n \qquad (4.d.21)$$

Finally, for *the bottom layer* we consider the bottom boundary condition to be *fixed* temperature (equal to $T_B = -2°\text{C}$ for sea ice overlying an ocean), or zero flux condition (over land).

Consider the zero flux condition first. In this case, $T_{\text{L}+1}^{n+1} = T_{\text{L}}^{n+1}$, where L + 1 is a "virtual" layer underlying the lowest actual layer in the model; thus, the finite difference equation becomes that for a general intermediate layer, or:

$$\left(-\overline{\kappa}_{\text{LL}-1}\, f_L^- \right) T_{\text{L}-1}^{n+1} + \left\{ \frac{\rho_{\text{L}} C_{\text{L}}}{\Delta t} + \overline{\kappa}_{\text{LL}-1}\, f_{\text{L}}^- \right\} T_{\text{L}}^{n+1} = + \left(\frac{\rho_{\text{L}} C_{\text{L}}}{\Delta t} \right) T_{\text{L}}^n. \qquad (4.d.22)$$

For the case of a fixed lower boundary temperature, we specify $T_{\text{L}+1}^{n+1} = T_B$, and use:

$$\overline{\kappa}_{\text{L}+1,\text{L}} = \kappa_\ell \qquad \Delta z_{\text{L}}^+ = z_{\text{L}} - \overline{z}_{\text{L}} \qquad f_{\text{L}}^+ = \frac{1}{\Delta z_{\text{L}} \Delta z_{\text{L}}^+}, \qquad (4.d.23)$$

which results in an equation of the form of (4.*d*.21).

The equations for T_ℓ^{n+1} $\ell = 1, 2, \ldots \mathrm{L}$ form a coupled set of linear equations of the form:

$$\begin{pmatrix} A_{11} & A_{12} & 0 & 0 & \ldots & 0 \\ A_{21} & A_{22} & A_{23} & 0 & \ldots & 0 \\ 0 & A_{32} & A_{33} & A_{34} & \ldots & 0 \\ \vdots & & \ddots & & \vdots & \\ 0 & \ldots & 0 & 0 & A_{\mathrm{L}-1,\mathrm{L}} & A_{\mathrm{LL}} \end{pmatrix} \begin{pmatrix} T_1^{n+1} \\ T_2^{n+1} \\ T_3^{n+1} \\ \vdots \\ T_{\mathrm{L}}^{n+1} \end{pmatrix} = \begin{pmatrix} b_1 \\ b_2 \\ \vdots \\ b_L \end{pmatrix}, \qquad (4.d.24)$$

or a set of $\mathrm{L} \times \mathrm{L}$ linear equations, where we can see the definitions of the $A(\mathrm{L} \times \mathrm{L})$ matrix and $b(\mathrm{L})$ vector, respectively, from the finite difference equations above.

A consistency check on the calculation can be done by evaluating the vertical sum of the thermal energy. Vertically summing equation 4.*d*.13, where the thermal flux divergence is defined by 4.*d*.14 yields:

$$E^{n+1} = \sum_{\ell=1}^{L} \rho_\ell C_\ell T_\ell^{n+1} (z_\ell - z_{\ell-1}), \qquad (4.d.25)$$

with a similar equation for E^n using the temperatures T_ℓ^n. Over land, with the zero thermal flux as the bottom boundary condition, the following condition is satisfied:

$$\frac{E^{n+1} - E^n}{\Delta t} = F_{\mathrm{net}}^n + \left.\frac{\partial F_{\mathrm{net}}}{\partial T_s}\right|_{T_1^n} (T_1^{n+1} - T_1^n). \qquad (4.d.26)$$

Over sea ice, an extra term arises due to the thermal flux from the underlying ocean.

e. Vertical Diffusion and Atmospheric Boundary Layer Processes

Local diffusion scheme

An explicit, non-local Atmospheric Boundary Layer (ABL) parameterization is incorporated into the vertical diffusion parameterization in CCM2. The ABL parameterization includes a determination of the boundary layer depth. Above the top of the ABL, CCM2 employs a standard local diffusion parameterization for the free atmosphere. In practice, the free atmosphere diffusivities are calculated first at all levels. The ABL scheme then determines the ABL depth and diffusivities and replaces the free atmosphere values for all levels within the ABL. The ABL parameterization, its implementation in CCM2, and its impact on the behavior of the model are discussed in Holtslag and Boville (1993), while the formalism only is discussed here.

The local form of the vertical diffusion terms of momentum, sensible heat, and moisture follows those described by Smagorinsky *et al.* (1965) and Manabe *et al.* (1965) where the tendencies are given by

$$\frac{\partial u}{\partial t} = -\frac{1}{\rho}\frac{\partial \tau_\lambda}{\partial z} = g\frac{\partial \tau_\lambda}{\partial p}, \qquad (4.e.1)$$

$$\frac{\partial v}{\partial t} = -\frac{1}{\rho}\frac{\partial \tau_\mu}{\partial z} = g\frac{\partial \tau_\mu}{\partial p}, \tag{4.e.2}$$

$$\frac{\partial T}{\partial t} = -\frac{1}{\rho c_p^*}\frac{\partial H}{\partial z} = \frac{g}{c_p^*}\frac{\partial H}{\partial p}, \tag{4.e.3}$$

$$\frac{\partial q}{\partial t} = -\frac{1}{\rho}\frac{\partial R}{\partial z} = g\frac{\partial R}{\partial p}, \tag{4.e.4}$$

where c_p^* is given by $c_p^* = \left[1 + \left(\frac{c_{pv}}{c_p} - 1\right) q\right] c_p$. Above the surface layer, the upward fluxes of momentum, sensible heat, and moisture due to turbulent motions are given by

$$\tau_\lambda = \rho\overline{w'u'} = -\rho K_m \frac{\partial u}{\partial z} = g\rho^2 K_c \frac{\partial u}{\partial p}, \tag{4.e.5}$$

$$\tau_\mu = \rho\overline{w'v'} = -\rho K_m \frac{\partial v}{\partial z} = g\rho^2 K_c \frac{\partial v}{\partial p}, \tag{4.e.6}$$

$$H = \rho\overline{w'\theta'} = -c_p^* \rho K_\theta \frac{\partial \theta}{\partial z} = c_p^* g\rho^2 K_c \frac{\partial \theta}{\partial p}, \tag{4.e.7}$$

$$R = \rho\overline{w'q'} = -\rho K_q \frac{\partial q}{\partial z} = g\rho^2 K_c \frac{\partial q}{\partial p}, \tag{4.e.8}$$

where $\theta = T\left(\frac{p^*}{p}\right)^\kappa$ and p^* is a reference pressure which in practice is taken to be p_s. The variables K_c, where $c \in (q, \theta, u, v)$ are "eddy-diffusivities" that are typically taken as functions of length scales ℓ_c and local vertical gradients of wind and virtual potential temperature, *e.g.*,

$$K_c = {\ell_c}^2 S F_c(Ri). \tag{4.e.9}$$

Here S is the local shear, defined by

$$S = \left|\frac{\partial \mathbf{V}}{\partial z}\right|, \tag{4.e.10}$$

and the mixing length ℓ_c is generally given by

$$\frac{1}{\ell_c} = \frac{1}{kz} + \frac{1}{\lambda_c}, \tag{4.e.11}$$

where again k is the Von Karman constant, and λ_c is the so-called asymptotic length scale, taken to be 30 m above the ABL. Since the lowest model level is always greater than 30 m in depth, ℓ_c is simply set to 30 m in CCM2. Furthermore, $F_c(Ri)$ denotes a functional dependence of K_c on the gradient Richardson number:

$$Ri = \frac{g}{\theta_v}\frac{\partial \theta_v / \partial z}{S^2}, \tag{4.e.12}$$

where θ_v is the virtual potential temperature,

$$\theta_v = \theta \left[1 + \left(\frac{R_v}{R} - 1 \right) q \right]. \tag{4.e.13}$$

For simplicity, in our present implementation of the local K approach, we specify the same stability functions F_c for all c. For unstable conditions ($Ri < 0$) we choose

$$F_c(Ri) = (1 - 18Ri)^{1/2}, \tag{4.e.14}$$

as in CCM1 (Williamson *et al.*, 1987), and we use (4.c.12) for stable conditions ($Ri > 0$). This means that no distinction is made between vertical diffusion of heat, scalars and momentum.

"Non-local" atmospheric boundary layer scheme

In a local diffusion approach, the turbulent flux of a quantity is proportional to the local gradient of that quantity (*e.g.*, (4.e.5)–(4.e.8)). In such an approach the eddy diffusivity depends on local gradients of mean wind and mean virtual temperature (see (4.e.9)). These are reasonable assumptions when the length scale of the largest turbulent eddies is smaller than the size of the domain over which the turbulence extends. In the Atmospheric Boundary Layer (ABL) this is typically true for neutral and stable conditions only. For unstable and convective conditions, however, the largest transporting eddies may have a similar size as the boundary layer height itself, and the flux can be counter to the local gradient (Deardorff, 1972; Holtslag and Moeng, 1991). In such conditions a local diffusion approach is no longer appropriate, and the eddy diffusivity is better represented with turbulent properties characteristic of the ABL. We will refer to such an approach as non-local diffusion.

To account for "non-local" transport by convective turbulence in the ABL, the local diffusion term for constituent c is modified as

$$\overline{w'C'} = -K_c \left(\frac{\partial C}{\partial z} - \gamma_c \right), \tag{4.e.15}$$

where K_c is the non-local eddy diffusivity for the quantity of interest. The term γ_c is a "non-local" transport term and reflects non-local transport due to dry convection. Eq. (4.e.15) applies to potential temperature, water vapor, and passive scalars. No countergradient term is applied to the wind components, so (4.e.1) and (4.e.2) remain unchanged. For stable and neutral conditions the non-local term is not relevant for any of the quantities. The eddy diffusivity formalism is, however, modified for unstable conditions.

In the non-local diffusion scheme the eddy diffusivity is given by

$$K_c = k \, w_t \, z \left(1 - \frac{z}{h} \right)^2, \tag{4.e.16}$$

where w_t is a turbulent velocity scale and h is the boundary layer height. Equation (4.e.16) applies for heat, water vapor and passive scalars. The eddy diffusivity of momentum K_m, is also defined as (4.e.16) but with w_t replaced by another velocity scale w_m. With proper formulation of w_t (or w_m) and h, it can be shown that equation (4.e.16) behaves well from very stable to very unstable conditions in horizontally homogeneous and quasi-stationary conditions. For unstable conditions w_t and w_m are proportional to the so-called convective velocity scale w_*, while for neutral and stable conditions w_t and w_m are proportional to the friction velocity u_*.

The major advantage of the present approach over the local eddy diffusivity approach is that large eddy transport in the ABL is accounted for and entrainment effects are treated implicitly. Above the ABL, $\gamma_c = 0$ so (4.e.15) reduces to a local form with K_c given by (4.e.9). Near the top of the ABL we use the maximum of the values by (4.e.9) and (4.e.16), although (4.e.16) almost always gives the larger value in practice.

The non-local transport term in (4.e.15), γ_c, represents non-local influences on the mixing by turbulence (Deardorff, 1972). As such, this term is small in stable conditions, and is therefore neglected in these conditions. For unstable conditions, however, most transport of heat and moisture is done by turbulent eddies with sizes on the order of the depth h of the ABL. In such cases, a formulation for γ_c consistent with the eddy formulation of (4.e.15) is given by

$$\gamma_c = a \frac{w_* (\overline{w'C'})_s}{{w_m}^2 h} \ , \tag{4.e.17}$$

where a is a constant and $(\overline{w'C'})_s$ is the surface flux (in kinematic units) of the transported scalar. The form of (4.e.17) is similar to the one proposed in Holtslag and Moeng (1991). The non-local correction vanishes under neutral conditions, for which $w_* = 0$.

The formulations of the eddy-diffusivity and the non-local terms are dependent on the boundary layer height h. We follow Troen and Mahrt (1986) and determine h iteratively by using

$$h = \frac{Ri_{cr} \left\{ u(h)^2 + v(h)^2 \right\}}{(g/\theta_s) \left(\theta_v(h) - \theta_s \right)} \ , \tag{4.e.18}$$

where Ri_{cr} is a critical bulk Richardson number for the ABL; $u(h)$ and $v(h)$ are the horizontal velocity components at h; g/θ_s is the buoyancy parameter; $\theta_v(h)$ is the virtual temperature at h; and θ_s is an appropriate temperature of air near the surface. The value of the critical bulk Richardson number Ri_{cr} in (4.e.18) depends generally on the vertical resolution of the model. For the standard model resolution, we use $Ri_{cr} = 0.5$.

Following Troen and Mahrt (1986), θ_s for unstable conditions is given by:

$$\theta_s = \theta_v (z_s) + b \frac{(\overline{w'\theta'_v})_s}{w_m} \ , \tag{4.e.19}$$

where b is a constant, $(\overline{w'\theta'_v})_s$ is the virtual heat flux at the surface, and unstable conditions are determined by $(\overline{w'\theta'_v})_s > 0$. In (4.e.19), $\theta_v(z_s)$ is a virtual temperature in the atmospheric surface layer (say at a height of 10 m). The second term on the right hand side of (4.e.19) represents a temperature excess, which is a measure of the strength of convective thermals in the lower part of the ABL. This value, and a similar one for moisture, is also used by the convection scheme.

The above described determination of h for unstable conditions incorporates both the effects of mean wind shear and convection. Note that in the limit of free convection, (4.e.18) provides that $\theta_v(h) = \theta_s$. For stable conditions $(\overline{w'\theta'})_s < 0$, we apply

$$\theta_s = \theta_v(z_s), \tag{4.e.20}$$

with $z_s = 10$ m. The latter virtual temperature is calculated from the temperature and moisture of the first model level and of the surface by applying the procedure in Geleyn (1988).

On the basis of (4.e.18), the boundary layer height h can be determined by iteration for all stability conditions, when the surface fluxes and the profiles of θ_v, u, and v are known. The computation starts by calculating the bulk Richardson number Ri between the level of θ_s and subsequent higher levels of the model. Once Ri exceeds the critical value, the value of h is derived by linear interpolation between the level with $Ri > Ri_{cr}$ and the level below.

Using the calculated value for h and the surface fluxes, we calculate the velocity scales, the eddy diffusivities with (4.e.16), and the countergradient terms with (4.e.17), for each of the transported constituents. Subsequently, the new profiles for θ, q, u, and v are calculated using an implicit diffusion formulation.

The turbulent velocity scale of (4.e.16) depends primarily on the relative height z/h (h is boundary layer height), and the stability within the ABL. Here stability is defined with respect to the surface virtual heat flux $(\overline{w'\theta'_v})_s$. Secondly, the velocity scales are also generally dependent on the specific quantity of interest. We will assume that the velocity scales for mixing of passive scalars and specific humidity are equal to the one for heat, denoted by w_t. For the wind components, the velocity scale is different and denoted by w_m. The specification of w_t and w_m is given in detail by Troen and Mahrt (1986). Holtslag *et al.*, (1990) have rewritten the velocity scale, in terms of the more widely accepted profile functions of Dyer (1974), and have given a new formulation for very stable conditions. Below we follow the latter approach.

For stable $((\overline{w'\theta'_v})_s < 0)$ and neutral surface conditions $((\overline{w'\theta'_v})_s = 0)$, the velocity scale for scalar transport is

$$w_t = \frac{u_*}{\phi_h}, \tag{4.e.21}$$

where u_* is the friction velocity defined by

$$u_* = \left[(\overline{u'w'})_s^2 + (\overline{v'w'})_s^2\right]^{1/4} . \qquad (4.e.22)$$

Furthermore, ϕ_h is the dimensionless vertical temperature gradient given by (Dyer, 1974),

$$\phi_h = 1 + 5\frac{z}{L} , \qquad (4.e.23)$$

for $0 \leq z/L \leq 1$. Here L is the Obukhov length, defined by

$$L = \frac{-u_*^3}{k(g/\theta_{v0})(\overline{w'\theta_v'})_0} . \qquad (4.e.24)$$

For $z/L > 1$,

$$\phi_h = 5 + \frac{z}{L} , \qquad (4.e.25)$$

which matches (4.e.23) for $z/L = 1$. Equation (4.e.25) is a simple means to prevent ϕ_h from becoming too large (and K_c too small) in very stable conditions. In stable conditions, the exchange coefficients for heat and momentum are often found to be similar. Therefore we may use w_m=w_t.

For unstable conditions $(\overline{w'\theta_v'})_s > 0$, we have that w_t and w_m differ in the surface layer ($z/h \leq 0.1$) and in the outer layer of the ABL ($z/h > 0.1$). For the surface layer, w_t is given by (4.e.21) with

$$\phi_h = \left(1 - 15\frac{z}{L}\right)^{-1/2} . \qquad (4.e.26)$$

Similarly, w_m is written as

$$w_m = \frac{u_*}{\phi_m} , \qquad (4.e.27)$$

where ϕ_m is the dimensionless wind gradient given by

$$\phi_m = \left(1 - 15\frac{z}{L}\right)^{-1/3} . \qquad (4.e.28)$$

In the surface layer, the scalar flux is normally given by

$$(\overline{w'c'})_0 = -\frac{ku_*z}{\phi_h}\left(\frac{\partial C}{\partial z}\right) . \qquad (4.e.29)$$

Comparison with (4.e.15) and (4.e.16) shows that, in the surface layer, we should have $a = 0$ in (4.e.17) for consistency.

For the outer layer, w_t and w_m are given by

$$w_t = w_m/Pr , \qquad (4.e.30)$$

where

$$w_m = \left(u_*^3 + c_1 w_*^3\right)^{1/3} , \qquad (4.e.31)$$

and

$$w_* = \left((g/\theta_{v0})\ (\overline{w'\theta_v'})_0 h\right)^{1/3} \qquad (4.e.32)$$

is the convective velocity scale. Furthermore, Pr is the turbulent Prandtl number and c_1 is a constant. The latter is obtained by evaluating the dimensionless vertical wind gradient ϕ_m by (4.e.28) at the top of the surface layer, as discussed by Troen and Mahrt (1986). This results in $c_1 = 0.6$. For very unstable conditions ($h \gg -L$ or $w_*/u_* \gg 0$), it can be shown with (4.e.30) that w_m is proportional to 0.85 w_*, while for the neutral case $w_m = u_*$. The turbulent Prandtl number Pr ($= K_m/K_h = w_m/w_t$) of (4.e.30) is evaluated from

$$Pr = \frac{\phi_h}{\phi_m}\left(\frac{z}{L}\right) + ak\frac{z}{h}\frac{w_*}{w_m} \tag{4.e.33}$$

for $z = 0.1h$. Equation (4.e.33) arises from matching (4.e.15), (4.e.16), (4.e.17), and (4.e.29) at the top of the surface layer. As in Troen and Mahrt we assume that Pr is independent of height in the unstable outer layer. Its value decreases from $Pr = 1$ for the neutral case ($z/L = 0$ and $w_* = 0$), to $Pr = 0.6$ for $w_*/u_* \simeq 10$ in very unstable conditions.

In very unstable conditions, the countergradient term of (4.e.17) approaches

$$\gamma_c = d\frac{\overline{wC}_0}{w_* h}\,, \tag{4.e.34}$$

where $d \simeq a/0.85^2$, because for very unstable conditions we obtain $w_m \simeq 0.85 w_*$. Since typically $d \simeq 10$ (Troen and Mahrt 1986), we have $a = 7.2$. Similarly, the temperature excess of (4.e.19) reads in this limit as $d(\overline{w'\theta'_v})_0/w_*$. This leads to b ($= 0.85\ d$) $= 8.5$ in (4.e.19).

Finally, using the velocity scales described above, the flux equation (4.e.15) is continuous in relative height (z/h) and in the boundary layer stability parameter (h/L or w_*/u_*).

In summary, the vertical diffusion tendency is given by the vertical derivative of the turbulent flux defined in (4.e.15):

$$\begin{aligned}\frac{\partial C}{\partial t} &= -\frac{1}{\rho}\frac{\partial}{\partial z}\left[\rho\overline{w'C'}\right] \\ &= \frac{1}{\rho}\frac{\partial}{\partial z}\left[\rho K_c\left(\frac{\partial C}{\partial z} - \gamma_c\right)\right].\end{aligned} \tag{4.e.35}$$

The vertical diffusion is implemented using a time-split implicit method, as in CCM1. The countergradient term in the non-local ABL scheme depends on the surface flux, the boundary layer depth and the velocity scale, but not explicitly on the diffused quantity. Therefore the countergradient term cannot be treated implicitly. Forward time differencing is used for the diffusion, whereas a leap frog (centered) method is used for the dynamics. Thus, the diffusive forward step is over two time steps. The time discretization then results in:

$$\frac{C^{n+1} - C^{n-1}}{2\Delta t} = \frac{1}{\rho^{n-1}}\frac{\partial}{\partial z}\left[\rho^{n-1}K_c^{n-1}\left(\frac{\partial C^{n+1}}{\partial z} - \gamma_c^{n-1}\right)\right], \tag{4.e.36}$$

where subscripts $n-1$ and $n+1$ refer to time levels, with K_c^{n-1} and γ_c^{n-1} evaluated using model variables at time $n-1$. The whole diffusion process is time split from all other processes so that time $n-1$ variables may already have contributions from the dynamics and other physical process. Equation (4.*e*.36) can be rewritten as

$$C^{n+1} = (1 - 2\Delta t G^{n-1})^{-1} C^*, \tag{4.e.37}$$

$$C^* = C^{n-1} - 2\Delta t H^{n-1}(\gamma_c^{n-1}), \tag{4.e.38}$$

where G and H are differential operators. There can be a problem in applying (4.*e*.38) for trace constituents, including water vapor, because these quantities are positive definite. The application of the countergradient term, $H^{n-1}(\gamma^{n-1})$ may result in negative values for C^*, which are not removed by the subsequent implicit diffusion step. This problem is not strictly numerical; it arises under highly non-stationary conditions for which the ABL formulation is not strictly applicable. In practice, we evaluate C^* and check for negative values in the constituent profiles. If a negative value is found, we set $C^* = C^{n-1}$ for that constituent profile (but not for other constituents at the same point). Note that (4.*e*.37) is just the normal diffusion equation, which is solved using the numerical techniques discussed in the next sub-section.

Numerical solution of nonlinear, time–split vertical diffusion

As described in section 2, the vertical diffusion is calculated prior to the main dynamical calculation. This time–split diffusion is

$$u_k^{n+1} = u_k^{n-1} + 2\Delta t \frac{\tau_{\lambda k+1/2}^{n+1} - \tau_{\lambda k-1/2}^{n+1}}{\rho_k \Delta z_k^{n-1}}, \tag{4.e.39}$$

$$v_k^{n+1} = v_k^{n-1} + 2\Delta t \frac{\tau_{\mu k+1/2}^{n+1} - \tau_{\mu k-1/2}^{n+1}}{\rho_k \Delta z_k^{n-1}}, \tag{4.e.40}$$

$$\theta_k^{n+1} = \theta_k^{n-1} + 2\Delta t \frac{g}{c_{p_k}^*} \frac{H_{k+1/2}^{n+1} - H_{k-1/2}^{n+1}}{\rho_k \Delta z_k^{n-1}}, \tag{4.e.41}$$

$$q_k^{n+1} = q_k^{n-1} + 2\Delta t \frac{R_{k+1/2}^{n+1} - R_{k-1/2}^{n+1}}{\rho_k \Delta z_k^{n-1}}, \tag{4.e.42}$$

where

$$c_{p_k}^* = c_p \left[1 + \left(\frac{c_{p_v}}{c_p} - 1 \right) q_k^{n-1} \right]. \tag{4.e.43}$$

The surface fluxes are given by the explicit forms (4.*c*.2)–(4.*c*.5):

$$R_{K+1/2}^{n+1} = R_{K+1/2}^{n} = L\rho \left(\overline{w'q'} \right)_s, \tag{4.e.44}$$

$$H_{K+1/2}^{n+1} = H_{K+1/2}^{n} = c_p \rho_1 \left(\overline{w'\theta'} \right)_s, \tag{4.e.45}$$

$$\tau_{\lambda K+1/2}^{n+1} = \tau_{\lambda K+1/2}^{n} = \rho_1 \left(\overline{w'u'}\right)_s , \tag{4.e.46}$$

$$\tau_{\mu K+1/2}^{n+1} = \tau_{\mu K+1/2}^{n} = \rho_1 \left(\overline{w'v'}\right)_s . \tag{4.e.47}$$

Note that these surface fluxes are explicit and ensure conservation of energy and moisture in the surface exchange. The surface stresses τ_λ and τ_μ could be made implicit without affecting this conservation. In the free atmosphere, for $k = 1$ to $K - 1$,

$$\tau_{\lambda k+1/2}^{n+1} = \left(\rho_{k+1/2}^{n-1}\right) K_{k+1/2}^{n-1} \frac{u_{k+1}^{n+1} - u_k^{n+1}}{z_{k+1}^{n-1} - z_k^{n-1}}, \tag{4.e.48}$$

$$\tau_{\mu k+1/2}^{n+1} = \left(\rho_{k+1/2}^{n-1}\right) K_{k+1/2}^{n-1} \frac{v_{k+1}^{n+1} - v_k^{n+1}}{z_{k+1}^{n-1} - z_k^{n-1}}, \tag{4.e.49}$$

$$R_{k+1/2}^{n+1} = \left(\rho_{k+1/2}^{n-1}\right) K_{k+1/2}^{n-1} \frac{q_{k+1}^{n+1} - q_k^{n+1}}{z_{k+1}^{n-1} - z_k^{n-1}}, \tag{4.e.50}$$

$$H_{k+1/2}^{n+1} = c_{p_{k+1/2}}^{*} \left(\rho_{k+1/2}^{n-1}\right) K_{k+1/2}^{n-1} \frac{\theta_{k+1}^{n+1} - \theta_k^{n+1}}{z_{k+1}^{n-1} - z_k^{n-1}}, \tag{4.e.51}$$

where

$$\rho_{k+1/2}^{n-1} = \frac{2p_{k+1/2}^{n-1}}{R\left(T_{k+1}^{n-1} + T_k^{n-1}\right)\left[1 + \left(\frac{R_v}{R} - 1\right)\frac{1}{2}\left(q_{k+1}^{n-1} + q_k^{n-1}\right)\right]}, \tag{4.e.52}$$

and

$$c_{p_{k+1/2}}^{*} = c_p \left[1 + \left(\frac{c_{p_v}}{c_p} - 1\right)\frac{1}{2}\left(q_{k+1}^{n-1} + q_k^{n-1}\right)\right]. \tag{4.e.53}$$

$K_{k+1/2}^{n-1}$ is then determined from the neutral K modulated by a function of Richardson number

$$K_{k+1/2}^{n-1} = \left(K_N^{n-1}\right)_{k+1/2} \cdot f\left(R_{I_{k+1/2}}\right), \tag{4.e.54}$$

with a minimum value for $K_{k+1/2}^{n-1}$ of $K_{min} = 0.01$.

$$f(R_I) = \begin{cases} \max\left(0, 1 - R_I/R_{IC}\right) & \text{for } R_I \geq 0 \text{ (stable)}, \\ \sqrt{1 - 18R_I} & \text{for } R_I < 0 \text{ (unstable)}, \end{cases} \tag{4.e.55}$$

with a critical Richardson number at which f goes to zero of

$$R_{IC} = 0.2 \ . \tag{4.e.56}$$

The neutral K_N is calculated by

$$\left(K_N^{n-1}\right)_{k+1/2} = \ell_{k+1/2}^2 \frac{p_{k+1/2}^{n-1}}{RT_{v_{k+1/2}}^{n-1}} \frac{\left[\left(u_{k+1}^{n-1} - u_k^{n-1}\right)^2 + \left(v_{k+1}^{n-1} - v_k^{n-1}\right)^2\right]}{\rho_k \Delta z_{k+1/2}^{n-1}}, \tag{4.e.57}$$

with

$$RT^{n-1}_{v_{k+1/2}} = R\left[1+\left(\frac{R_v}{R}-1\right)\frac{1}{2}\left(q^{n-1}_{k+1}+q^{n-1}_{k}\right)\right]\frac{1}{2}\left(T^{n-1}_{k+1}+T^{n-1}_{k}\right), \tag{4.e.58}$$

$$\Delta z^{n-1}_{k+1/2} = z^{n-1}_{k+1} - z^{n-1}_{k}, \tag{4.e.59}$$

and $\ell_{k+1/2}$ is determined from (4.e.11) and (4.e.13). The Richardson number in the free atmosphere is calculated from

$$\begin{aligned} R_{I_{k+1/2}} = & \frac{2g\left(z^{n-1}_{k}-z^{n-1}_{k+1}\right)}{\left(\theta^{n-1}_{v_k}+\theta^{n-1}_{v_{k+1}}\right)} \\ & \times\left[\frac{\theta^{n-1}_{v_k}-\theta^{n-1}_{v_{k+1}}}{\left(u^{n-1}_{k+1}-u^{n-1}_{k}\right)^2+\left(v^{n-1}_{k+1}-v^{n-1}_{k}\right)^2}\right]. \end{aligned} \tag{4.e.60}$$

Within the diagnosed atmospheric boundary layer, the diffusivities are modified by the non-local atmospheric boundary layer scheme described earlier. At the top of the model, the fluxes are set to 0,

$$\tau^{n+1}_{\lambda 1/2} = \tau^{n+1}_{\mu 1/2} = R^{n+1}_{1/2} = H^{n+1}_{1/2} = 0. \tag{4.e.61}$$

The diffusion equations can be summarized as

$$u^{n+1}_{k} - \left\{u^{n-1}\right\}_k = a_k\left(u^{n+1}_{k+1}-u^{n+1}_{k}\right) - c_k\left(u^{n+1}_{k}-u^{n+1}_{k-1}\right), \tag{4.e.62}$$

$$v^{n+1}_{k} - \left\{v^{n-1}\right\}_k = a_k\left(v^{n+1}_{k+1}-v^{n+1}_{k}\right) - c_k\left(v^{n+1}_{k}-v^{n+1}_{k-1}\right), \tag{4.e.63}$$

$$q^{n+1}_{k} - \left\{q^{n-1}\right\}_k = a_k\left(q^{n+1}_{k+1}-q^{n+1}_{k}\right) - c_k\left(q^{n+1}_{k}-q^{n+1}_{k-1}\right), \tag{4.e.64}$$

$$T^{n+1}_{k} - \left\{T^{n-1}\right\}_k = a_k\left[\theta^{n+1}_{k+1}-\theta^{n+1}_{k}\right] - c_k\left[\theta^{n+1}_{k}-\theta^{n+1}_{k-1}\right], \tag{4.e.65}$$

for $1 \le k \le K-1$,

$$\left\{u^{n-1}\right\}_k = u^{n-1}_k, \tag{4.e.66}$$

$$\left\{v^{n-1}\right\}_k = v^{n-1}_k, \tag{4.e.67}$$

$$\left\{q^{n-1}\right\}_k = q^{n-1}_k, \tag{4.e.68}$$

$$\left\{T^{n-1}\right\}_k = T^{n-1}_k, \tag{4.e.69}$$

and for $k = K$,

$$\left\{u^{n-1}\right\}_K = u^{n-1}_K + \frac{2\Delta t}{\rho_{K+\frac{1}{2}}\Delta z^{n-1}_K}\tau^{n+1}_{\lambda K+1/2}, \tag{4.e.70}$$

$$\left\{v^{n-1}\right\}_K = v^{n-1}_K + \frac{2\Delta t}{\rho_{K+\frac{1}{2}}\Delta z^{n-1}_k}\tau^{n+1}_{\mu K+1/2}, \tag{4.e.71}$$

$$\left\{q^{n-1}\right\}_K = q_K^{n-1} + \frac{2\Delta t}{\rho_{K+\frac{1}{2}} \Delta z_K^{n-1}} R_{K+1/2}^{n+1} \,, \tag{4.e.72}$$

$$\left\{\theta^{n-1}\right\}_K = \theta_K^{n-1} + \frac{2\Delta t}{c_{p_K}^* \rho_{K+\frac{1}{2}} \Delta z_K^{n-1}} H_{K+1/2}^{n+1} \,, \tag{4.e.73}$$

where

$$a_k = \frac{2\Delta t}{\Delta p_k \left(p_{k+1} - p_k\right)} \left(\frac{g\rho_{k+1/2}^{n-1}}{p_s^{n-1}}\right)^2 K_{k+1/2}^{n-1} \qquad 1 \le k \le K-1, \tag{4.e.74}$$

$$a_K = 0, \tag{4.e.75}$$

$$c_1 = 0, \tag{4.e.76}$$

$$c_k = \frac{2\Delta t}{\Delta p_k^{n-1} \left(p_k^{n-1} - p_{k-1}^{n-1}\right)} \left(g\bar{\rho}_{k-1/2}^{n-1}\right) K_{k-1/2}^{n-1} \qquad 2 \le k \le K. \tag{4.e.77}$$

The left-hand side of (4.e.65) can be written in terms of T because it is represented as a difference.

Following Richtmeyer and Morton (1967, pp. 198–201), the solutions for u, v, θ, and q have the form,

$$u_k^{n+1} = Fu_k + E_k u_{k+1}^{n+1}, \tag{4.e.78}$$

where for $k = 1$,

$$Fu_1 = \frac{\left\{u^{n-1}\right\}_1}{b_1}, \tag{4.e.79}$$

$$E_1 = \frac{a_1}{b_1}, \tag{4.e.80}$$

and for $2 \le k \le K-1$,

$$Fu_k = \frac{\left\{u^{n-1}\right\}_k + c_k Fu_{k-1}}{b_k - c_k E_{k-1}}, \tag{4.e.81}$$

$$E_k = \frac{a_k}{b_k - c_k E_{k-1}}, \tag{4.e.82}$$

and for $k = K$,

$$E_K = 0, \tag{4.e.83}$$

$$Fu_K = \frac{\left\{u^{n-1}\right\}_K + c_K Fu_{K-1}}{b_K - c_K E_{K-1}}. \tag{4.e.84}$$

In the above, the diagonal coefficient is given by

$$b_k = 1 + a_k + c_k. \tag{4.e.85}$$

Note that, since the model actually forecasts vorticity and divergence, the new diffused velocity fields u_k^{n+1} and v_k^{n+1} are not explicitly carried by the model, and the corresponding diffused vorticity and divergence are not calculated. Rather, the net effects of the diffusion $F_{u_V}\left(u^{n+1}\right)$ and $F_{v_V}\left(v^{n+1}\right)$ are saved for addition to the nonlinear terms n_U and n_V in the vorticity and divergence equations (after multiplication by $\cos\phi$),

$$F_{u_V} = \frac{u^{n+1} - u^{n-1}}{2\Delta t}, \tag{4.e.86}$$

$$F_{v_V} = \frac{v^{n+1} - v^{n-1}}{2\Delta t}. \tag{4.e.87}$$

The heating rate due to the diffusion is also calculated,

$$F_{T_V} = \frac{T^{n+1} - T^{n-1}}{2\Delta t}, \tag{4.e.88}$$

and added to the nonlinear term in the temperature tendency equation. The frictional heating associated with (4.e.86) and (4.e.87) is also added to the nonlinear term in the thermodynamic equation. The individual heating rates $F_{T_V}\left(T^{n+1}\right), -u^{n-1}F_{u_V}\left(u^{n+1}\right)/c_p^*$, and $-v^{n-1}F_{v_V}\left(v^{n+1}\right)/c_p^*$ are saved for diagnostic purposes. The new moisture q^{n+1} is retained as the basis for the next time–split step in the moisture equation. The moisture tendency due to vertical diffusion is also saved for diagnostic purposes,

$$F_{q_V}\left(q^{n+1}\right) = \frac{q^{n+1} - q^{n-1}}{2\Delta t}. \tag{4.e.89}$$

f. Gravity Wave Drag

Vertically propagating gravity waves can be excited in the atmosphere where stably stratified air flows over an irregular lower boundary. These waves are capable of transporting significant quantities of horizontal momentum between their source regions and regions where they are absorbed or dissipated. Previous GCM results have shown that the large-scale momentum sinks resulting from breaking gravity waves play an important role in determining the structure of the large-scale flow, particularly for higher resolution truncations. The CCM2 incorporates the stationary orographic gravity wave drag parameterization described by McFarlane (1987). We will discuss the implementation details here, and refer the reader to McFarlane's paper for a discussion of fundamental theoretical aspects of gravity wave drag effects.

As with all CCM2 physical parameterizations, non-resolvable-scale effects of vertically propagating gravity waves are determined in physical space on the transform

grid. The wave drag force in pressure coordinates is written as

$$\frac{\partial \mathbf{V}}{\partial t} = g\,\frac{\partial \vec{\tau}}{\partial p} = \vec{n}\,\frac{\partial}{\partial p}\,(g\tau)\,, \tag{4.f.1}$$

where

$$\tau = -\alpha A^2 \rho N \mathcal{U} = -\frac{\alpha A^2 p N \mathcal{U}}{H} = -M\mathcal{U}\,; \tag{4.f.2}$$

$\vec{n}$ is a unit vector parallel to the reference level flow $\mathbf{V}_o$; $\mathcal{U}$ is the component of the local flow which is parallel to the reference level flow

$$\mathcal{U} = \mathbf{V}\cdot\mathbf{V}_o/\mid \mathbf{V}_o \mid; \tag{4.f.3}$$

N is the local Brunt-Väisällä frequency defined as

$$N = \left(\frac{-g^2 p}{\theta}\,\frac{\partial\theta}{\partial p}\right)^{1/2}\,; \tag{4.f.4}$$

$A(z)$ is the local wave amplitude; H is the local scale height; and the "tunable" parameter α is defined as

$$\alpha = E\mu_e/2, \tag{4.f.5}$$

where μ_e is a representative horizontal wavenumber and E is an efficiency factor assumed to be less than unity. The wave amplitude at the reference level is defined in terms of the subgrid-scale orographic variance, but constrained so that the local Froude number does not exceed some critical value denoted by F_c. Thus

$$A_o = \min\{2S_d, F_c\mathcal{U}_o/N_o\}\,, \tag{4.f.6}$$

where S_d is the standard deviation of the subgrid-scale orography associated with horizontal space scales assumed to be most responsible for the generation of vertically propagating gravity waves. The wave momentum flux at the surface is written as

$$-g\tau_o = \alpha A_o^2 p_o N_o \mathcal{U}_o/H_o\,. \tag{4.f.7}$$

The wave momentum flux above the reference level is assumed to be constant with height, except in regions of wave saturation. Thus at all model levels above the reference level, the local wave amplitude is computed in terms of the wave amplitude of the layer below, so that the wave momentum flux is constant except in saturation regions where

$$A = F_c\mathcal{U}/N\,. \tag{4.f.8}$$

The wave momentum flux at some level k is then given by

$$[-g\tau]_k = \min\left\{[-g\tau]_{k+1}\,,\ \left[\frac{\alpha p N\mathcal{U}}{H}\left(\frac{F_c\mathcal{U}}{N}\right)^2\right]_k\right\}. \tag{4.f.9}$$

Numerical approximations

The gravity wave drag parameterization is applied immediately after the nonlinear vertical diffusion. The interface temperatures are first determined from

$$T_{k+1/2}^{n-1} = T_k^{n-1} + \frac{T_{k+1}^{n-1} - T_k^{n-1}}{\ln\left(\frac{p_{k+1}^{n-1}}{p_k^{n-1}}\right)} \ln\left(p_{k+1/2}^{n-1}/p_k^{n-1}\right) . \qquad (4.f.10)$$

The projection of the interface winds on the reference level wind is evaluated as

$$\mathcal{U}_{k+1/2} = \mathcal{V}_k + \frac{\mathcal{V}_{k+1} - \mathcal{V}_k}{\ln\left(\frac{p_{k+1}^{n-1}}{p_k^{n-1}}\right)} \ln\left(\frac{p_{k+1/2}^{n-1}}{p_k^{n-1}}\right) , \qquad (4.f.11)$$

where

$$\mathcal{V}_k \equiv u_k^{n-1} \left(\frac{u_K^{n-1}}{\mid \mathbf{V} \mid_K^{n-1}}\right) + v_k^{n-1} \left(\frac{v_K^{n-1}}{\mid \mathbf{V} \mid_K^{n-1}}\right) , \qquad (4.f.12)$$

while the interface Brunt-Väisällä frequencies are given by

$$N_{k+1/2} = \left\{ \frac{-g^2}{R} \frac{p_{k+1/2}^{n-1}}{\left(T_{k+1/2}^{n-1}\right)^2} \left(\frac{T_{k+1}^{n-1} - T_k^{n-1}}{p_{k+1}^{n-1} - p_k^{n-1}}\right) - \kappa \frac{T_{k+1/2}^{n-1}}{p_{k+1/2}^{n-1}} \right\}^{1/2} . \qquad (4.f.13)$$

The top interface Brunt-Väisällä frequency is evaluated assuming an isothermal atmosphere above the top model layer so that

$$N_{1/2} = \left(\frac{g^2}{c_p T_1^{n-1}}\right)^{1/2} . \qquad (4.f.14)$$

Assuming that the magnitude of the reference level wind exceeds a critical value of 2 m s^{-1}, and that the subgrid-scale standard deviation exceeds a critical value of 5 m, the surface momentum flux is given by

$$\tau_{g_{K+1/2}} = \frac{E\mu_e}{2H_K} h_e^2 p_K N_{K-1/2} \mid \mathbf{V}_K^{n-1} \mid, \qquad (4.f.15)$$

where

$$h_e = \min\left(2S_d, F_c \mathcal{U}_{K-1/2}/N_{K-1/2}\right) , \qquad (4.f.16)$$

S_d is the subgrid-scale orographic standard deviation, F_c is the critical Froude number taken as $\frac{1}{2}$, and H is the local scale height. The remaining momentum fluxes are computed from the lowest level upwards using

$$\tau_{g_{k+1/2}} = \min\left\{\tau_{g_{k+3/2}}, \frac{E\mu_e F_c^2 \mathcal{U}_{k+1/2}^3 p_{k+1/2}^{n-1}}{2H_k N_{k+1/2}}\right\} , \qquad (4.f.17)$$

with the exception of the top interface level, where the momentum flux is calculated assuming the top interface is located an equal increment in $\ln p$ above the two interfaces

immediately below, and that all variables are constant above the uppermost integer level

$$\tau_{g_{1/2}} = \min\left\{\tau_{g_{3/2}}, \frac{E\mu_e F_c^2 \mathcal{U}_{3/2}^3 p_{1/2}^{n-1}}{2H_1 N_{1/2}}\right\}. \qquad (4.f.18)$$

The momentum tendencies (stress divergence) are then evaluated as

$$\left(\frac{\partial u}{\partial t}\right)_{g_k} = \frac{-u_K^{n-1}}{|\mathbf{V}_K^{n-1}|}\left\{\frac{\tau_{g_{k+1/2}} - \tau_{g_{k-1/2}}}{p_{k+1/2}^{n-1} - p_{k-1/2}^{n-1}}\right\} \qquad (4.f.19)$$

$$\left(\frac{\partial v}{\partial t}\right)_{g_k} = \frac{-v_K^{n-1}}{|\mathbf{V}_K^{n-1}|}\left\{\frac{\tau_{g_{k+1/2}} - \tau_{g_{k-1/2}}}{p_{k+1/2}^{n-1} - p_{k-1/2}^{n-1}}\right\}. \qquad (4.f.20)$$

The magnitude of the vector momentum tendency is evaluated as

$$\left(\frac{\partial \mathbf{V}}{\partial t}\right)_{g_k} = \left(\left(\frac{\partial u}{\partial t}\right)_{g_k}^2 + \left(\frac{\partial v}{\partial t}\right)_{g_k}^2\right)^{1/2} \qquad (4.f.21)$$

and limited to a maximum of 250 m s^{-1} day^{-1} (denoted by $(\partial \mathbf{V}/\partial t)_{\max}$) so that (4.f.19) and (4.f.20) become

$$\left(\frac{\partial u}{\partial t}\right)_{g_k} = \left(\frac{\partial u}{\partial t}\right)_{g_k} \min\left\{\left(\frac{\partial \mathbf{V}}{\partial t}\right)_{\max}, \left(\frac{\partial \mathbf{V}}{\partial t}\right)_{g_k}\right\} \Big/ \left(\frac{\partial \mathbf{V}}{\partial t}\right)_{g_k} \qquad (4.f.22)$$

and

$$\left(\frac{\partial v}{\partial t}\right)_{g_k} = \left(\frac{\partial v}{\partial t}\right)_{g_k} \min\left\{\left(\frac{\partial \mathbf{V}}{\partial t}\right)_{\max}, \left(\frac{\partial \mathbf{V}}{\partial t}\right)_{g_k}\right\} \Big/ \left(\frac{\partial \mathbf{V}}{\partial t}\right)_{g_k}. \qquad (4.f.23)$$

The component momentum tendencies are then added to the nonlinear terms n_U and n_V in the vorticity and divergence equations (along with the previously saved tendencies in (4.e.86) and (4.e.87));

$$F_U = \cos\phi\left(F_{u_V} + \left(\frac{\partial u}{\partial t}\right)_g\right), \qquad (4.f.24)$$

and

$$F_V = \cos\phi\left(F_{v_V} + \left(\frac{\partial v}{\partial t}\right)_g\right). \qquad (4.f.25)$$

The frictional heating associated with the momentum tendencies in (4.f.22) and (4.f.23), $-\left(u^{n-1}\left(\frac{\partial u}{\partial t}\right)_g + v^{n-1}\left(\frac{\partial v}{\partial t}\right)_g\right)\Big/ c_p^*$ is also added to the non-linear term in the thermodynamic equation.

g. Rayleigh Friction

For stratospheric applications of the CCM2, a Raleigh friction term has been included in the zonal momentum equation to provide a crude parameterization of the effect of breaking gravity waves in the mesosphere and to prevent reflection of waves from

the top boundary. This term is implemented in the form

$$\frac{\partial \mathbf{V}}{\partial t} = -K_R \mathbf{V} \tag{4.g.1}$$

The friction coefficient is determined from

$$K_R = \frac{1}{3}\left[1 + \tanh\left(\frac{z - 63 \times 10^3}{7.5 \times 10^3}\right)\right] \text{ days}^{-1}, \tag{4.g.2}$$

where

$$z = -h \ln(A + B), \tag{4.g.3}$$

and $h = 7 \times 10^3$ m. This term, which is not intended to be a faithful representation of mesospheric dynamics is inactive in the standard model configuration.

4.2 Adjustment Physics

After the new temperatures and mixing ratios are computed from (2.c.1) and (2.c.4), a series of convective adjustment schemes is applied to create mutually adjusted T and q fields. If the predicted atmosphere is not saturated and the lapse rate exceeds the dry adiabatic lapse rate, the temperatures are reset to give a dry adiabatic lapse rate, but only in the "stratospheric" region (i.e., top three levels in the standard configuration) of the model. The moisture field is assumed to be mixed by this process as well and is reset to the average value. The stability–dependent vertical diffusion provides for dry turbulent vertical mixing in the troposphere. Thus, in practice, momentum is mixed as well as heat and moisture. If the atmosphere is moist adiabatically unstable, the moisture and temperature fields are simultaneously modified in accordance with a simple model of moist convection. If the atmosphere is stable but supersaturated, the moisture field is adjusted to be saturated and the temperature field is simultaneously adjusted to reflect the heating due to the release of latent heat. When the moisture field is changed to eliminate supersaturation, the change is assumed to go into precipitation. The details of these processes are presented in the following sections, where we use the notation (T, q) to denote values before the adjustment, and $(\hat{T}, \hat{q})$ after the adjustment.

h. Moist Convection

The large-scale budget equations for dry static energy and total water can be written as

$$\begin{aligned}\frac{\partial \overline{s}}{\partial t} &= -\nabla \cdot \overline{\mathbf{V}}\,\overline{s} - \frac{\partial \overline{\omega}\,\overline{s}}{\partial p} - \frac{\partial}{\partial p}\left(\overline{\omega' s'_\ell}\right) + L\mathcal{R} + c_p Q_R \\ &= \left.\frac{\partial \overline{s}}{\partial t}\right|_{R.S.} - \frac{\partial}{\partial p}\left(\overline{\omega' s'_\ell}\right) + L\mathcal{R}\end{aligned} \tag{4.h.1}$$

and

$$\frac{\partial \overline{q}}{\partial t} = -\nabla \cdot \overline{\mathbf{V}}\,\overline{q} - \frac{\partial \overline{\omega}\,\overline{q}}{\partial p} - \frac{\partial}{\partial p}\left(\overline{\omega'\left(q'+\ell'\right)}\right) - \mathcal{R}$$

$$= \left.\frac{\partial \overline{q}}{\partial t}\right|_{R.S.} - \frac{\partial}{\partial p}\left(\overline{\omega'\left(q'+\ell'\right)}\right) - \mathcal{R}, \qquad (4.h.2)$$

where $s \equiv c_p T + gz$ is the dry static energy; ℓ represents liquid water; $s_\ell \equiv s - L\ell$ is the static energy analogue of the liquid water potential temperature introduced by Betts (1975); $\mathcal{R}$ is the "convective-scale" liquid water sink (sometimes denoted by $C - E$); and Q_R is the net radiative heating rate. The subscript $R.S.$ denotes the resolvable-scale contributions to the large-scale budget. Note that variations of the mean liquid water on the large scale have been neglected. It is generally agreed that the remaining terms in (4.h.1) and (4.h.2) are the major convective-scale contributors to the large-scale thermodynamic budget (*i.e.,* horizontal eddy flux transports can be neglected). The barred quantities represent horizontal averages over an area large enough to contain a collection of cloud elements, but small enough so as to cover only a fraction of a large-scale disturbance. By writing the mean thermodynamic variables in terms of their average cloud and environment properties, and assuming that the convection occupies only a small fraction of the averaging area, we can approximate the vertical eddy transports $\overline{\omega' s'_\ell}$ and $\overline{\omega'\left(q'+\ell'\right)}$ by the difference between the upward flux inside a typical convective element and the downward flux (*i.e.,* induced subsidence) in the environment (cf. Yanai *et al.*, 1973). Mathematically, this approximation takes the form

$$F_{s_\ell}(p) = -\frac{1}{g}\left(\overline{\omega' s'_\ell}\right) \approx -M_c(p)\left(\overline{s}(p) - s_c(p) + L\ell(p)\right) \qquad (4.h.3)$$

and

$$F_{q+\ell}(p) = -\frac{1}{g}\left(\overline{\omega'\left(q'+\ell'\right)}\right) \approx -M_c(p)\left(\overline{q}(p) - q_c(p) - \ell(p)\right), \qquad (4.h.4)$$

where M_c is a convective mass flux, and s_c, q_c, and ℓ represent cloud-scale properties. Thus, (4.h.1) and (4.h.2) can be written as

$$\frac{\partial \overline{s}}{\partial t} = \left.\frac{\partial \overline{s}}{\partial t}\right|_{R.S.} + g\frac{\partial}{\partial p}F_{s_\ell} + L\mathcal{R}\,, \qquad (4.h.5)$$

and

$$\frac{\partial \overline{q}}{\partial t} = \left.\frac{\partial \overline{q}}{\partial t}\right|_{R.S.} + g\frac{\partial}{\partial p}F_{q+\ell} - \mathcal{R}\,. \qquad (4.h.6)$$

Let us now turn our attention to a vertically discrete model atmosphere and consider the case where layers k and $k+1$ are moist adiabatically unstable, *i.e.,* a non-entraining parcel of air at level $k+1$ (with moist static energy h_c) would be unstable if raised to level k. We assume the existence of a non-entraining convective element with roots in level $k+1$, condensation and rainout processes in level k, and limited detrainment in level $k-1$ (see Figure 3). In accordance with (4.h.5) and (4.h.6), the discrete dry static

energy and specific humidity budget equations for these three layers can be written as

$$\hat{\overline{s}}_{k-1} = \overline{s}_{k-1} + \frac{2\Delta tg}{\Delta p_{k-1}} \left\{ \beta m_c \left(s_c - \overline{s}_{k-\frac{1}{2}} - L\ell_k \right) \right\} , \tag{4.h.7}$$

$$\hat{\overline{s}}_k = \overline{s}_k + \frac{2\Delta tg}{\Delta p_k} \left\{ m_c \left(s_c - \overline{s}_{k+\frac{1}{2}} \right) - \beta m_c \left(s_c - L\ell_k - \overline{s}_{k-\frac{1}{2}} \right) + LR_k \right\} , \tag{4.h.8}$$

$$\hat{\overline{s}}_{k+1} = \overline{s}_{k+1} + \frac{2\Delta tg}{\Delta p_{k+1}} \left\{ m_c \left(\overline{s}_{k+\frac{1}{2}} - s_c \right) \right\} , \tag{4.h.9}$$

$$\hat{\overline{q}}_{k-1} = \overline{q}_{k-1} + \frac{2\Delta tg}{\Delta p_{k-1}} \left\{ \beta m_c \left(q_c - \overline{q}_{k-\frac{1}{2}} \right) \right\} , \tag{4.h.10}$$

$$\hat{\overline{q}}_k = \overline{q}_k + \frac{2\Delta tg}{\Delta p_k} \left\{ m_c \left(q_c - \overline{q}_{k+\frac{1}{2}} \right) - \beta m_c \left(q_c - \overline{q}_{k-\frac{1}{2}} \right) - R_k \right\} , \tag{4.h.11}$$

$$\hat{\overline{q}}_{k+1} = \overline{q}_{k+1} + \frac{2\Delta tg}{\Delta p_{k+1}} \left\{ m_c \left(\overline{q}_{k+\frac{1}{2}} - q_c \right) \right\} , \tag{4.h.12}$$

where the subscript c denotes cloud properties in the ascent region, m_c is a convective mass flux at the bottom of the condensation layer (level $k+\frac{1}{2}$, "cloud base"), and β is a yet to be determined "overshoot parameter" at level $k-\frac{1}{2}$ that will take a value between zero and one. Note that the convective-scale liquid water sink $\mathcal{R}$ has been redefined in terms of mass per unit area per unit time (denoted by R), and the resolvable-scale components have been dropped for the convenience of the following discussion. In the general case, the thermodynamic properties of the updraft region can be assumed to be equal to their large-scale values in the sub-cloud layer, level $k+1$, plus some arbitrary thermodynamic perturbation; i.e.,

$$s_c = \overline{s}_{k+1} + s', \tag{4.h.13}$$

$$q_c = \overline{q}_{k+1} + q', \tag{4.h.14}$$

and

$$h_c = s_c + Lq_c. \tag{4.h.15}$$

The perturbation quantities q' and s' are in practice provided by the Atmospheric Boundary Layer (ABL) scheme as discussed earlier.

The liquid water generation rate at level k is given by

$$m_c\ell_k = m_c \left[q_c - (q_c)_k \right] . \tag{4.h.16}$$

Using the saturation relation

$$(q_c)_k = \overline{q}_k^* + \frac{\gamma_k}{1+\gamma_k} \frac{1}{L} \left(h_c - \overline{h}_k^* \right) , \tag{4.h.17}$$

where $\overline{q}^*$ denotes the saturated specific humidity

$$\overline{q}^* = \epsilon \frac{e_s}{p - (1-\epsilon)e_s} , \tag{4.h.18}$$

h^* denotes the saturated moist state energy, e_s is the saturation vapor pressure (determined from a precomputed table), and $\gamma \equiv (L/c_p)\left(\partial \overline{q}^*/\partial \overline{T}\right)_p$, and assuming that the large-scale liquid water divergence in layer k is zero, (4.*h*.16) can be manipulated to give the rainout term in layer k as

$$LR_k \equiv L(1-\beta)m_c\ell_k = (1-\beta)m_c\left\{\overline{s}_k - s_c + \frac{1}{1+\gamma_k}\left(h_c - \overline{h}_k^*\right)\right\}, \qquad (4.h.19)$$

and the liquid water flux into layer $k-1$ as

$$\beta m_c L\ell_k = \beta m_c\left\{\overline{s}_k - s_c + \frac{1}{1+\gamma_k}\left(h_c - \overline{h}_k^*\right)\right\}. \qquad (4.h.20)$$

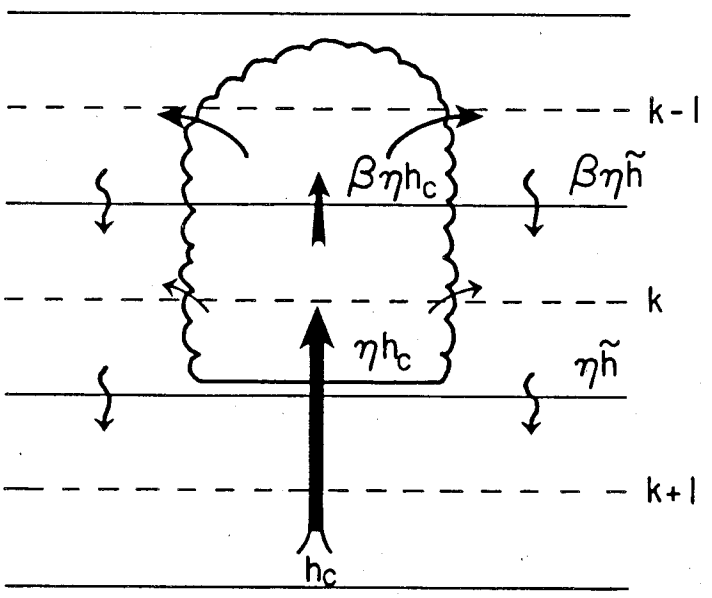

Figure 3. Conceptual three-level non-entraining cloud model

Equations (4.*h*.9) and (4.*h*.12) can be combined to give an equation for moist static energy in layer $k+1$

$$\frac{\partial \overline{h}_{k+1}}{\partial t} = \frac{g}{\Delta p_{k+1}} m_c\left(\overline{h}_{k+\frac{1}{2}} - h_c\right) \approx \frac{\partial h_c}{\partial t}, \qquad (4.h.21)$$

where the approximation follows from the assumption that $\partial h'/\partial t$ can be neglected. Using the relation $(1+\gamma_k)\frac{\partial \overline{s}_k}{\partial t} = \frac{\partial \overline{h}_k^*}{\partial t}$, (4.*h*.8) can be manipulated to give an expression for the

time rate of change of saturated moist static energy in layer k

$$\frac{\partial \overline{h}_k^*}{\partial t} = \frac{g m_c}{\Delta p_k} (1+\gamma_k) \left\{ \left(s_c - \overline{s}_{k+\frac{1}{2}} + L\ell_k \right) - \beta \left(s_c - \overline{s}_{k-\frac{1}{2}} \right) \right\} . \tag{4.h.22}$$

Subtracting (4.h.22) from (4.h.21) results in

$$\begin{aligned} \frac{\partial \left(h_c - \overline{h}_k^* \right)}{\partial t} = m_c \Big\{ & \frac{g}{\Delta p_{k+1}} \left(\overline{h}_{k+\frac{1}{2}} - h_c \right) \\ & - \frac{g}{\Delta p_k} (1+\gamma_k) \left[\left(\overline{s}_k - \overline{s}_{k+\frac{1}{2}} \right) - \beta \left(s_c - \overline{s}_{k-\frac{1}{2}} \right) \right] \Big\} , \end{aligned} \tag{4.h.23}$$

from which the convective mass flux m_c can be written as

$$m_c = \frac{h_c - \overline{h}_k^*}{g\tau \left\{ \frac{(1+\gamma_k)}{\Delta p_k} \left[\left(s_c - \overline{s}_{k+\frac{1}{2}} + L\ell_k \right) - \beta \left(s_c - \overline{s}_{k-\frac{1}{2}} \right) \right] - \frac{1}{\Delta p_{k+1}} \left[\overline{h}_{k+\frac{1}{2}} - h_c \right] \right\}} \tag{4.h.24}$$

where τ is a characteristic convective adjustment time scale.

Physically realistic solutions require that the convective mass flux m_c be positive, implying the following constraint on the overshoot parameter β

$$\beta (1+\gamma_k) \left(s_c - \overline{s}_{k-\frac{1}{2}} \right) < (1+\gamma_k) \left(s_c - \overline{s}_{k+\frac{1}{2}} + L\ell_k \right) - \frac{\Delta p_k}{\Delta p_{k+1}} \left(\overline{h}_{k+\frac{1}{2}} - h_c \right) . \tag{4.h.25}$$

A second physical constraint is that the adjustment process must not supersaturate the "detrainment layer", $k-1$. Using the relation $(1+\gamma_{k-1}) \frac{\partial s_{k-1}}{\partial t} = \frac{\partial \overline{h}_{k-1}^*}{\partial t}$, (4.h.7) can be written as

$$\frac{\partial \overline{h}_{k-1}^*}{\partial t} = \frac{g}{\Delta p_{k-1}} m_c \beta \left\{ (1+\gamma_{k-1}) \left(s_c - \overline{s}_{k-\frac{1}{2}} - L\ell_k \right) \right\} . \tag{4.h.26}$$

Equations (4.h.7) and (4.h.10) can also be combined to give

$$\frac{\partial \overline{h}_{k-1}}{\partial t} = \frac{g}{\Delta p_{k-1}} m_c \beta \left\{ h_c - \overline{h}_{k-\frac{1}{2}} - L\ell_k \right\} . \tag{4.h.27}$$

Equations (4.h.26) and (4.h.27) may also be written in discrete form, respectively, as

$$\hat{\overline{h}}_{k-1}^* = \overline{h}_{k-1}^* + \frac{g}{\Delta p_{k-1}} m_c 2\Delta t \beta \left\{ (1+\gamma_{k-1}) \left(s_c - \overline{s}_{k-\frac{1}{2}} - L\ell_k \right) \right\} , \tag{4.h.28}$$

and

$$\hat{\overline{h}}_{k-1} = \overline{h}_{k-1} + \frac{g}{\Delta p_{k-1}} m_c 2\Delta t \beta \left\{ h_c - \overline{h}_{k-\frac{1}{2}} - L\ell_k \right\} . \tag{4.h.29}$$

Subtracting we have

$$\frac{\left(\overline{h}_{k-1}^* - \overline{h}_{k-1} \right) \Delta p_{k-1}}{g m_c 2\Delta t} > \beta \left\{ h_c - \overline{h}_{k-\frac{1}{2}} - s_c + \overline{s}_{k-\frac{1}{2}} + \gamma_{k-1} \left(\overline{s}_{k-\frac{1}{2}} - s_c + L\ell_k \right) \right\} . \tag{4.h.30}$$

Substituting for m_c from (4.*h*.24), (4.*h*.30) can be further manipulated to give the following constraint on the overshoot parameter, β:

$$\frac{1}{\Delta p_k}\left[(1+\gamma_k)\left(s_c-\overline{s}_{k+\frac{1}{2}}+L\ell_k\right)\right]-\frac{1}{\Delta p_{k+1}}\left[\overline{h}_{k+\frac{1}{2}}-h_c\right]>$$
$$\beta\Bigg\{\left(\frac{2\Delta t}{\tau}\right)\frac{h_c-\overline{h}_k^*}{\left(\overline{h}_{k-1}^*-\overline{h}_{k-1}\right)\Delta p_{k-1}}\left[\gamma_{k-1}\left\{\overline{s}_{k-\frac{1}{2}}-s_c+L\ell_k\right\}\right. \tag{4.h.31}$$
$$\left.+h_c-\overline{h}_{k-\frac{1}{2}}-s_c+\overline{s}_{k-\frac{1}{2}}\right]+\frac{1}{\Delta p_k}(1+\gamma_k)\left(s_c-\overline{s}_{k-\frac{1}{2}}\right)\Bigg\}.$$

Finally, in order to minimize the introduction of $2\Delta\eta$ computational structures in the thermodynamic field, we enforce one final constraint on the overshoot parameter β which does not allow the procedure to increase the vertical gradient of h when $\frac{\partial h}{\partial p}<0$ in the upper pair of layers. Mathematically this constraint is formulated by discretizing in time the moist static energy equations in layers k and $k-1$ which can be written as

$$\hat{\overline{h}}_k-\hat{\overline{h}}_{k-1}=\overline{h}_k-\overline{h}_{k-1}+gm_c2\Delta t\Bigg\{\frac{1}{\Delta p_k}\left[h_c-\overline{h}_{k+\frac{1}{2}}\right]-\beta\left[h_c-\overline{h}_{k-\frac{1}{2}}-L\ell_k\right] \tag{4.h.32}$$
$$\left(\frac{1}{\Delta p_k}+\frac{1}{\Delta p_{k-1}}\right)\Bigg\}.$$

We enforce the condition that $\hat{\overline{h}}_k-\hat{\overline{h}}_{k-1}\geq G$, where G is an arbitrary gradient, which gives rise to the relation

$$\frac{\overline{h}_k-\overline{h}_{k-1}-G}{(h_c-\overline{h}_k^*)}\left(\frac{\tau}{2\Delta t}\right)\left(\frac{1}{\Delta p_h}\left[(1+\gamma_k)(s_c-\overline{s}_{k+\frac{1}{2}}+L\ell_k)\right]-\frac{1}{\Delta p_{k+\frac{1}{2}}}\left[\overline{h}_{k+\frac{1}{2}}-h_c\right]\right)$$
$$+\frac{1}{\Delta p_k}\left[h_c-\overline{h}_{k+\frac{1}{2}}\right]$$
$$\geq\beta\Bigg\{\frac{\overline{h}_k-\overline{h}_{k-1}-G}{h_c-\overline{h}_k^*}\left(\frac{\tau}{2\Delta t}\right)\left(\frac{1+\gamma_k}{\Delta p_k}\right)\left(s_c-\overline{s}_{k-\frac{1}{2}}\right)$$
$$+\left(h_c-\overline{h}_{k-\frac{1}{2}}-L\ell_k\right)\left(\frac{1}{\Delta p_k}+\frac{1}{\Delta p_{k+1}}\right)\Bigg\}. \tag{4.h.33}$$

The first guess for the overshoot parameter, β, comes from a crude buoyancy argument where

$$\beta = \max \begin{cases} \beta_{\min} \\ \\ \min \begin{cases} \beta_{\max} \\ 1 + \frac{(h_c - \overline{h}^*_{k-1})\Delta p_{k-1}}{(h_c - \overline{h}^*_k)\Delta p_k} \end{cases} \end{cases}, \tag{4.h.34}$$

and $\beta_{\min}$ is assumed to be 0.10 (i.e., 10% overshoot). Since β effectively determines the actual autoconversion from cloud water to rainwater, $\beta_{\max}$ is determined from a minimum autoconversion requirement which is mathematically written as

$$\beta_{\max} = \max \begin{cases} \beta_{\min} \\ \\ 1 - c_0 \left(\delta z - \delta z_{\min}\right), \end{cases} \tag{4.h.35}$$

where c_0 is a constant autoconversion coefficient assumed to be equal to 1.0×10^{-4} m^{-1}, δz is the depth of contiguous convective activity (i.e., layers in which condensation and rainout takes place) including and below layer k, and $\delta z_{\min}$ is a minimum depth for precipitating convection. The physical constraints on the adjustment process are then applied to determine the actual value of β appropriate to the stabilization of levels k and $k+1$.

In summary, the adjustment procedure is applied as follows. A first guess at β is determined from (4.*h*.34) and (4.*h*.35), and further refined using (4.*h*.25), (4.*h*.31), and (4.*h*.33). The convective mass flux, m_c, is then determined from (4.*h*.23), followed by application of budget equations (4.*h*.7) – (4.*h*.12) to complete the thermodynamic adjustment in layers $k-1$ through $k+1$. By repeated application of this procedure from the bottom of the model to the top (see Figure 4), the thermodynamic structure is stabilized, and a vertical profile of the total cloud mass flux, M_c (where $M_{c_{k+\frac{1}{2}}} = m_{c_{k+\frac{1}{2}}} + \beta\, m_{c_{k+\frac{3}{2}}}$) can be constructed. This mass flux profile can also be used to estimate the convective-scale transport of arbitrary passive scalars. The total convective precipitation rate is obtained by vertically integrating the convective-scale liquid water sink

$$P = \frac{1}{\rho_{\mathrm{H_2O}}} \sum_{k=1}^{K} R_k. \tag{4.h.36}$$

The free parameters for the scheme consist of a minimum convective overshoot, $\beta_{\min}$, a characteristic adjustment time scale for the convection, τ, a cloud-water to rain-water autoconversion coefficient c_0, and a minimum depth for precipitating convection $\delta z_{\min}$.

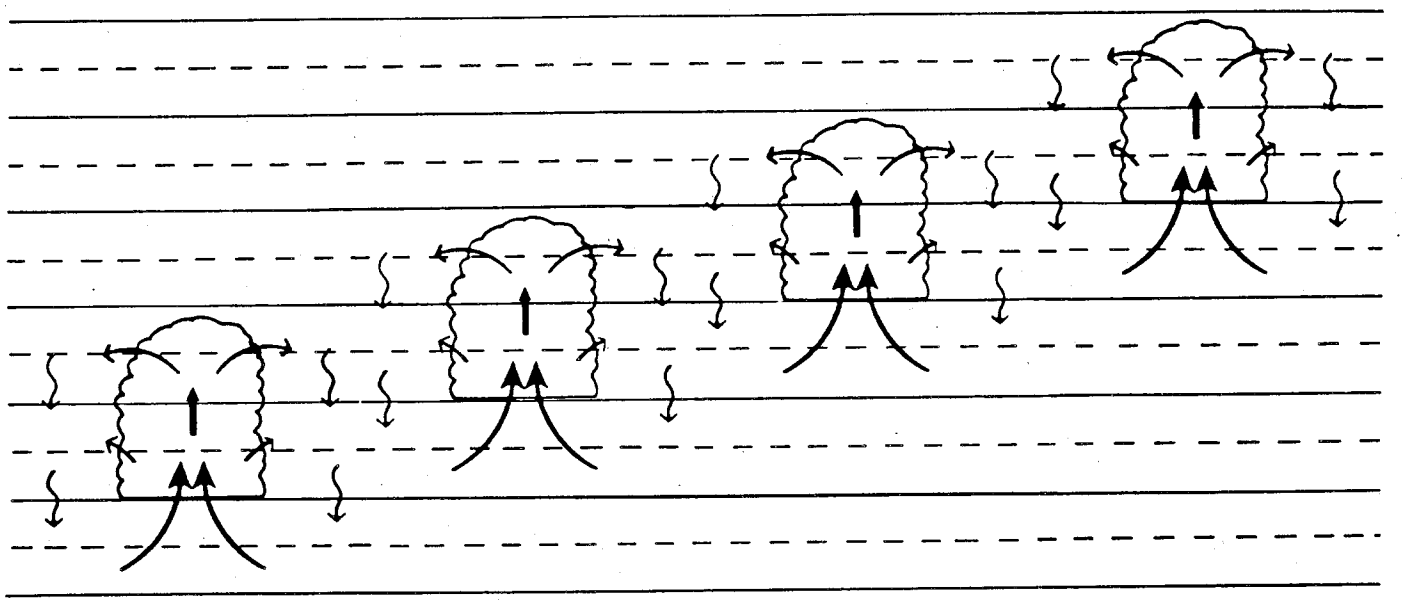

Figure 4. Successive application of cloud model

i. Stable Condensation

If the lapse rate is stable, but the moisture is supersaturated at a point, *i.e.*, if

$$\frac{q_k}{q_k^*} > 1.0 \quad , \tag{4.i.1}$$

the temperature and moisture are adjusted simultaneously so that the point is just saturated. The new specific humidity is given by

$$\hat{q}_k = \left[q_k^* + \frac{dq_k^*}{dT} \left(\hat{T}_k - T_k \right) \right], \tag{4.i.2}$$

where q_k^* is given by $(4.h.18)$. The temperature change due to the release of latent heat during condensation is

$$\left(\hat{T}_k - T_k\right) = \frac{L}{c_p}\left(q_k - \hat{q}_k\right). \tag{4.i.3}$$

Substitution of $(4.i.3)$ into $(4.i.2)$ gives the adjusted specific humidity,

$$\hat{q}_k = q_k - \left(q_k - q_k^*\right) / \left(1 + \frac{L}{c_p}\frac{dq_k^*}{dT}\right). \tag{4.i.4}$$

Equations $(4.i.4)$ and $(4.i.3)$ are iterated twice. The corresponding stable precipitation rate at level k is given by

$$R_{s_k} = \left(\hat{q}_k - q_k\right)\Delta p_k / \left(2\Delta tg\right). \tag{4.i.5}$$

The stable precipitation rate over the entire column is given by

$$P_s = \sum_{k=1}^{K} R_{s_k} / \rho_{H_2 0}. \tag{4.i.6}$$

j. Dry Adiabatic Adjustment

If a layer is unstable with respect to the dry adiabatic lapse rate, dry adiabatic adjustment is performed. The layer is stable if

$$\frac{\partial T}{\partial p} < \frac{\kappa T}{p}. \tag{4.j.1}$$

In finite–difference form, this becomes

$$T_{k+1} - T_k < C1_{k+1}(T_{k+1} + T_k) + \delta, \tag{4.j.2}$$

where

$$C1_{k+1} = \frac{\kappa(p_{k+1} - p_k)}{2p_{k+1/2}}. \tag{4.j.3}$$

If there are any unstable layers in a column, the temperature is adjusted so that $(4.j.2)$ is satisfied everywhere in the column. The variable δ represents a convergence criterion. The adjustment is done so that sensible heat is conserved,

$$c_p(\hat{T}_k \Delta p_k + \hat{T}_{k+1}\Delta p_{k+1}) = c_p(T_k \Delta p_k + T_{k+1}\Delta p_{k+1}), \tag{4.j.4}$$

and so that the layer has neutral stability:

$$\hat{T}_{k+1} - \hat{T}_k = C1_{k+1}(\hat{T}_{k+1} + \hat{T}_k). \tag{4.j.5}$$

As mentioned above, the hats denote the variables after adjustment. Thus, the adjusted temperatures are given by

$$\hat{T}_{k+1} = \frac{\Delta p_k}{\Delta p_{k+1} + \Delta p_k C2_{k+1}} T_k + \frac{\Delta p_{k+1}}{\Delta p_{k+1} + \Delta p_k C2_{k+1}} T_{k+1}, \tag{4.j.6}$$

and

$$\hat{T}_k = C2_{k+1}\hat{T}_{k+1}, \tag{4.j.7}$$

where

$$C2_{k+1} = \frac{1 - C1_{k+1}}{1 + C1_{k+1}}. \qquad (4.j.8)$$

Whenever the two layers undergo dry adjustment, the moisture is assumed to be completely mixed by the process as well. Thus, the specific humidity is changed in the two layers in a conserving manner to be the average value of the original values,

$$\hat{q}_{k+1} = \hat{q}_k = (q_{k+1}\Delta p_{k+1} + q_k \Delta p_k)/(\Delta p_{k+1} + \Delta p_k). \qquad (4.j.9)$$

The layers are adjusted iteratively. Initially, $\delta = 0.01$ in the stability check $(4.j.2)$. The column is passed through from $k = 1$ to a user-specifiable lower level (set to 3 in the standard model configuration) up to 15 times; each time unstable layers are adjusted until the entire column is stable. If convergence is not reached by the 15th pass, the convergence criterion is doubled, a message is printed, and the entire process is repeated. If δ exceeds 0.1 and the column is still not stable, the model stops.

As indicated above, the dry convective adjustment is only applied to the top three levels of the standard model. The vertical diffusion provides the stabilizing vertical mixing at other levels. Thus, in practice, momentum is mixed as well as moisture and potential temperature in the unstable case.

5. INITIAL AND BOUNDARY DATA

a. Initial Data

The previous section describes the central time loop of the model. In this section, we describe how the loop is started from data consistent with the spectral truncation. The basic initial data for the model consist of values of u, v, T, q, Π, and Φ_s on the Gaussian grid at time $t = 0$. From these, U, V, T', and Π are computed on the grid using (3.a.11), and (3.a.49). The Fourier coefficients of these variables U^m, V^m, T'^m, Π^m, and Φ_s^m are determined via an FFT subroutine (3.b.23), and the spherical harmonic coefficients $T_n'^m, \Pi_n^m$, and $(\Phi_s)_n^m$ are determined by Gaussian quadrature (3.b.24). The relative vorticity ζ and divergence δ spherical harmonic coefficients are determined directly from the Fourier coefficients U^m and V^m using the relations,

$$\zeta = \frac{1}{a(1-\mu^2)}\frac{\partial V}{\partial \lambda} - \frac{1}{a}\frac{\partial U}{\partial \mu}, \tag{5.a.1}$$

$$\delta = \frac{1}{a(1-\mu^2)}\frac{\partial U}{\partial \lambda} + \frac{1}{a}\frac{\partial V}{\partial \mu}. \tag{5.a.2}$$

The relative vorticity and divergence coefficients are obtained by Gaussian quadrature directly, using (3.b.27) for the λ–derivative terms and (3.b.30) for the μ–derivatives.

Once the spectral coefficients of the prognostic variables are available, the grid–point values of ζ, δ, T', Π, and Φ_s may be calculated from (3.b.47), the gradient $\nabla\Pi$ from (3.b.50) and (3.b.51), and U and V from (3.b.56) and (3.b.57). The absolute vorticity η is determined from the relative vorticity ζ by adding the appropriate associated Legendre function for f (3.b.4). This process gives grid–point fields for all variables, including the surface geopotential, that are consistent with the spectral truncation even if the original grid–point data were not. These grid–point values are then convectively adjusted (including the mass and negative moisture corrections).

The first time step of the model is forward semi–implicit rather than centered semi–implicit, so only variables at $t = 0$ are needed. The model performs this forward step by setting the variables at time $t = -\Delta t$ equal to those at $t = 0$ and by temporarily dividing $2\Delta t$ by 2 for this time step only. This is done so that formally the code and the centered prognostic equations of section 4 also describe this first forward step and no additional code is needed for this special step. The model loops through as indicated sequentially in section 4. The time step $2\Delta t$ is set to its original value before beginning the second time step.

b. Boundary Data

In addition to the initial grid–point values described in the previous section, the model also requires lower boundary conditions. The required data are surface temperature

(T_s) at each ocean point, the surface geopotential at each point, and a flag at each point to indicate whether the point is land, ocean, or sea ice. A surface temperature and three subsurface temperatures must also be provided at non-ocean points.

The sea–surface temperatures, sea–ice locations, and snow cover are changed to reflect the seasonal changes. The sea–surface temperatures and sea–ice distributions are specified from the monthly mean analyses of Shea *et al.*, (1990). The mean monthly sea–surface temperature and sea ice distribution are assigned the mid–month date and updated every time step at each grid point using linear interpolation.

The radiation parameterization requires monthly mean ozone volume mixing ratios to be specified as a function of the latitude grid, 23 vertical pressure levels, and time. The ozone path lengths are evaluated from the mixing–ratio data. The path lengths are interpolated to the model η–layer interfaces for use in the radiation calculation. As with the sea–surface temperatures, the seasonal version assigns the monthly averages to the mid–month date and updates them every 12 hours via linear interpolation. The actual mixing ratios used in the standard version were derived by Chervin (1986) from analyses of Dütsch (1978).

The radiation parameterization also requires that surface albedo be specified on the model grid for land points. The land albedos are constants (independent of time or moisture conditions); land albedos for snow–covered points are weighted values of snow albedos and the constant land albedos depending on snow depth and local roughness length. The surface albedo data are composed of five quantities—the fraction of strong zenith–angle dependence and four surface albedos (two zenith angles and two spectral range groups). The original source of these data is the Matthews (1983) $1° \times 1°$ global 32–type vegetation data set, which was reduced to ten vegetation types. Narrow–band (0.2–0.5 μm, 0.5–0.7 μm, 0.7–0.85 μm, and 0.85–4.0 μm) spectral albedos (for diffuse incident radiation) were ascribed to each of these ten types (Briegleb, 1992). The ten surface types were segregated into two groups, based on solar zenith–angle dependence (strong or weak) and averaged to the spectral intervals (0.2–0.7 μm, 0.7–4.0 μm). The $1° \times 1°$ data set was then averaged to the required horizontal resolution of the CCM2.

Roughness length and potential evaporation factor were determined in an analogous fashion from Mathews (1983) $1° \times 1°$ data (see Section 4c) and Table 1. The sub-grid scale standard deviation of surface orography was specified in the following manner. The variance is first evaluated from the global Navy $10'$ topographic height data over $2° \times 2°$ grid for T42 and lower resolutions, $1.67° \times 1.67°$ for T63, and $1.0° \times 1.0°$ for T106 resolution, and is assumed to be isotropic. Once computed on the appropriate grid, the standard deviations are binned to the CCM2 Gaussian grid (*i.e.,* all values whose latitude and longitude centers fall within each Gaussian grid box are averaged together). Finally, the standard deviation is smoothed twice with a 1–2–1 spatial filter. Values over ocean are set to zero.

6. STATISTICS CALCULATIONS

At specified times during a model run, selected global average statistics are computed for diagnostic purposes. Let $\int_3$ denote a global and vertical average and $\int_2$ a horizontal global average. For an arbitrary variable ψ, these are defined by

$$\int_3 \psi dV = \sum_{k=1}^{K}\sum_{j=1}^{J}\sum_{i=1}^{I} \psi_{ijk} w_j \left(\frac{\Delta p_k}{\pi}\right) \Big/ 2I, \tag{6.a.1}$$

and

$$\int_2 \psi dA = \sum_{j=1}^{J}\sum_{i=1}^{I} \psi_{ijk} w_j / 2I, \tag{6.a.2}$$

where recall that

$$\sum_{j=1}^{J} w_j = 2. \tag{6.a.3}$$

The quantities monitored are:

$$\text{global rms } (\zeta + f)(\text{s}^{-1}) = \left[\int_3 (\zeta^n + f)^2 dV\right]^{1/2}, \tag{6.a.4}$$

$$\text{global rms } \delta(\text{s}^{-1}) = \left[\int_3 (\delta^n)^2 dV\right]^{1/2}, \tag{6.a.5}$$

$$\text{global rms } T \text{ (K)} = \left[\int_3 (T^r + T'^n)^2 dV\right]^{1/2}, \tag{6.a.6}$$

$$\text{global average mass times } g \text{ (Pa)} = \int_2 \pi^n dA, \tag{6.a.7}$$

$$\text{global average mass of moisture (kg m}^{-2}) = \int_3 \pi^n q^n / g dV. \tag{6.a.8}$$

APPENDIX A—Terms in Equations

The terms of (3.*b*.18) are

$$\underline{V} = \underline{(\zeta + f)}^{n-1}, \tag{A1}$$

$$\underline{V}_\lambda = 2\Delta t\, \underline{n}_V^n, \tag{A2}$$

$$\underline{V}_\mu = 2\Delta t\, \underline{n}_U^n. \tag{A3}$$

The terms of (3.*b*.19) are

$$\underline{D} = \underline{\delta}^{n-1}, \tag{A4}$$

$$\underline{D}_\lambda = 2\Delta t\, \underline{n}_U^n, \tag{A5}$$

$$\underline{D}_\mu = 2\Delta t\, \underline{n}_V^n, \tag{A6}$$

$$\begin{aligned} \underline{D}_\nabla = {} & 2\Delta t \left[\underline{E}^n + \Phi_s \underline{1} + R\mathbf{H}^r \underline{T}'^n\right] \\ & + \Delta t \left[R\mathbf{H}^r \left(\left(\underline{T}'\right)^{n-1} - 2(\underline{T}')^n\right) + R\left(\underline{b}^r + \underline{h}^r\right)\left(\Pi^{n-1} - 2\Pi^n\right)\right] . \end{aligned} \tag{A7}$$

The terms of (3.*b*.20) are

$$\underline{T} = \left(\underline{T}'\right)^{n-1} + 2\Delta t\, \underline{\Gamma}^n - \Delta t \mathbf{D}^r \left[\underline{\delta}^{n-1} - 2\underline{\delta}^n\right] , \tag{A8}$$

$$\underline{T}_\lambda = 2\Delta t \underline{(UT')}^n, \tag{A9}$$

$$\underline{T}_\mu = 2\Delta t \underline{(VT')}^n. \tag{A10}$$

The nonlinear term in (3.b.21) is

$$\begin{aligned} PS = {} & \Pi^{n-1} - 2\Delta t \frac{1}{\pi^n} \left[\left(\underline{\delta}^n\right)^T \left(\underline{\Delta p}^n\right) + \left(\underline{\mathbf{V}}^n\right)^T \nabla \Pi^n \pi^n \underline{\Delta B}\right] \\ & - \Delta t \left[\left(\underline{\Delta p}^r\right)^T \frac{1}{\pi^r}\right] \left[\underline{\delta}^{n-1} - 2\underline{\delta}^n\right] . \end{aligned} \tag{A11}$$

The spectral transformation of the terms in the vorticity equation (3.*b*.33) is given by

$$\underline{VS}_n^m = \sum_{j=1}^{J} \left[\underline{V}^m(\mu_j) P_n^m(\mu_j) + im \underline{V}_\lambda^m(\mu_j) \frac{P_n^m(\mu_j)}{a(1-\mu_j^2)} + \underline{V}_\mu^m(\mu_j) \frac{H_n^m(\mu_j)}{a(1-\mu_j^2)}\right] w_j. \tag{A12}$$

The spectral transformation of the explicit terms in the divergence equation (3.*b*.34) is

$$\underline{DS}_n^m = \sum_{j=1}^{J} \left\{ \left[\underline{D}^m(\mu_j) + \frac{n(n+1)}{a^2} \underline{D}_\nabla^m(\mu_j) \right] P_n^m(\mu_j) \right.$$
$$\left. + im\underline{D}_\lambda^m(\mu_j) \frac{P_n^m(\mu_j)}{a(1-\mu_j^2)} - \underline{D}_\mu^m(\mu_j) \frac{H_n^m(\mu_j)}{a(1-\mu_j^2)} \right\} w_j. \tag{A13}$$

The spectral transformation of the explicit term of the thermodynamic equation (3.*b*.35) is

$$\underline{TS}_n^m = \sum_{j=1}^{J} \left[\underline{T}^m(\mu_j) P_n^m(\mu_j) - im\underline{T}_\lambda^m(\mu_j) \frac{P_n^m(\mu_j)}{a(1-\mu_j^2)} + \underline{T}_\mu^m(\mu_j) \frac{H_n^m(\mu_j)}{a(1-\mu_j^2)} \right] w_j. \tag{A14}$$

The spectral transformation of the explicit terms of the surface pressure tendency equation (3.*b*.36) is

$$PS_n^m = \sum_{j=1}^{J} PS^m(\mu_j) P_n^m(\mu_j) w_j. \tag{A15}$$

APPENDIX B—Physical Constants

Following the American Meteorological Society convention, the model uses the International System of Units (SI) (see August 1974 *Bulletin of the American Meteorological Society,* **Vol. 55,** No. 8, pp. 926–930).

a	=	6.37122×10^6 m	Radius of earth
g	=	9.80616 m s^{-2}	Acceleration due to gravity
Ω	=	7.292×10^{-5} s^{-1}	Earth's angular velocity
σ_B	=	5.67×10^{-8} W m^{-2} K^{-4}	Stefan–Boltzmann constant
R	=	287.04 J kg^{-1} K^{-1}	Gas constant for dry air
c_p	=	1.00464×10^3J kg^{-1} K^{-1}	Specific heat capacity of dry air at constant pressure
κ	=	R/c_p	
ϵ	=	.622	Ratio of molecular weight of water vapor to that of dry air
L_v	=	2.5104×10^6 J kg^{-1}	Latent heat of vaporization
L_i	=	3.336×10^5 J kg^{-1}	Latent heat of fusion
R_v	=	4.61×10^2 J kg^{-1} K^{-1}	Gas constant for water vapor
ρ_{H_2O}	=	1.0×10^3 kg m^{-3}	Density of liquid water
c_{p_v}	=	1.81×10^3 J kg^{-1} K^{-1}	Specific heat capacity of water vapor at constant pressure
T_{melt}	=	273.16°K	Melting point of ice

The model code defines these constants to the stated accuracy. We do not mean to imply that these constants are known to this accuracy nor that the low–order digits are significant to the physical approximations employed.

ACKNOWLEDGMENTS

The authors wish to acknowledge other members of the Climate Modeling Section, Linda Bath, Lawrence Buja, Jerry Olson, Jim Rosinski, John Truesdale, Mariana Vertenstein, and Gloria Williamson for all their contributions to the development of the CCM2. We are also indepted to Gordon Bonan for his careful review of this technical note, and are particularly grateful to Mariana Vertenstein for her exceptionally thorough and insightful reviews of several versions of this technical note. We also wish to thank Ronna Bailey and Janet Rodina for their invaluable help in the preparation of this document.

REFERENCES

Anthes, R. A., 1986: Summary of workshop on the NCAR community climate/forecast models 14–26 July 1985, Boulder, Colorado. *Bull. Amer. Meteor. Soc.*, **67,** 94–198.

Asselin, R., 1972: Frequency filter for time integrations. *Mon. Wea. Rev.*, **100,** 487–490.

Baede, A. P. M., M. Jarraud, and U. Cubasch, 1979: *Adiabatic formulation and organization of ECMWF's model.* ECMWF Technical Report No. 15, 40 pp.

Bath, L. M., M. A. Dias, D. L. Williamson, G. S. Williamson, and R. J. Wolski, 1987: *Users' Guide to NCAR CCM1.* NCAR Technical Note NCAR/TN–286+IA, Boulder, Colorado, 173 pp..

——, J. Rosinski, and J. Olson, 1992: *User's Guide to CCM2.* NCAR Technical Note/TN–379+IA, Boulder, Colorado, 127 pp.

Beljaars, A. C. M., and A. A. M. Holtslag, 1991: Flux parameterization over land surfaces for atmospheric models. *J. Appl. Meteorol.*, **30**, 327–341.

Betts, A. K., 1975: Parametric interpretation of trade-wind cumulus budget studies. *J. Atmos. Sci.*, **32**, 1934–1945.

Bhumralkar, C.M., 1975: Numerical Experiments on the Computation of Ground Surface Temperature in an Atmospheric General Circulation Model. *J. Appl. Meteorol.*, 14, 1246–1258.

Bonan, G.B., 1993: Comparison of the land surface climatology of the NCAR CCM2 at R15 and T42 resolutions with implications for sub-grid land surface heterogeneity. submitted to *J. Geophys. Res.*.

Bourke, W., B. McAvaney, K. Puri, and R. Thurling, 1977: Global modeling of atmospheric flow by spectral methods. *Methods in Computational Physics,* **17,** Academic Press, 267–324.

Briegleb, B. P., 1992: Delta-Eddington approximation for solar radiation in the NCAR Community Climate Model. *J. Geophys. Res.*, **97**, 7603–7612.

——, and V. Ramanathan, 1982: Spectral and diurnal variations in clear sky planetary albedo. *J. Climate Appl. Meteor.*, **21**, 1160–1171.

——, P. Minnis, V. Ramanathan, and E. Harrison, 1986: Comparison of regional clear–sky albedos inferred from satellite observations and model computations. *J. Climate Appl. Meteor.*, **25,** 214–226.

Budyko, M. I., 1956: *Heat Balance of the Earth's Surface.* Gidrometeozidat, Leningrad, 255 pp.

Cess, R.D., 1985: Nuclear war: Illustrative effects of atmospheric smoke and dust upon solar radiation. *Clim. Change*, **7**, 237-251.

Chervin, R. M., 1986: Interannual variability and seasonal climate predictability. *J. Atmos. Sci.,* **43,** 233–251.

Climate Modeling Section, 1993: Climate statistics of the NCAR Community Climate Model (CCM2). Submitted to *J. Geophys. Res.*.

Coakley, J.A., R.D. Cess and F.B. Yurevich, 1983: The effect of tropospheric aerosols on the Earth's radiation budget: A parameterization for climate models. *J. Atmos. Sci.*, **40**, 116-138.

Daley, R., C. Girard, J. Henderson, and I. Simmonds, 1976: Short–term forecasting with a multi–level spectral primitive equation model. Part I—Model formulation. *Atmosphere,* **14,** 98–116.

Deardorff, J. W., 1972: Parameterization of the planetary boundary layer for use in general circulation models. *Mon. Wea. Rev.,* **100,** 93–106.

Dickinson, R.E., A. Henderson-Sellers, and P.J. Kennedy, 1993: *Biosphere-Atmosphere Transfer Scheme (BATS) Version 1e as coupled to the NCAR Community Climate Model.* NCAR Technical Note, in preparation.

——, ——, ——, and M.S. Wilson, 1986: *Biosphere-Atmosphere Transfer Scheme (BATS) for the NCAR Community Climate Model.* NCAR Technical Note NCAR/TN-275+STR, Boulder, Colorado, 69 pp.

Dütsch, H. V., 1978: Vertical ozone distribution on a global scale. *Pure Appl. Geophys.,* **116,** 511–529.

Dyer, A.J., 1974: A review of flux-profile relationships. *Boundary-Layer Meteor.*, **7**, 363–372.

Errico, R.M., 1986: *A Description of Software for Determination of Normal Modes of the NCAR Community Climate Model.* NCAR Tech. Note, NCAR/TN-217+STR, National Center for Atmospheric Research, Boulder, Colo., 86 pp.

——, and B.E. Eaton, 1987: *Nonlinear Normal Mode Initialization of the NCAR CCM.* NCAR Tech. Note, NCAR/TN-303+IA, National Center for Atmospheric Research, Boulder, Colo., 106 pp.

Forderhase, K., W.M. Washington, R.M. Chervin, V. Ramanathan, D.L. Williamson, and D.J. Knight, 1980: *Lower boundary conditions for the NCAR Global Circulation Model: Ocean surface temperatures, sea ice, snow cover, continental surface albedos and surface emissivity, subsurface continental temperatures and mountain heights.* NCAR Tech. Note, NCAR/TN-157+STR, National Center for Atmospheric Research, Boulder, Colo., 58 pp.

Geleyn, J. F., 1988: Interpolation of wind, temperature and humidity values from model levels to the height of measurement. *Tellus*, **40A**, 347–351.

Griffith, K. T., S. K. Cox, and R. G. Knollberg, 1980: Infrared radiative properties of tropical cirrus clouds inferred from aircraft measurements. *J. Atmos. Sci.*, **37**, 1077–1087.

Hack, J.J., 1993: Parameterization of moist convection in the NCAR Community Climate Model (CCM2). Submitted to *J. Geophys. Res.*

——, L. M. Bath, G. W. Williamson and B. A. Boville, 1989: *Modifications and Enhancements to the NCAR Community Climate Model (CCM1).* NCAR Technical Note NCAR/TN-336+STR, NTIS PB89-215594/AS, 97 pp.

Holloway, J. L., Jr., and S. Manabe, 1971: Simulation of climate by a global general circulation model. 1. Hydrologic cycle and heat balance. *Mon. Wea. Rev.*, **99**, 335–370.

Holtslag, A.A.M., and B.A. Boville, 1993: Local versus nonlocal boundary–layer diffusion in a global climate model, *J. Climate*, in press.

——, and C.-H. Moeng, 1991: Eddy diffusivity and countergradient transport in the convective atmospheric boundary layer. *J. Atmos. Sci.*, **48**, 1690–1698.

——, and A. C. M. Beljaars, 1989: Surface flux parameterization schemes: Developments and experiences at KNMI.Proceedings of the ECMWF workshop on Parameterization of fluxes over land surface, ECMWF Reading UK, 121–147 (Also available as KNMI Sci. Rep. 88–06, De Bilt NL, 27p.).

——, E.I.F. de Bruijn, and H.-L. Pan, 1990: A high resolution air mass transformation model for short-range weather forecasting. *Mon. Wea. Rev.*, **118**, 1561-1575

Joseph, J.H., W.J. Wiscombe and J.A. Weinman, 1976: The delta-Eddington approximation for radiative flux transfer. *J. Atmos. Sci.*, **33**, 2452-2459.

Kasahara, A., 1974: Various vertical coordinate systems used for numerical weather prediction. *Mon. Wea. Rev.*, **102**, 509–522.

Kiehl, J. T., 1991: Modelling and validation of clouds and radiation in the NCAR Community Climate Model. *Proc. ECMWF/WCRP Workshop on Clouds, Radiative Transfer and the Hydrological Cycle*, Reading, *12-15 November 1990*, 413-450.

____, and B.P. Briegleb, 1991: A new parameterization of the absorptance due to the 15 μm band system of carbon dioxide. *J. Geophys. Res.*, **96**, 9013-9019.

____, and V. Ramanathan, 1990: Comparison of cloud forcing derived from the earth radiation budget experiment with that simulated by the NCAR Community Climate Model. *J. Geophys. Res.*, **95**, 11679–11698.

____, and ____, 1983: CO_2 radiative parameterization used in climate models: Comparison with narrow band models and with laboratory data. *J. Geophys. Res.*, **88**, 5191-5202.

____, J. J. Hack, and B.P. Briegleb, 1993: The simulated earth radiation budget of the NCAR CCM2 and Comparisons with the Earth Radiation Budget Experiment (ERBE). Submitted to *J. Geophys. Res.*.

____, R. J. Wolski, B. P. Briegleb, and V. Ramanathan, 1987: *Documentation of Radiation and Cloud Routines in the NCAR Community Climate Model (CCM1).* NCAR Technical Note NCAR/TN–288+IA, Boulder, Colorado.

Louis, J.F., 1979: A parametric model of vertical eddy fluxes in the atmosphere. *Bound.-Layer Meteorol.*, **17**, 187–202.

Machenhauer, B., 1979: The spectral method. *Numerical Methods Used in Atmospheric Models. GARP Publication Series 17,* 121–275, World Meteorological Organization, Geneva, Switzerland.

Manabe, S., 1969: Climate and ocean circulation. 1. The atmosphere circulation and the hydrology of the earth's surface. *Mon. Wea. Rev.,* **97,** 739–773.

____, J. Smagorinsky, and R. F. Strickler, 1965: Simulated climatology of a general circulation model with a hydrologic cycle. *Mon. Wea. Rev.,* **93,** 769–798.

Matthews, E., 1983: Global vegetation and land use: New high–resolution data bases for climate studies. *J. Clim. Appl. Meteor.,* **22,** 474–487.

Mayer, T.A., 1988: *Generation of CCM Format History Tapes from Analyzed Data.* NCAR Tech. Note, NCAR/TN-322+STR, National Center for Atmospheric Research, Boulder, Colorado, 68 pp..

McAvaney, B. J., W. Bourke, and K. Puri, 1978: A global spectral model for simulation of the general circulation. *J. Atmos. Sci.,* **35,** 1557–1583.

McFarlane, N.A., 1987: The effect of orographically excited wave drag on the general circulation of the lower stratosphere and troposphere. *J. Atmos. Sci.*, **44**, 1775-1800.

Nieuwstadt, F.T.M., 1984: Some aspects of the turbulent stable boundary layer. *Boundary-Layer Meteor.*, **30**, 31–55.

Orszag, S. A., 1974: Fourier series on spheres. *Mon. Wea. Rev.,* **106,** 405–412.

Paltridge, G.W. and C.M.R. Platt, 1976: *Radiative Processes in Meteorology and Climatology*, Elsevier Scientific Publishing Co., Amsterdam, Oxford-New York, 318pp.

Pitcher, E. J., R. C. Malone, V. Ramanathan, M. L. Blackmon, K. Puri, and W. Bourke, 1983: January and July simulations with a spectral general circulation model. *J. Atmos. Sci.,* **40,** 580–604.

Ramanathan, V., and P. Downey, 1986: A nonisothermal emissivity and absorptivity formulation for water vapor. *J. Geophys. Res.,* **91,** 8649–8666.

_____, and R. E. Dickinson, 1979: The role of stratospheric ozone in the zonal and seasonal radiative energy balance of the earth–troposphere system. *J. Atmos. Sci.,* **36,** 1084–1104.

_____, E. J. Pitcher, R. C. Malone, and M. L. Blackmon, 1983: The response of a spectral general circulation model to refinements in radiative processes. *J. Atmos. Sci.,* **40,** 605–630.

Rasch, P. J., and D. L. Williamson, 1991: The sensitivity of a general circulation model climate to the moisture transport formulation. *J. Geophys. Res.*, **96**, 13,123–13,137.

_____, and _____, 1990: Computational aspects of moisture transport in global models of the atmosphere. *Quart. J. Roy. Meteor. Soc.*, **116**, 1071–1090.

Richtmeyer, R. D., and K. W. Morton, 1967: *Difference Methods for Initial–Value Problems,* Second Edition. Interscience Publishers, New York, 405 pp.

Robert, A. J., 1966: The integration of a low order spectral form of the primitive meteorological equations. *J. Meteor. Soc. Japan,* **44,** 237–245.

Royer, J–F., 1986: Correction of negative mixing ratios in spectral models by global horizontal borrowing. *Mon. Wea. Rev.,* **114,** 1406–1410.

Sato, R. K., L. M. Bath, D. L. Williamson, and G. S. Williamson, 1983: *User's Guide to NCAR CCMOB.* NCAR Technical Note NCAR/TN–211+IA, Boulder, Colorado, NTIS No. PB83 263988, 133 pp.

Sellers, W.D., 1965: *Physical Climatology*, The University of Chicago Press, Chicago and London, 272 pp.

Shea, D.J., K.E. Trenberth, R.W. Reynolds, 1990: *A Global Monthly Sea Surface Temperature Climatology.* NCAR Technical Note NCAR/TN–345+STR, Boulder, Colorado, 167 pp.

Simmons, A. J., and R. Strüfing, 1981: *An energy and angular-momentum conserving finite-difference scheme, hybrid coordinates and medium-range weather prediction.* ECMWF Technical Report No. 28, 68pp.

——, B. J. Hoskins, and D. M. Burridge, 1978: Stability of the semi–implicit method of time integration. *Mon. Wea. Rev.,* **106,** 405–412.

Slingo, A., 1989: A GCM parameterization for the shortwave radiative properties of water clouds. *J. Atmos. Sci.*, **46**, 1419–1427.

Slingo, J.M., 1987: The development and verification of a cloud prediction scheme for the ECMWF model. *Quart. J. Roy. Meteor. Soc.*, **113**, 899-927.

Smagorinsky, J., 1963: General circulation experiments with the primitive equations, 1. The basic experiment. *Mon. Wea. Rev.,* **91,** 98–164.

——, S. Manabe, and J. L. Holloway, Jr., 1965: Numerical results from a nine–level general circulation model of the atmosphere. *Mon. Wea. Rev.,* **93,** 927–768.

Smith, G.D., 1965: *Numerical Solution of Partial Differential Equations*, Oxford University Press, New York and London, 179 pp.

Troen, I., and L. Mahrt, 1986: A simple model of the atmospheric boundary layer; Sensitivity to surface evaporation. *Boundary-Layer Meteor.*, **37**, 129-148.

Verstraete, M.M., 1988: *Defining the Thermal Properties of Continental Surfaces in GCMs*, unpublished manuscript (NCAR MS. 8076/88–1), pp. 12.

Washington, W. M., 1982: *Documentation for the Community Climate Model (CCM), Version* ∅. NCAR report, Boulder, Colorado, NTIS No. PB82 194192.

——, and L. VerPlank, 1986: *A Description of Coupled General Circulation Models of the Atmosphere and Oceans Used for Carbon Dioxide Studies.* NCAR Technical Note, NCAR/TN-271+EDD, National Center for Atmospheric Research, Boulder, Colo., 29 pp.

Williamson, D. L., 1990: Semi-Lagrangian moisture transport in the NMC spectral model. *Tellus*, **42A**, 413–428.

——, 1983: *Description of NCAR Community Climate Model (CCM0B).* NCAR Technical Note NCAR/TN-210+STR, Boulder, Colorado, NTIS No. PB83 231068, 88 pp.

——, and P.J. Rasch, 1993: Water vapor transport in the NCAR CCM2. *Tellus*, in press.

——, and ——, 1989: Two-dimensional semi-Lagrangian transport with shape preserving interpolation. *Mon. Wea. Rev.*, **117**, 102-129.

——, and G. S. Williamson, 1984: *Circulation Statistics from January and July Simulations with the NCAR Community Climate Model (CCM0B).* NCAR Technical Note NCAR/TN-224+STR, Boulder, Colorado, NTIS No. PB85 165637/AS, 112 pp.

——, J.T. Kiehl, V. Ramanathan, R.E. Dickinson and J.J Hack, 1987: *Description of NCAR Community Climate Model (CCM1).* NCAR Tech. Note, NCAR/TN-285+STR, National Center for Atmospheric Research, Boulder, Colo., 112 pp.

——, L.M. Bath, R.K. Sato, T.A. Mayer, and M.L. Kuhn, 1983: *Documentation of NCAR CCM0B Program Modules.* NCAR Technical Note NCAR/TN-212+IA, Boulder, Colorado, NTIS No. PB83 263996, 198 pp.

Williamson, G.S., and D.L. Williamson, 1987: *Circulation Statistics from Seasonal and Perpetual January and July Simulations with the NCAR Community Climate Model (CCM1):R15.* NCAR Tech. Note, NCAR/TN-302+STR, National Center for Atmospheric Research, Boulder, Colorado., 199 pp.

Yanai, M., S. Esbensen and J.-H. Chu, 1973: Determination of bulk properties of tropical cloud clusters from large-scale heat and moisture budgets. *J. Atmos. Sci.*, **30**, 611–627.